

Final Report

**Design, Fabrication, and Testing of an
External-Fuel [UO₂], Full-Length Thermionic Converter**

Prepared

under

Contract JPL 952277

for

Thermionic Reactor Systems Project
Propulsion Research and Advanced Concepts Section
Jet Propulsion Laboratory
4800 Oak Grove Drive
Pasadena, California 91103



Reproduced by
**NATIONAL TECHNICAL
INFORMATION SERVICE**
U S Department of Commerce
Springfield VA 22151

(NASA-CR-126142) DESIGN, FABRICATION, AND TESTING OF AN EXTERNAL FUEL (UO₂), FULL-LENGTH THERMIONIC CONVERTER Final Report A. Schock, et al (Fairchild Hiller Corp.) 15 Sep. 1971 166 p CSCL 18E G3/22 N72-22664 Unclas 15234

CAT. 22

PCD-TR-71-5
FHR 3641A
PC004R5101

15 September 1971

Final Report

**Design, Fabrication, and Testing of an
External-Fuel [UO₂], Full-Length Thermionic Converter**

Prepared
under
Contract JPL 952277
for

Thermionic Reactor Systems Project
Propulsion Research and Advanced Concepts Section
Jet Propulsion Laboratory
4800 Oak Road Drive
Pasadena, California 91103

JPL Technical Managers:

J. P. Davis
J. F. Mondt
W. M. Phillips

Report Prepared by:

A. Schock
B. Raab

A. Schock



This work was performed for the Jet Propulsion Laboratory,
California Institute of Technology, as sponsored by the National
Aeronautics and Space Administration under Contract NAS7-100.

PREFACE

This report contains information prepared by Fairchild Industries under JPL subcontract. Its content is not necessarily endorsed by the Jet Propulsion Laboratory, California Institute of Technology, or the National Aeronautics and Space Administration.

The work described here extended from November 1, 1968, to July 30, 1971. The report was prepared by A. Schock and B. Raab. In carrying out this program they were supported, at various times, by F. Giorgio and B. Wolk of Fairchild Industries, and by S. Basham and W. Zielenbach of the Battelle Columbus Laboratories. The latter organization, under Subcontract No. 106573, conducted a nuclear mock-up test to determine the required fuel enrichment, advised on BRR safety requirements, submitted the safety evaluation for approval, and assembled the in-pile vacuum system and all requisite safety circuitry.

The program, at various times, was under the general direction of J. P. Davis, J. F. Mondt, and W. M. Phillips of the Jet Propulsion Laboratory.

CONTENTS

| <u>Section</u> | | <u>Page</u> |
|----------------|---|-------------|
| 1. | INTRODUCTION | 1 |
| 2. | CONCLUSIONS | 2 |
| 3. | DESIGN DESCRIPTION | 5 |
| | 3.1 Fuel-Emitter Assembly | 5 |
| | 3.2 Collector Assembly | 7 |
| | 3.3 Cooling and Electrical Arrangement | 8 |
| | 3.4 Containment | 9 |
| | 3.5 Fission Gas Collection | 10 |
| | 3.6 In-Pile Test Arrangement | 11 |
| 4. | CONVERTER FABRICATION | 12 |
| | 4.1 Emitter Body | 12 |
| | 4.2 Emitter Assembly | 14 |
| | 4.3 Joints | 15 |
| | 4.4 Assembly Sequence | 17 |
| 5. | DIODE PROCESSING AND TEST ARRANGEMENT | 18 |
| | 5.1 RF Feedthrough | 18 |
| | 5.2 Converter Processing | 19 |
| | 5.3 Out-Of-Pile Installation | 20 |
| | 5.4 Emitter Temperature | 21 |
| 6. | OUT-OF-PILE TEST OF CONVERTER NO. 1 | 25 |
| | 6.1 Test Conditions and Results | 25 |
| | 6.2 Heat Balance and Efficiency | 26 |
| | 6.3 Comparison With Predicted Performance | 27 |
| | 6.4 Test Operation | 28 |
| | 6.5 Fission Gas Vent | 30 |
| | 6.6 Fuel Body Leak | 31 |
| 7. | CONVERTER NO. 2 | 32 |
| | 7.1 Description | 32 |
| | 7.2 Discussion | 32 |
| | 7.3 Fabrication and Processing | 33 |
| | 7.4 Out-of-Pile Test | 33 |
| | 7.5 Test Results | 35 |

| <u>Section</u> | | <u>Page</u> |
|----------------|--|-------------|
| 8. | PREPARATION FOR IN-PILE TEST | 37 |
| 8.1 | Fuel-Emitter Thermocouples | 37 |
| 8.2 | Secondary Containment | 39 |
| 8.3 | Discussion | 40 |
| 8.4 | Fission Gas Collection Assembly | 41 |
| 8.5 | Assembly Plate | 44 |
| 8.6 | In-Pile Test Chamber and Vacuum System | 45 |
| 8.7 | External Controls and Instrumentation | 49 |
| 8.8 | Final Assembly | 50 |
| 9. | DESIGN ALTERNATIVES | 52 |
| 9.1 | Introduction | 52 |
| 9.2 | Heatpipe-Cooled Converter Module | 52 |
| 9.3 | Single-Ended Converter | 53 |
| 9.4 | Emitter Body Geometry | 54 |
| 9.5 | Axial Reflector | 55 |
| 9.6 | Emitter Flanges | 56 |
| 9.7 | Collector Assembly | 56 |
| 9.8 | Converter Assembly | 57 |
| | REFERENCES | 59 |

APPENDIX

| | | |
|----|---|-----|
| A. | Predicted Thermionic Performance and Estimate of Required Thermal Power | 60 |
| B. | Nuclear Analysis | 68 |
| C. | Nuclear Mock-up Experiments | 73 |
| D. | Thermal Stress Analysis | 83 |
| E. | Hydraulic-Electric Design Details | 88 |
| F. | Electron-Beam Welding of Refractory Metals | 95 |
| G. | Fabrication and Assembly Steps | 98 |
| H. | New Technology | 108 |

SUMMARY

The development of a double-ended full-core-length external-fuel converter, a prototypical fuel module for a 200- to 300-ekw thermionic reactor, is described. The converter design is based on a revolver-shaped tungsten emitter body, with six peripheral fuel chambers loaded with enriched UO_2 pellets. The columbium collector is water-cooled through a sub-atmospheric adjustable-pressure helium gap. The converter employs graded metal-ceramic seals, and its double-ended construction is made possible by bellows to compensate for differential axial expansion. Fission gases are vented from the fuel chambers and collected in an accumulator designed for continuous monitoring of the pressure buildup. Component fabrication, assembly sequence, and joining methods are described; also the test procedures, and the converter load control. All tests are performed in vacuum. During in-pile testing, the fuel is triply contained, with thermal insulation between the secondary and tertiary containers. Before insertion in-pile, the fully fueled converter is qualification-tested by rf-induction heating, using a specially-developed high-vacuum rf-feedthrough.

Two converters were built and tested. The first was operated for 1100 hours, at a maximum emitter temperature of 2000°K , producing a total of 480 kilowatt-hours, with a peak output of 530 watts, or 7.1 w/cm^2 at a conversion efficiency of 11.5%. The second converter, which exhibited equivalent performance, was tested for 300 hours, after which it was equipped with fuel-emitter thermocouples and encapsulated in the secondary container and thermal insulation. A fission gas collection system with differential pressure transducers, and an in-pile test assembly plate with the required electrical and coolant feedthroughs were also built. Final joining of these subassemblies is to take place at the reactor site.

SECTION 1

INTRODUCTION

This report describes the development of a full-length external-fuel thermionic converter for in-pile testing. The development program includes out-of-pile performance testing of the fully fueled-converter, using rf-induction heating, before its installation in the in-pile test capsule.

An external-fuel converter is cylindrical in shape, and consists of an inner, centrally cooled collector, and an outer emitter surrounded by nuclear fuel. The term "full-length" denotes that the converter is long enough to extend over the full height of the reactor core. Thus, the converter under development is not a scaled-down test device, but a full-scale fuel element of the thermionic reactor, Potential advantages of this design were discussed in earlier reports (1, 2).

The external-fuel converter concept permits a number of different design options, particularly with respect to the fuel composition and shape, and the collector cooling arrangement. The converter described here was developed for the Jet Propulsion Laboratory, and is based on their concept for a thermionic reactor with uninsulated collector cooling as described in an earlier paper (2). The converter is double-ended, with through-flow cooling, and with ceramic seals and emitter and collector power take-offs at both ends. The design uses a revolver-shaped tungsten emitter body, with the central emitter hole surrounded by six peripheral fuel holes loaded with cylindrical UO_2 pellets.

SECTION 2

CONCLUSIONS

The work performed under this program is described in Section 3 through Section 8. The results of that work have led to the following conclusions:

- (1) Fabrication of revolver-shaped tungsten bodies for use as fuel containers in external-fuel thermionic converters is feasible.
- (2) External-fuel revolver fuel elements can be employed as emitter bodies in cylindrical thermionic converters at least as long as eight inches.
- (3) Vacuum-tight joints between tungsten and/or tungsten-alloy components can be reliably achieved by EB-welding with appropriate pre- and post-heating. Hermetic joints between columbium and tungsten can be made by an EB-self-brazing technique. EB-weld joints between columbium components are easy to achieve and highly reliable.
- (4) Fully-fueled external-fuel diodes can be tested out-of-pile by rf-induction heating. Such testing is valuable in permitting adjustment of the external load and cooling arrangements, based on actual operating parameters.
- (5) While arc-cast tungsten can be successfully machined and welded, subsequent grain growth in high-temperature service makes long-term hermeticity of this material questionable. A converter employing an arc-cast tungsten fuel element exhibited considerable grain growth with two grain-boundary leaks in its fuel chamber wall after 1100 hours of operation.
- (6) A thoriated-tungsten fuel-emitter evidenced relatively little grain growth following three hundred hours of out-of-pile testing, and remained leaktight for this period.
- (7) A converter employing a thoriated-tungsten emitter body yielded performance comparable to one using an arc-cast tungsten emitter, at least to 1700°C.

- (8) Converter performance remained stable for the 300-hour test period, despite the presence of 2 wt% thoria in the tungsten emitter. (The thoria may actually serve to enhance the thermionic performance.)
- (9) Eight-inch long fueled cylindrical diodes with small (0.010") interelectrode gaps can withstand extended high-temperature operation and numerous thermal cycles without shorting. This confirms the experience of earlier non-fueled out-of-pile tests.
- (10) In spite of higher ohmic losses in long converters, overall performance was quite good, yielding typical power densities of 5 to 7 watt/cm² at 1700°C emitter temperatures, and conversion efficiencies at 11 to 12%, after the electrical and thermal losses in the emitter leads.
- (11) The high-voltage rf-feedthrough developed in this program permits reliable rf-heating for diode processing and out-of-pile testing in a high-vacuum test chamber. Power transfer of approximately 35 kW was achieved.
- (12) Water-cooling the collector through a gas gap is quite practical, using a single-component (helium) gas with pressure adjustment to control the collector temperature.
- (13) A thin-walled (0.005") large-diameter (1.5-inch OD) nested columbium bellows can reliably be made by EB-welding.
- (14) Although the yield of the high-pressure inert gas autoclaving process used for making the graded columbium-alumina seals was relatively poor (30%), the four seals actually used in the converters proved quite reliable.
- (15) Continuous monitoring of pressure buildup in the fission gas accumulator and the secondary container appears to be feasible, although the radiation hardness of the transducers remains to be verified.

- (16) A double-ended, full-core-length external-fuel thermionic converter can be fabricated without any braze joints in the cesium envelope.
- (17) In future converters, the need for leaktight tungsten or tungsten-alloy welds should be minimized or eliminated.
- (18) In general, an external-fuel thermionic converter for operation in a test reactor is much more difficult to design and build than a similar converter for use in the actual thermionic reactor. This is so primarily because the former converter requires individual collection of fission gases as well as the double containment of the fuel element, its thermocouple leads, and the fission gas collector.
- (19) Although, in contrast to the flashlight converter design, the external-fuel configuration makes possible the direct measurement of the temperature of fuel-emitter body via thermocouples, such measurement leads to considerable complications because of the double-containment requirement.

SECTION 3

DESIGN DESCRIPTION

The in-pile converter design is illustrated by the isometric cutaway view shown in Figure 1 and by the cross-sectional views of Figures 2 and 3. The latter figure also shows the fission gas collection system and the lower half of the test capsule. (In the following discussion superscript numerals refer to figure callouts; references are designated by numerals in parentheses).

3.1 Fuel-Emitter Assembly

The tungsten emitter body¹ has an outer diameter of 1.5 inches, and an 8-inch active length. The 0.5-inch central emitter hole² is surrounded by six 0.4-inch fuel holes³. The revolver¹ has minimum web thicknesses of 0.060 inch between emitter and fuel, 0.040 inch between fuel and the outside, and 0.110 inch between neighboring fuel holes.

With these dimensions, the fuel chambers occupy 42.8% of the converter cross-section. Assuming a reactor core made up of such elements separated by 0.060-inch vacuum gaps, the fuel chambers would occupy 36.0% of the core volume. However, the outer boundary of the converter can be hexagonalized, to permit closer packing and higher fuel volume fractions. For example, with the same thicknesses of webs and vacuum gaps as above, and with the emitter and fuel hole diameters increased to 0.66 and 0.51 inch, respectively, the fuel chambers would occupy 45% of the core volume, as illustrated in Section 9.4.

The converters are loaded with annular cylindrical fuel pellets⁴ of 0.396-inch O.D., 0.200-inch I.D., and 0.51-inch length. The fuel is UO₂ of 92% theoretical density and 9% enrichment. As described in Appendix C, the fuel enrichment is based on the results of a mock-up test in the Battelle Research Reactor, where the in-pile test will be conducted. The design loading per converter is 58 gm of U₂₃₅.

The emitter body contains six thermocouple wells, not shown in these figures, located at various points of the fuel element periphery. Each well is a slanted hole of 0.040-inch diameter, penetrating to a depth of 0.2 inches into the web between fuel chambers⁸. The external-fuel design lends itself to detailed monitoring of the emitter body temperature distribution. For example, during the in-pile test the converter will be located not at the center of the core, but nearer to one of its corners. Thus, the use of diametrically opposed thermocouples on the emitter body will show how much transverse temperature gradient is produced by the existing flux gradient. Another interesting point is that the presence of thermocouples at the top, middle, and bottom of the revolver makes it possible to observe the effect of UO₂ redistribution within the fuel chamber on the axial temperature profile of the emitter.

To aid in venting the released fission gases during the in-pile test, there is a tungsten snorkel tube⁵ at the center of each fuel chamber, extending over the full length of the fuel element; it has 0.040-inch perforations at 0.5-inch intervals, and is welded to a tungsten cover disk⁹ at its upper end. All fuel holes are connect to a common fission gas plenum at the top of the emitter body.

The ends of the emitter body are joined to W-25Re end caps¹⁰. These seal the fuel chambers, except for a single W-25Re vent tube¹¹ of 0.060-inch O.D. and 0.040-inch I.D., which is connected to the upper end cap. Integral with each end cap is a half-inch long emitter lead¹² of 0.050-inch wall thickness. The resultant emitter lead resistance is close to the optimum for this diode.

Each emitter lead is connected to a metal-ceramic seal¹³ and to a high-conductance power take-off flange¹⁴. During in-pile testing, these flanges also serve as part of the secondary containment chamber, together with a 0.020-inch thick cylindrical tungsten sleeve¹⁵ connecting them. To permit rf-induction heating of the emitter body during out-of-pile testing, the secondary containment sleeve¹⁵ is not emplaced until after the completion of that test.

3.2 Collector Assembly

The columbium collector⁶, which is separated from the emitter by a 0.010-inch cesium gap², has a wall thickness of 0.135-inch. To avoid the complexity of operating a liquid metal loop in the test chamber, the collector is water-cooled across a 0.003-inch wide helium gap (cold), and its temperature is varied by adjusting the helium pressure in the sub-atmospheric range.

The ends of the columbium collector¹⁶, beyond the active length of the diode, are expanded to a 0.8-inch outer diameter, to reduce ohmic losses. To center the collector within the emitter hole, each end of the collector is positioned by eight sapphire balls¹⁷ of 0.040-inch diameter, which are seated in hemispherical cavities in the collector at 45° intervals. These sapphire balls are in contact with the cool end of each emitter lead.

In addition, there are three anti-shortening spacers¹⁸ within the active region of the diode: one at the center, and the others one inch from each end. These spacers, which are not shown in Figure 1, consist of split and grooved alumina rings inserted into corresponding collector grooves, where they are retained by W-25Re wire snap-rings. The W-25Re wires extend 0.005-inch beyond the radius of the collector, and do not touch the emitter when the collector is properly centered.

The collector is joined to the metal-ceramic seal at the upper end of the converter. At the lower end, a columbium bellows¹⁹ is interposed between collector and seal, to allow for the differential thermal expansion of the emitter and collector assemblies. The columbium bellows has a nested configuration and contains fourteen convolutions of 1.375-inch O.D., 0.9-inch I.D., and 0.005-inch wall thickness.

The bottom end of the collector is joined to the cesium reservoir²⁰ by a 0.8-inch long cesium leg²¹ of 0.156-inch O.D.; both are of columbium. Heat conduction to the reservoir through the cesium leg is less than 7 watts, but during in-pile testing the reservoir receives an additional input of 40 watts from gamma heating. The reservoir is water-cooled via a split cooling clamp, not shown.

Fine temperature control of the cesium reservoir is effected by means of electrical heaters²² ; two independent heaters are provided, for redundancy. The floor of the reservoir is connected to a columbium tube²³ for diode outgassing, cesium charging, and final pinch-off.

3.3 Cooling and Electrical Arrangement

The collector cooling water flows through a 0.204-inch O.D. by 0.152-inch I.D. stainless steel tube⁷. Circular ridges projecting from this stainless steel tube at 0.5-inch intervals provide for centering within the collector, to maintain a uniform 0.003-inch cold helium gap. Beyond the active length of the diode the helium gap is increased to at least 0.025-inch, to reduce heat transfer and prevent over-cooling the collector ends¹⁶.

The upper end of the coolant tube⁷ is joined to a small, hydroformed, stainless steel bellows²⁴, to permit thermal expansion of the collector relative to the coolant tube. These bellows are joined to a stainless steel top cap²⁵ which seals the helium space, except for a helium port²⁶ to allow adjustment of the gas pressure during diode operation.

Since this is a double-ended diode, there are four converter terminals. These terminals are considered to be the upper and lower emitter power take-off flanges¹⁴ and the upper and lower collector hubs²⁷. Thus, the diode terminal voltage, power output, and efficiency reported later are the values obtained after the electrical and thermal losses in the optimized emitter leads. Any losses beyond these terminals are considered to be merely part of the experimental arrangement, rather than an inherent characteristic of the converter.

The collector cooling water flows through the collector coolant tube⁷ in an upward direction. A typical flow rate is 0.5 gpm and 8.2 ft/sec. The water inlet and outlet tubes²⁸, which are made of copper, simultaneously serve as the high-current collector leads. To avoid overcooling the collector hubs²⁷ below the cesium reservoir temperature, these hubs are connected to the water-cooled copper tubes²⁸ by thermal chokes²⁹.

Similarly, water-cooled copper tubes³⁰ serve to conduct the upper and lower emitter currents. Again, thermal chokes³¹ must be employed to avoid over-cooling the W-Re emitter power take-off flanges¹⁴. Each of these thermal chokes consists of a molybdenum skirt with a rectangular cooling channel³² at its outer end, with each cooling channel connected to water inlet and outlet tubes³⁰ at 180° intervals. The thermal resistance of the emitter heat chokes³¹ is sized so as to maintain the temperature of the power take-off flanges¹⁴ at 600 to 800°C during normal diode operation. Thus, the ceramic seals¹³ and the columbium bellows¹⁹ are lifetested at a temperature which realistically simulates their operating condition in a thermionic reactor.

In addition to their thermal and electrical functions, the molybdenum skirts³¹ also serve two other purposes: they are used for mechanical support⁵² of the converter during out-of-pile and in-pile testing, and they make it possible to maintain the tungsten and tungsten-alloy components of the converter above their ductile-brittle transition temperature during reactor shutdown, by means of an electrical heater³³ (not shown in Figure 1) brazed to the inner surface of each Mo skirt.

3.4 Containment

Nuclear safety rules at the test reactor require that the fuel be triply contained. In addition to the integrity of the sealed fuel chamber, the emitter power take-off flanges¹⁴ and the connecting tungsten sleeve¹⁵ form part of the secondary container; and the 2.75-inch diameter outer wall of the test capsule³⁴, made of 0.057-inch thick stainless steel, serves as the tertiary container.

The secondary containment volume is sealed under vacuum after completion of the out-of-pile testing. The tertiary containment volume, which contains the thermal radiation shielding³⁵ consisting of 50 layers of thoriated tungsten foil, is an active vacuum. During the in-pile test it is pumped by a pair of 350-liter/sec ion pumps, a 7500-liter/sec titanium sublimation pump for intermittent duty, and a liquid-nitrogen cold trap.

As illustrated, there are four 0.125-inch O.D. columbium tubes³⁶ joined to the upper emitter power take-off flange¹⁴. These tubes form part of the secondary containment enclosure. Three of the four are cover tubes for the six emitter thermocouples. The W-25Re and W-3Re thermocouples employ multi-strand wire, and have bare junctions that are knotted rather than spot-welded, to avoid embrittlement. The thermocouple leads are beryllia-insulated in the vicinity of the hot emitter body¹, and are sheathed in four-hole alumina insulators within the columbium cover tubes³⁶. During in-pile testing, the thermocouple cover tubes extend for approximately seven feet above the top of the reactor core, in order to move the required insulating vacuum feedthroughs to a region of lower neutron flux.

3.5 Fission Gas Collection

The fourth of the above columbium tubes³⁷ serves as the secondary container around the W-Re fission gas vent tube¹¹. As illustrated in Figure 3, the vent tube is joined to a fission gas accumulator³⁸, and the cover tube³⁷ is joined to the secondary containment shell³⁹ which surrounds the accumulator. Both connections are made via bellows⁴⁰ to allow for differences in expansion. The fission gas collection system, which is made of stainless steel, is not joined to the converter assembly until after completion of the out-of-pile test and installation of the secondary container¹⁵. Note that there are two separate tubes for sequential vacuum pumpdown and pinch-off, one for the accumulator and fuel volume⁴¹ and one for the secondary containment shell⁴².

The fission gas accumulator³⁸ has a 2-inch diameter and 6-inch length. It is sized so as to develop a maximum pressure of 100 torr after 10,000 hours of operation, assuming complete release of xenon and krypton. There are two differential pressure transducers, one⁴³ to measure the pressure difference between the accumulator and the secondary container, and the other⁴⁴ to measure the difference between the secondary and tertiary containers. Thus, the system is designed not only to monitor the extent of fission gas venting from the fuel element, but also to detect the occurrence of leaks from the fuel element or the fission gas collection system into the secondary container.

The two transducers, which are located 3 feet above the top of the reactor core, are radiation-hardened versions of the LVDT (linear, variable differential transformer) type. As shown in Figure 3, the two pressures whose difference is to be measured are separated by a 2.375-inch diameter diaphragm⁴⁵. This diaphragm is connected to a rod-shaped magnetic core⁴⁶, whose displacement is measured by a set of coaxial transformer coils⁴⁷. The transducers have a theoretical resolution of 0.5 torr.

3.6 In-Pile Test Arrangement

Figure 3 shows the lower end of the in-pile test capsule wall. At the bottom of the capsule is a centering hub⁴⁸ for seating the capsule in the reactor grid plate. Above this hub there are eighteen 1-inch diameter inlet ports⁴⁹ for the forced circulation of the reactor cooling water. Above the reactor core, the 2.75-inch diameter capsule wall³⁴ is expanded to a 6-inch pipe⁵⁰ by means of an eccentric transition section⁵¹.

An overview of the whole test capsule, showing its location in the test reactor, is presented in Figure 4. As can be seen, the top of the previously shown 6-inch diameter pipe is connected to a tee-section, whose top is sealed by a 8.5-inch diameter assembly plate. The converter and the fission gas collection system are suspended from this assembly plate. It contains numerous insulated feedthroughs for the diode and heater leads, water and helium lines, thermocouples and voltage probes. To minimize axial stress, all solid lines are connected via bellows, with flexible high-conductance bypass straps on all current-carrying lines.

Above the assembly plate is an offset 6-inch diameter dry-well, through which the various instrumentation and plumbing lines are brought to the top of the reactor pool. The side port of the tee-section is connected via 8-inch plumbing to the previously described vacuum ion pump system at the top of the reactor bridge.

SECTION 4

CONVERTER FABRICATION

The converter consists of five major subassemblies three of which are illustrated in Figure 5; the emitter assembly, the collector assembly, and the coolant assembly. The fourth subassembly, consisting of the secondary containment sleeve and the thermal radiation shielding, and the fifth, the fission gas collection system, are added after completion of the out-of-pile testing. The columbium components of the collector assembly and the stainless steel parts of the coolant assembly and of the fission gas collection system are all prepared by standard machining techniques. Only the more unusual components of the emitter assembly warrant a more detailed discussion.

4.1 Emitter Body

The first step in making the revolver-shaped emitter body is to EDM (electric-discharge-machine) the central emitter hole in the cylindrical tungsten billet. Brass electrodes and copper-impregnated tungsten electrodes have both been successfully employed in the EDM process. To minimize the danger of radial drift, the 8-inch long hole is machined in two parts; i.e., half way from each end of the tungsten billet. Tubular electrodes are employed, and the central tungsten core drops out when the two holes meet in the middle. If desired, the EDM process would lend itself well to machining blind holes, as well as non-circular holes.

After machining, the surface of the emitter hole is honed. The honing process removes a layer of approximately 0.002-inch, which is important because it is this layer which is most likely to contain surface microcracks as the result of the electric discharge process.

After finishing the emitter hole, the ends of the tungsten billet are ground to provide the inner and outer lips required to join it to the end caps. The six peripheral fuel holes are then electric-discharge-machined and honed, in the same manner as the central emitter hole. Finally, the outer surface of the revolver is

ground to size, and the six slanted thermocouple walls are introduced by the EDM technique; two of the six are faintly visible in the emitter photograph in Figure 5. The last step is to electropolish the outer surface and end faces of the emitter body. Wherever possible, this process is used as the final step on all tungsten components, because of its sensitivity in revealing any surface defects.

A total of six tungsten revolvers were prepared by the above technique, and it was demonstrated that tool drift can be sufficiently well-controlled so that hole alignment and web thicknesses can be maintained within satisfactory tolerance limits.

The first three emitter bodies had been prepared from sintered and forged powder-metallurgy tungsten billets. Although two of the resultant revolver bodies appeared to be leaktight after machining, subsequent electropolishing of their outer surface revealed the existence of cracks, possibly the result of improper fixturing, which precluded their use in diodes. However, one of these tungsten revolvers was employed for the nuclear mock-up test in the Battelle Research Reactor, which was needed to determine the required fuel enrichment.

The next two emitter bodies were prepared from arc-cast and hot-extruded tungsten billets. Both were leaktight and showed no surface defects after electropolishing. However, one of the units developed two leaks (not near the weld joints) during subsequent thermal processing. The cause of these defects has not been defined. The second of the arc-cast emitter bodies was successfully fabricated into the first of the two diodes built and tested under this program.

Finally, the sixth emitter body was prepared from a thoriated tungsten billet formed by powder-metallurgy techniques and extrusion. The material used (GE-17) contained 2 wt% thoria. The resultant emitter body, which was machined without difficulty by the same techniques as the all-tungsten revolvers, was then used to fabricate the second diode, described in Section 7.

4.2 Emitter Assembly

The 9%-enriched UO_2 fuel pellets were cold-pressed to 70% theoretical density, hydrogen-sintered to 92% density, and finish-ground to the desired dimensions. The oxygen-to-uranium ratio was 2.005, and the impurity content was below the measurable limits for all species tested. The tungsten snorkel tubes were prepared by chemical vapor deposition from WF_6 , and the perforations required for venting the fission gases were introduced by electric-discharge machining.

The rest of the emitter assembly consists of an upper and lower sub-assembly. As illustrated in Figure 5, each of these subassemblies contains an end cap, a graded metal-ceramic seal, a power take-off flange, and a thermal choke with water coolant connections. In addition, the upper subassembly contains the vent tube and four cover tubes, and the lower assembly includes the columbium bellows.

The end caps and the power take-off flanges were prepared from powder-metallurgy tungsten-25% rhenium stock. They were roughed out by electric-discharge-machining, and finished by grinding and electropolishing, with intermediate annealing steps. The 0.040-inch I.D. vent tube, which is joined to the upper end cap, was made by chemical vapor deposition of W-25Re.

The metal-ceramic seals were prepared by autoclaving graded layers of columbium and alumina powders encapsulated in a Cb-1Zr jacket. At the central plane of each assembly is a 0.060-inch thick alumina (Lucalox) wafer. On each side of this wafer are several layers of mixed powders, with compositions gradating from ceramic-rich to metal-rich. The assembly is consolidated by hot isostatic compaction at approximately 1650°C and 10,000 psi. After autoclaving, the seal is finished by machining, ultrasonic drilling, and diamond grinding. Before use in a diode, each seal is acceptance-tested by leak checking after 25 thermal cycles to 1000°C.

The emitter heat chokes, which are identified as "emitter-terminals" in Figure 5, are made of molybdenum, with water inlet and outlet ports of columbium. The photograph also shows the previously mentioned electrical heaters brazed to their inner surface. Nichrome heaters with magnesia insulation and inconel sheathing were used.

Finally, the emitter expansion bellows consists of fourteen nested convolutions, joined by EB (electron-beam) welding. Each convolution consists of two diaphragm rings, which are stamped and shaped from 0.005-inch columbium foil. Individual convolutions are first prepared by EB-welding pairs of diaphragm rings along their inner edges, while their outer edges are separated by a sacrificial molybdenum spacer ring. These convolutions are then joined by EB-welding along their outer edges, after which the molybdenum spacers are chemically removed by dissolution in a mixture of concentrated nitric and sulfuric acids.

4.3 Joints

All emitter assembly components were joined by electron-beam welding. The most difficult joints to work out were those between tungsten and tungsten-rhenium components. These include joining the W-Re end caps to the W emitter body, to the W-Re power take-off flanges, and to the W-Re vent tube.

Our welding experience with these joints is described in detail in Appendix F. As explained there, when the arc-cast tungsten revolver was first welded to the W-Re end cap, it developed leaks; not at the weld joints but about 0.25-inch away, at a region where the tungsten revolver had been preheated by a defocused electron beam. However, once satisfactory methods of pre-heating and post-heating these components by means of a radiant furnace within the welding chamber had been worked out, it was found that joints between W and W-Re could be EB-welded with very high reliability. After welding, each of these joints was stress-relieved by vacuum-annealing for one hour at 1300°C.

To salvage the defective revolver discussed above, a half-inch long section containing the leaky region was cut off, and the cut end remachined. This shortened revolver was then incorporated in Converter No. 1, using a specially

machined W-Re end cap transition. As a result, the active length of this diode is only 7.5 inches, instead of the 8-inch design value. Converter No. 2, which incorporated the thoriated tungsten emitter body, was welded without difficulty and has the normal 8-inch design length.

Contrary to expectations, pre-heating was also found to be necessary in joining the end caps to the power take-off flange and to the vent tube, joints in which both components consisted of nominally ductile W-Re alloys.

Another class of joints is that between tungsten-rhenium and columbium. In making these joints, which include the end-cap-to-seal and the top-flange-to-cover-tubes, it was found that weld joints which depended on the formation of an alloy between W-Re and Cb tended to be unreliable. However, by shifting the electron beam to the columbium side of the joint, to avoid melting the W-Re, leaktight joints could be made with good reliability, provided pre- and post-heating was applied. Such joints are not really EB-welds; they should more accurately be called "electron-beam selfbrazes", since in effect the melted part of the columbium acts as a braze alloy for the unmelted part of the component.

The joints between the W-Re power-take-off flanges and the Mo heat chokes were EB-welded without difficulty. However, these joints need not be leaktight, since they only serve mechanical and conductive functions.

All joints in the converter between columbium and columbium were made by electron-beam welding, with good reliability. Thus, all joints in the cesium envelope are EB-welded, except the metal-ceramic seals which are pressure-bonded. After EB-welding the power take-off flanges to the end caps (emitter leads), backbrazes of a palladium-nickel-silver alloy (1052°C) were added to these joints, for enhanced thermal and electrical conductance.

Finally, all joints between stainless steel components were also made by EB-welding. Brazing was only used for joining dissimilar metals, such as columbium to stainless steel, and stainless steel to copper. Thus, the only brazes in the converter are the joints at the top and bottom of the diode between

the collector cooling assembly and the collector heat chokes. These were rf-heated vacuum brazes, again using a palladium-nickel-silver alloy (1052°C).

4.4 Assembly Sequence

The converter assembly sequence is illustrated in Figure 5. Individual components are first joined to form the upper and lower emitter subassemblies. Next, the lower subassembly is joined to the emitter body, the inner lips by means of an axial weld, and the outer lips by a radial weld. The emitter body is then loaded with fuel and snorkels, and the fueled assembly is vacuum-fired at the emitter operating temperature, after which it is sealed by joining it to the upper subassembly. The finished fuel element can be leak-checked through the vent tube.

Since the diameter of the collector ends exceeds that of the emitter hole, the collector assembly must be fabricated in two parts. After insertion of the spacer rings and sapphire balls, the lower part of the collector assembly, which includes the cesium reservoir and the diode pump-down leg, is inserted into the emitter hole, and the collector extension with sapphire balls in place is inserted into the top of the emitter assembly. Union between the two collector halves is effected by means of an axial EB-weld at the upper collector well. Two additional welds seal the diode.

Finally, the stainless steel coolant assembly is inserted into the top of the collector hole, and the helium space is sealed by means of the two vacuum brazes. The right photograph in Figure 5 shows the completed diode, ready for outgassing and charging with cesium.

SECTION 5

DIODE PROCESSING AND TEST ARRANGEMENT

Converter outgassing takes place in the same vacuum chamber, and with the same rf-induction heating arrangement, as subsequent out-of-pile testing. RF-induction heating had also been employed in previously reported (1) out-of-pile testing of unfueled diodes. In that test program, the converter was located inside a water-jacketed quartz vacuum chamber, and the rf-induction coil was located outside the vacuum chamber, as shown in Figure 6. Such an arrangement is very convenient, because operation of the induction coil in air eliminates the need for rf-vacuum feedthroughs, and also permits easy adjustment of the position and spacing of the heating coil during the course of a test.

However, there were also some serious disadvantages to this mode of operation. Since the ends of the quartz tube were sealed by organic O-rings, the resultant vacuum in the test chamber was relatively poor. Moreover, since the double-ended diode needed high-conductance current leads and instrumentation feedthroughs at both ends of the test chamber, it was a rather cumbersome procedure to install the diode for testing or to open the chamber for any minor adjustments (e. g., of the thermocouples).

For these reasons, it was decided that the present program would employ a more conventional all-metal belljar using a crushable copper gasket, metal-ceramic vacuum feedthroughs, and with the rf-induction coil located within the test chamber. This would make possible a much better vacuum, and greatly simplify the test installation.

5.1 RF Feedthrough

To achieve these advantages, however, it was first necessary to develop a reliable high-vacuum high-power rf-feedthrough, since the required unit does not appear to be commercially available. As shown in Figure 7, the rf-feedthrough that evolved is a co-axial unit, with a brazed metal-ceramic seal. The unit is sealed to the test chamber baseplate by means of copper-gasketed knife edges. A co-axial rather than parallel feedthrough design is used, to avoid excessive induction heating of the test chamber wall.

In addition to the ceramic seal at the feedthrough's outer end, there is a slip-fitted ceramic spacer at its inner end. This is to provide centering for the high-voltage copper tube, to minimize the danger of breakdown. However, with the spacer design shown in Figure 7, some difficulty was encountered with rf-breakdown at approximately 7 kilovolts, due to surface conduction along the inner end-face of the ceramic spacer. The radial arc resulted in melt-through of the central copper tube at that point, with consequent release of water into the test chamber.

The problem was corrected by modifying the spacer design to provide a considerably larger conduction path. The coaxial feedthrough with the modified ceramic spacer was then successfully tested to the maximum 12-kilovolt output of the rf-power supply, and has since operated without difficulties for hundreds of hours at about 8 kilovolts and 35 kVA.

5.2 Converter Processing

The general arrangement for processing and out-of-pile testing the converter is illustrated in Figures 8, 9, and 10. Figure 8 shows a close-up view. Figure 9 illustrates the diode outgassing and cesium charging procedure, and Figure 10 presents an overview of the test arrangement.

The ends of the converter⁵³ can be seen projecting from the rf-induction coil⁵⁴. The induction coil is connected to the previously shown coaxial feedthrough⁵⁵, whose outer ends are connected to a 75-kw, 450 kHz rf-power supply⁵⁶. Water-cooled copper tubes act as high-conductance current leads to the diode, two tubes to the collector⁵⁷ and four for the emitter⁵⁸. These tubes enter the test chamber through ceramic feedthroughs⁵⁹. The 18-inch diameter base-plate⁶⁰ and the 30-inch high belljar⁶¹ of the stainless steel test chamber are both water cooled. During diode outgassing and out-of-pile testing, the fission gas vent tube is open to the vacuum chamber.

To reduce confusion, the photographs were taken before the installation of the thermocouples and voltage probes. W-3Re and W-25Re thermocouples were used at the emitter body, and chromel-alumel thermocouples everywhere else,

including the emitter power take-off flanges¹⁴, the collector ends²⁷, and the cesium reservoir²⁰.

Figure 8 shows the cesium reservoir⁶² and its heater⁶³ before installation of the reservoir cooling clamp. Emerging from the bottom of the reservoir is an S-shaped copper tube⁶⁴ which passes through a feedthrough at the bottom of the baseplate. This S-tube is used for outgassing the diode and subsequently charging it with cesium. As shown in Figure 9, after this tube⁶⁴ emerges from the vacuum chamber it is connected to a 0.75-inch diameter extension⁶⁵, which contains the glass ampoules with the cesium charge. Below this point, the tube is connected to a 15-liter/sec ion pump⁶⁶ used for outgassing the inside of the diode. The test chamber itself is evacuated by a separate 400-liter/sec ion pump⁶⁷.

During outgassing, the emitter body was heated to a maximum of 1900°C, and the S-tube⁶⁴ and cesium ampoule container⁶⁵ were resistively heated to 200°C. All parts of the converter were at or above their normal operating temperatures. To ensure this, a 500-ampere alternating current was passed between the upper and lower collector leads²⁸, to duplicate the ohmic heating in the collector heat chokes²⁹ during diode operation.

Heating was continued for several days, to reduce the pressure at the diode ion pump⁶⁶ to 10^{-8} torr, at which point the ampoule container⁶⁵ was squeezed to crush the glass ampoules. After some additional pumping to remove any gas released from the cesium ampoules, the diode pumpdown leg⁶⁸ was pinched off. The converter was then cooled and removed from the test chamber, and the liquid cesium was decanted into the S-tube, with care taken to avoid transfer of crushed glass particles. After pinching off the ampoule container⁶⁸ with the crushed glass, the liquid cesium was transferred from the S-tube⁶⁴ into the diode. Once this transfer was verified by x-ray observation, the diode was sealed by pinching off the columbium tube just below the cesium reservoir.

5.3 Out-Of-Pile Installation

After processing, the converter was again installed in the test chamber and instrumented for testing. In addition to the thermocouples used during the

outgassing, voltage probes were attached to the upper and lower collector hubs²⁷ and emitter power take-off flanges¹⁴, as well as to the six current leads at the points where these emerge from the test chamber⁷⁰. These six points were also provided with thermometers with a resolution of 0.1°C. This instrumentation is used to measure the temperature rise of the three coolant streams and the ohmic losses in the diode leads within the test chamber, quantities which are needed later to compute the converter's efficiency.

Figure 10 presents an overview of the out-of-pile test arrangement. It shows the test chamber⁶¹ and its ion pump⁶⁷, the 75-kw rf-power supply⁵⁶, the heater controls⁷¹ and coolant flow meters⁷², the helium pressure regulating system⁷³ with its own vacuum pump⁷⁴ for subatmospheric operation, and a balancing potentiometer for thermocouple readout⁷⁵.

The temperature of the emitter body could be measured not only by thermocouples but also by a micro-optical pyrometer⁷⁶ through a window⁷⁷ in the vacuum belljar. This window was kept clean by means of a mask, that could be temporarily moved aside by a magnetically coupled actuator⁷⁸. All pyrometric readings were corrected, with corrections based on the emissivity of clean tungsten.

5.4 Emitter Temperature

It should be emphasized that the "emitter temperature" measured, whether by pyrometer or thermocouples, is really the temperature at the outside of the emitter body and not at the actual emitter surface. The temperature difference between these points can be quite significant, particularly during the rf-heated out-of-pile test, where most of the heat is generated near the outside of the emitter body.

At a radio frequency of 450 kilohertz, the skin depth or 1/e attenuation distance in 1700°C tungsten is approximately 0.026 inch. Figure 11 presents a typical computed temperature distribution in a transverse cross-section of the emitter body, before significant fuel redistribution has taken place. As can be

seen, the average emitter temperature is more than 100°C below that measured at outside of the emitter body.

By contrast, during in-pile testing most of the heat is generated by fissions within the fuel chambers. Under these conditions, the temperature difference between the inside and outside of the revolver is typically only 50°C, as illustrated by the calculated temperature map presented in Figure 12. This calculation took account of gamma heating as well as fissions. In a thermal test reactor, gamma heating of the massive tungsten revolver contributes about 25 percent of the total heat generated in the fueled emitter body. Note that, at most, there is roughly a 70°C temperature drop within the fuel, resulting in a maximum UO₂ temperature of less than 1900°C, far below its melting point.

The calculation illustrated in Figure 12 had an additional purpose: to estimate the effect of locating the converter near the outside of the reactor, with a consequent transverse flux gradient. A 20% fission density difference between opposite fuel chambers was measured in a mock-up experiment. As can be seen, this difference leads to a transverse temperature difference of 70°C which would cause only negligible bowing. Moreover, it can be seen that the 20% fission density variation produces a peripheral emitter temperature variation of only 10°C.

5.5 Load Control

Figure 10 also shows the voltage and current meters⁷⁹, an xy-recorder⁸⁰ for tracing the current-voltage characteristics of the diode, and the diode current leads⁸¹.

Early in the program, considerable effort had been devoted to devising a remotely adjustable power load, to be located within the test chamber, directly at the upper and lower ends of the converter. Such an arrangement would be very desirable, because of the very high currents (~ 1000 amperes) generated by this diode. Even with water-cooled high-conductance copper leads, delivering such currents to an externally located adjustable load consumes more power

than that generated by the diode. Ohmic losses in the leads are particularly severe in the case of the in-pile test, where the current must be delivered from the core to the top of the reactor pool. To overcome these lead losses requires a high-current dc-power supply, which could be eliminated if a remotely adjustable load were available.

The load design which was investigated is illustrated in Figure 13 for the lower end of the converter. The emitter and collector power take-off flanges⁸² are connected by a flexible molybdenum strap⁸³ in series with a 0.25-inch diameter columbium chamber⁸⁴ partially filled with sodium. This chamber, which acts as a variable-resistance load, is connected to a liquid metal reservoir⁸⁵. The liquid metal level in the load is adjusted by remote control of the inert gas pressure⁸⁶ above the sodium reservoir. To decrease the sensitivity of the liquid level to changes in the inert gas pressure or the sodium vapor pressure, inert gas at a fairly high pressure (~ 1 atm) was trapped above the liquid metal in the load chamber⁸⁷.

Even with that precaution, however, this load control system proved to be inherently unstable. To understand the cause of the instability, suppose the partially filled load chamber under equilibrium operation were to experience, for some reason, a small drop in the liquid level. This would raise the resistance of the load and increase the ohmic heating. The resultant temperature rise expands the trapped inert gas, forcing more of the liquid metal out of the load chamber. This continues until the chamber is completely dry. Conversely, an initial rise in the liquid level would lead to the reverse condition, tending to fill the load chamber. Thus, there was a strong tendency for the load to switch to either its maximum or minimum resistance condition; intermediate levels were very difficult to maintain.

The above stability problem may be solvable by resorting to higher gas pressures, or by more effective cooling of the load tube. The latter remedy, however, is limited because of the need to maintain the desired high temperatures at the collector hubs and the emitter flanges. In any event, it was decided to

abandon the remotely adjustable load concept, and bring the diode current out of the vacuum chamber to a more conventional external power supply.

A high-current dc power supply was therefore built. It employs a 5-kw Y-to-Y-connected variable autotransformer, to vary the ac input voltage delivered to a three-phase full-wave silicon rectifier bank. This rectifier bank is water cooled, to permit a maximum current capability of 1200 amperes.

The positive output side of the full-wave rectifier stack is divided into two parallel branches, which are connected to the two collector ends of the converter. Calibrated shunts are used to measure the individual current. Each side of the rectifier has a single-section-inductance input LC filter, where L is about 3 microhenries and C is 0.46 farads.

At a typical operating point, with the converter producing 800 amperes at 0.6 volt, the power supply delivered 1.8 volts. Thus, a total of 2.4 volts was consumed in overcoming the various lead resistances in out-of-pile testing.

If desired, the in-pile test could be operated without an external power supply, by installing a fixed load resistance (e.g., 0.001-ohm) at each end of the converter. However, such an arrangement was rejected because it would sacrifice the ability of adjusting the load resistance during the in-pile test, to compensate for the possible deviation of the fission density from its predicted value.

SECTION 6

OUT-OF-PILE TEST OF CONVERTER NO. 1

6.1 Test Conditions

All performance measurements were made under steady-state d. c. condition, since sweep measurements- unless made at very slow sweep rates - would tend to be affected by inductive interactions between the high-current diode leads.

During early measurements, there was appreciable imbalance in the current leads between the upper and lower diode terminals and the external power supply. Since this is a double-ended diode, this imbalance resulted in significant differences between the two output voltages and among the four output currents.

Under these conditions, there is some ambiguity as to the correct way of computing the total power output of the converter. The most rigorous method is to subtract the power delivered by the external power supply from the electrical power consumed in overcoming the resistance of the current leads. However, it was found that even with badly unbalanced voltages and currents, the rigorously computed diode power can be matched within a fraction of a percent simply by multiplying the total diode current by the arithmetic average of the two terminal voltages. In any event, the current-lead imbalance mentioned above was later corrected by changing the diameter of some of the copper lead tubes.

A typical current-voltage characteristic of this converter is shown by the solid curve in Figure 14. This was obtained by stepwise variation of the dc power supply output voltage, while maintaining a constant setting of the rf-power supply. At each step, the collector temperature (helium pressure) and reservoir temperature were reoptimized, and the diode was allowed to equilibrate.

Figure 14 also shows an illustrative operating point, at an emitter body temperature of 1940°K, a diode current of 735 amperes or 9.8 amp/cm^2 ,

and a terminal voltage of 0.72 after the emitter lead losses. This corresponds to a power output of 530 watts, or a power density of 7.1 w/cm^2 for the 75-cm^2 emitter.

6.2 Heat Balance and Efficiency

As indicated earlier, the converter efficiency and the thermal power supplied to the emitter are computed by applying an energy balance to the diode and the current leads within the test chamber. For example, for the illustrative operating point depicted in Figure 14, the collector cooling water flowed at a rate of 0.550 gpm and experienced a temperature rise of 25.6°C between the inlet and outlet points at the test chamber feedthroughs. This corresponds to a total heat input of 3717 watts to the collector coolant within the test chamber. From this we must subtract 259 watts, the ohmic heating at the upper collector heat choke and the upper collector lead within the test chamber; and 266 watts, the analogous ohmic loss at the bottom of the collector. Therefore, the true heat loss from collector to coolant, which includes radiation, electron heating, ohmic losses within the collector, and thermal conduction across the cesium gap, is 3192 watts. Note that this value includes diode end losses, i. e., thermal conduction through the ceramic seals.

Similarly, the upper and lower emitter lead coolant streams picked up 636 and 554 watts, respectively, within the test chamber. Subtracting the ohmic heat generation in the emitter heat choke and the emitter test leads, we obtain heat loss rates of 464 and 369 watts from the upper and lower emitter power take-off flanges. This represents the rate at which heat is transferred, by conduction and radiation, from the ends of the emitter body to the power take-off flanges.

Thus, the emitter heating rate, which is the actual rf-induced heating rate less the radiative heat loss from the uninsulated outer surface of the emitter body, consists of four terms: the 3192 watts lost to the collector, the 464 and 369 watts lost to the upper and lower emitter leads, and the 530 watts transformed into electrical energy, making a total of 4555 watts.

The corresponding conversion efficiency is $530/4555 = 11.6\%$. This does not include the effect of extraneous losses, such as electrical losses in the rf-power supply and induction coil, thermal radiation from the outside of the emitter body, and ohmic losses in passing the diode current through the heat chokes and bringing it to the outside of the vacuum test chamber. These losses are merely the result of the particular test arrangement used, and would not be present in a properly insulated thermionic reactor. The efficiency quoted does include all those losses that are an inherent characteristic of the converter, such as ohmic losses within each electrode, electrical and thermal losses in the emitter leads, and thermal losses through the ceramic seals.

6.3 Comparison with Predicted Performance

Finally, it is of interest to compare the measured converter performance with that predicted by theoretical calculations. This comparison is presented in Figure 15. Predicted current voltage characteristics (dotted curves) are shown both for constant thermal power and for constant maximum emitter temperature.

The method of computing the predicted performance of the converter was described in some detail in an earlier report (3). In essence, each point on the predicted performance curves represents the simultaneous solution of two Laplacian equations, to determine the axial variation of the emitter temperature, inter-electrode potential, current and power densities, and emitter heat flux. The computations employ performance data generated by the SIMCON analysis (4). If desired, our converter analysis program can also calculate the location and shape of the isothermal cavity after UO_2 redistribution in the fuel chamber.

Inspection of Figure 15 shows that the slope of the measure performance curve is intermediate between those of the predicted constant-emitter-temperature curves and the constant-thermal-power curves, but closer to the slope of the latter. This is precisely as it should be. Although the measured performance curve was obtained at constant rf-induction power, the emitter heat flux was not exactly constant. At lower current densities there is less electron

cooling, the emitter temperature goes up, more heat is lost by radiation from the outer surface, and the emitter heat flux drops. Therefore, with constant thermal input, a converter would be expected to have a steeper I-V characteristic without thermal insulation than with exterior insulation.

Comparison of the measured illustrative operating point in Figure 15 with the predicted performance curves reveals two discrepancies: For a 4500-watt heat input, the measured power output is significantly less than predicted, i. e., the conversion efficiency is lower. On the other hand, for the given emitter temperature, the measured output is appreciably above prediction; particularly since the actual emitter temperature may have been as much as 100°C lower than the 1940°K measured on the outside of the emitter body, as illustrated earlier in Figure 11.

The reasons for the second discrepancy are not clear. The first one, the seemingly low conversion efficiency, could be due to a combination of factors: First, the SIMCON (4) performance analysis may simply be over-optimistic, particularly, in estimating the radiative heat loss from emitter to collector. Second, the inferred measurement of the converter heat rejection rate may be overly conservative, since it neglects any radiative heat transfer from the outside of the uninsulated hot emitter body to the three coolant lines which go to the top of the diode. As a result, the net heat input to the converter may be several hundred watts lower than the inferred value of 4555 watts. And, third, thermal end losses may be significantly higher for a water-cooled converter than for liquid-metal-cooled devices, because of radiation, helium conduction and natural convection from the collector extensions to the cold water.

6.4 Test Operation

Converter No. 1 was subjected to an extended qualification test. During the initial period of this out-of-pile test, the diode experienced numerous startups and shutdowns, primarily because of malfunctions of various peripheral items. We have already mentioned the initial difficulties with the rf vacuum feedthrough, which were eliminated by modifying the design of the ceramic spacer bushing.

Another difficulty encountered was the development of small leaks between the helium line and the vacuum test chamber. These were eliminated by using only brazed connections in the helium line within the test chamber; compression fittings are satisfactory for water lines, but tend to relax at elevated temperatures.

Other peripheral malfunctions causing occasional test interruptions included failure of the cesium reservoir heater, which was easily replaced, and automatic shutdown of the rf-power supply. The latter tended to occur on humid days, when condensation of atmospheric moisture on the water-cooled lines inside the rf-unit resulted in high-voltage arcing. This problem was eliminated by cooling the rf-supply with a recirculating water system, operating above the atmospheric dew point. However, the converter itself was still cooled with fresh water at house pressure, because of the possible failure of the recirculating pump. Although such failure would automatically shutdown the rf-power supply, the heat retained in the massive high-temperature emitter body would probably melt the stainless steel cooling assembly if the water flow were stopped.

No difficulties at all were encountered with the nested columbium bellows, which contain thirty EB-welds and are exposed to high-temperature cesium vapor; but, ironically, we did have problems with the standard-production hydroformed stainless steel bellows, which are only exposed to cold water and helium. These problems were probably due to manufacturing defects. After 400 hours of out-of-pile operations, the converter test had to be interrupted because of a very small bellows leak, permitting cooling water to enter the helium space. The defective stainless steel bellows were replaced, and the out-of-pile test continued. After 1100 hours of operation, and a total energy production of 480 kilowatt-hours, the qualification test was stopped and Converter No. 1 removed from the test chamber. The dimensions of the fueled emitter body were unchanged. The arc-cast tungsten appeared very clean, but its typical grain size had grown to approximately 1-to-2 mm during the out-of-pile test.

6.5 Fission Gas Vent

As described in Section 3.5, the fuel chamber of the converter is vented via a chemically vapor-deposited W-Re tube¹¹ welded to the underside of the W-Re fuel top cap¹⁰. This tube has a very large length-to-diameter ratio (4 inch/0.060 inch) and, because of grain growth, is undoubtedly embrittled in the vicinity of the weld joint. While the middle 2.5 inches of the vent tube is surrounded by 0.085 inch I.D. cover tube, there was no provision for lateral support in the case of Converter No. 1.

Although not noticed at the time it happened, it was later found that the W-Re tube had broken off immediately above the weld joint, well within the hole in the fuel chamber top cap¹⁰. Presumably, this occurred because of either inadvertent jostling or excessive vibration. To minimize this danger in Converter No. 2, a lateral support sleeve was added, not to be removed until completion of the out-of-pile test and encapsulation in the secondary container.

To repair Converter No. 1, it was decided to vacuum braze a new columbium vent tube to the fuel top cap, using a columbium-vanadium eutectic braze alloy (60 wt % V, 1810°C melting point). In a preliminary brazing test with identical components, a leaktight seal was obtained on the first try. However, repeated brazing attempts on the actual converter failed to establish a leaktight joint, possibly because of contamination (UO₂) at the joint interface. The problem was magnified by the inaccessible location of the joint, as shown in Figure 1.

It was therefore decided to remove the vent tube by electron beam melting and to drill out the top cap hole in order to obtain a clean surface. The latter step, which was carried out at Battelle Columbus Laboratories (BCL), required the use of a 0.060"-diameter drill long enough to pass through the vent cover tube³⁷. To prevent buckling of the drill bit, lateral support was provided between the upper emitter flange¹⁴ and the fuel top cap¹⁰.

After the fuel chamber vent hole had been drilled out, the converter was returned to Fairchild for brazing in a new W-Re vent tube¹¹, using a

platinum braze ring over a molybdenum bridge ring prepared at BCL. Since the braze ring was not in direct thermal contact with the W-Re end cap¹⁰, the latter had to be heated above 2000°C before melting took place.

6.6 Fuel Body Leak

Only after the new vent tube had been brazed in place was it again possible to check the leaktightness of the fuel chamber. The check revealed that, sometime after converter fabrication, a leak had developed between one of the six fuel chambers³ and the outside of the emitter body¹. It could not be determined whether this had occurred during the 1100-hour out-of-pile test or during one of the subsequent high-temperature braze operations.

The leak was large enough for direct observation of argon bubbles through a pool of alcohol. Thus, its location (approximately 2.5 inches from the lower end of the emitter body) could be precisely defined and examined under a microscope. This examination revealed two distinct leaks, located near each other. One of these is shown in the photograph in Figure 16, taken with the incident light beam coming from the top of the picture, at a very low angle. As can be seen, several of the large grains on the outer surface of the tungsten revolver have been lifted up, out of that surface. The leak occurred at the indicated point on a dislocated grain boundary. There is no evidence of any intra-granular cracks.

While the work carried out under this program does not provide an adequate basis for forming generalized conclusions, the results obtained cast doubt on the ability of arc-cast tungsten to maintain hermeticity under emitter operating conditions. Although it may be possible to seal the above fuel chamber leaks, e. g. , by means of a chemically vapor deposited tungsten seal coat, it was decided instead to ship Converter No. 1 to JPL for further out-of-pile operation, and to substitute Converter No. 2 for the in-pile test.

SECTION 7

CONVERTER NUMBER 2

7.1 Description

The second converter built under this program is shown in Figure 17. It was essentially identical to the first, except for the following differences:

- a. The emitter body¹ was machined from tungsten containing 2 wt% thoria, instead of pure tungsten. The raw billet was produced by powder metallurgy, instead of the arc-cast billet used in the case of Diode No. 1.
- b. The secondary container¹⁵ consisted of rolled W-25Re half-sleeves, joined by two electron-beam seam welds, in contrast to the chemically vapor-deposited tungsten sleeve prepared for Diode No. 1.
- c. The vent tube¹¹ was protected by a temporary lateral support, to prevent accidental breakage during converter assembly, processing, and out-of-pile testing.
- d. The active diode length is at its 8-inch design value compared to the shortened 7.5-inch length of Diode No. 1.

7.2 Discussion

The material choice for the emitter body of Diode No. 2 was influenced by the initial difficulties in machining and welding the arc-cast tungsten revolvers, as described earlier. The use of thoriated tungsten offered the prospect of better machinability, and of less grain growth and higher creep strength at high temperatures. It did, however, introduce the danger of thermionic performance instability as the result of thoria decomposition. This possibility is discussed in Section 7.4.

As for the secondary container¹⁵, a seam-welded W-25Re sleeve had originally been prepared for Diode No. 1. However, when that diode was shortened by 0.5 inch, it was decided to use this full-length sleeve for Diode No. 2, and prepare a shortened all-tungsten sleeve for Diode No. 1. The tungsten sleeve was made in one piece, by the hydrogen reduction of tungsten hexafluoride vapor. Although the tungsten-rhenium alloy would be preferable because of its lower ductile-to-brittle transition temperature, fabrication of the first containment sleeve had proved this approach to be very difficult and costly. Moreover, the use of a CVD tungsten sleeve eliminates the two potentially unreliable seam welds.

The need for a protective lateral support sleeve to avoid accidental breakage of the W-Re vent tube¹¹ has been explained previously. This support sleeve was anchored to the relatively sturdy 0.125-inch diameter columbium cover tube³⁷ which surrounds the fragile vent tube. Except when it was moved aside to permit leakchecking the fuel chamber, the protective sleeve completely enveloped the vent tube.

7.3 Fabrication and Processing

As expected, the thoriaated tungsten proved to be significantly easier to machine (EDM) than the arc-cast tungsten used earlier. However, some difficulty was encountered in EB-welding the emitter body ends to their respective end caps. Two of the four weld joints had to be rewelded, one repeatedly, before leaktightness was achieved. Except for these delays, fabrication and processing of Diode No. 2 proceeded quite smoothly, without any of the problems initially encountered with Diode No. 1.

7.4 Out-Of-Pile Test

The electrically heated qualification test of Converter No. 2 also was carried out without incidents or difficulties. Because of budgetary constraints, the out-of-pile test was stopped after only 300 hours, to prepare the diode for in-pile operation.

Of major concern had been the effect of the thoria additive on the thermionic performance of the emitter. Thoriated tungsten cathodes have, of course, been extensively employed to increase electron emission in vacuum tubes. By activating such cathodes at very high temperatures (e. g. , 2200°C) thoria is decomposed, and the resultant coating of free thorium on the emitter surface lowers its work function.

In a high-pressure cesium diode the effect of free thorium would be deleterious, by raising the cesium pressure required to achieve a given emitter work function. The question arises whether, even without the high-temperature activation step, a significant surface coating of free thorium would form after extended diode operation. While the duration of this out-of-pile test was too short to permit any long-term predictions, at least over this operating period (300 hours) there was no significant change in performance.

Although it had been intended to limit the emitter temperature to avoid thoria decomposition, parts of the emitter body operated at temperatures much higher than planned. This was the result of a deliberately uneven spacing of the rf-induction coil⁵⁴ used for heating the emitter body. With a uniformly spaced induction coil, fringing of the magnetic field results in some temperature drop-off near the ends of the heated body. In order to minimize this effect and achieve a more uniform axial temperature profile, the coil used for heating Diode No. 2 was very densely bunched near the ends of the emitter, with almost no turns in its middle third.

Unfortunately, this stratagem was overdone. During most of this test, the middle half of the emitter body operated at an outer-surface temperature of 1600°C, corresponding to a pyrometer reading of ~1475°C before emissivity correction. But the two regions approximately 2 inches from each end of the emitter body, where the induction coil was most densely wound, gave pyrometer readings as much as 200°C higher. It is difficult to say how much of this difference in readings really represented a higher temperature and how much of it was merely the result of internal reflections from the densely packed induction coil, creating a higher effective emissivity.

Thus, while most of the emitter body's outer surface was at 1600°C, part of it was probably above 1700°C. On the other hand, it should be remembered that the temperature of the emitter surface is about 100°C below that of the outside, as illustrated in Figure 11.

7.5 Test Results

Unlike the first converter, the second unit was not subjected to parametric performance mapping, because of time limitations. A favorable operating point, not necessarily optimum, was chosen at the beginning of the test, and the rf-power setting, reservoir temperature, helium pressure and load impedance remained fixed throughout the first half of the test. Typically, the converter yielded an output of 400 watts (650 amperes at 0.6 volt), corresponding to an emitter power density of $\sim 5 \text{ watt/cm}^2$.

After 160 hours of operation, a significant change occurred. At a fixed rf-power supply setting, the emitter temperature dropped by $\sim 100^\circ\text{C}$. The reason for this is not clear. It appears unlikely that the reduced emitter temperature was due to a deposit on the collector which increased the latter's emissivity. The relative abruptness of the change, occurring within a one-hour period, argues against that interpretation. More likely, the temperature change was caused by some alteration within the rf-power supply, a conjecture supported by the fact that one of the rf-oscillator tubes failed completely, shortly after the completion of the out-of-pile test.

The 100°C drop in emitter temperature reduced the power output by 15%. However, this output loss was fully recovered by more careful optimization of the operating conditions, particularly by increasing the collector temperature. For the remainder of the test the converter had a steady output of 410 watts, in spite of the very low emitter temperature (i. e., 1500 to approximately 1600°C on the outside of the emitter, and about 100°C lower at the emitter surface). The conversion efficiency was 10.8%, determined in the same manner as has been described for the first converter.

Although the power output (410 W) of the second converter was appreciably lower than the maximum output (530 W) of the first, this is consistent with its lower operating temperature. Thus, as far as can be judged, the performance of the thoriated tungsten emitter appears to be equivalent to that of the all-tungsten emitter used in Diode No. 1. Moreover, the performance of Diode No. 2 was stable for 300 hours, at which time the test was stopped to prepare the converter for installation in the test reactor.

SECTION 8

PREPARATION FOR IN-PILE TEST

After conclusion of the out-of-pile test and dismounting of the converter from the test chamber, stainless steel extension tubes (about 18 inches long) were joined onto the W-Re fission gas vent tube¹¹, its Cb cover tube³⁷, and the three thermocouple Cb cover tubes³⁶. These cover tubes, it will be recalled, are part of the secondary container enclosure.

The 0.060" O.D. vent tube¹¹ was connected to its 0.125" O.D. extension via a columbium transition section. The joints were vacuum-brazed, using a palladium-nickel-silver alloy (1052°C). The same braze alloy was used for joining the 0.125" O.D. thermocouple cover tubes³⁶ to their 0.125" O.D. extensions. In the case of the 0.125" O.D. vent cover tube³⁷, a stainless steel transition to a 0.250" O.D. extension was used, to accommodate the larger vent tube extension. These were brazed with a palladium-copper-silver alloy (950°C), to avoid opening the internal vent tube joint.

8.1 Fuel-Emitter Thermocouples

Next, the emitter body was instrumented with six W-3Re versus W-25Re thermocouples, at the location shown below:

| <u>Thermocouple Number</u> | <u>Azimuthal Angle Clockwise from Vent Tube</u> | <u>Distance from Top of Emitter Body</u> |
|--------------------------------|---|--|
| 1 | 150° | 1/2" |
| 2 | 270° | 2" |
| 3 | 150° | 4" |
| 4 | 30° | 4" |
| 5 | 270° | 6" |
| 6 | 30° | 7-1/2" |

Each thermocouple lead was spun from eight strands of 0.003"-diameter wire, and each junction was inserted into a slanted hole of 0.040" diameter, penetrating to a depth of 0.2 inch into the emitter body webs⁸ between fuel chambers.

Originally, it had been planned to tie a knot at each thermocouple junction, but such knots proved to be difficult to insert into the wells and unnecessary. Good contact to the emitter body could be achieved by making a 180°-bend near the end of each stranded lead, and stuffing the two bent ends into the appropriate thermocouple well.

Each of the three thermocouple cover tubes³⁶ enclosed four of the stranded thermocouple leads. In the high temperature region below the emitter flange the thermocouple leads were insulated by two-hole beryllia sleeves. Within the cover tubes and their extensions, the thermocouple leads were insulated by four hole alumina sleeves. Both types of insulator sleeves had 0.065-inch outer diameters and 0.016-inch holes. The beryllia sleeves were tied by tungsten-rhenium wires to the outside of the emitter body, to prevent accidental dislocation of the thermocouple junction during subsequent processing and shipment.

Since the thermocouple cover tube extensions are part of the secondary containment enclosure, insulating seals are required where these leads pass from the secondary to the tertiary containment volume. It had been decided to use epoxy cement for making these seals. Therefore, to minimize the danger of neutron-induced radiation damage, the seals had to be located as far from the reactor core as possible, i. e., near the assembly plate at the top of the test capsule.

Initially, it had been planned to extend the stranded thermocouple leads through the full seven foot length of the cover tube extensions and the epoxy seals. However, preliminary tests indicated difficulty in achieving hermetic seals with stranded wires. Single-strand leads could be sealed with much greater reliability.

Consequently, the multi-strand leads were cut off where they emerged from the 0.125" O.D. cover tube extensions, approximately 18 inches above the top of the converter, and each lead joined to a 0.010"-diameter single-strand extension of the same composition (W-3Re, W-25Re). Joining of the multi-strand and single-strand leads was carried out by inserting their overlapping ends into a 0.25-inch long stainless steel capillary sleeve, together with a short length

of soft copper wire. The stainless steel sleeve was then crimped by means of a four-jaw crimping tool.

Since the crimped sleeves were too thick to fit through the 0.016-inch holes of the four-hole alumina insulators, larger diameter (Mullite) insulators were used from this region upward. These made it necessary to expand the stainless steel cover tube extensions from 0.125" to 0.250" diameter.

8.2 Secondary Containment

Figure 17 shows the converter after installation of the vent and cover tube extensions and of the tungsten-rhenium thermocouples, ready to receive the secondary container sleeve¹⁵. The tungsten-rhenium container sleeve had been fabricated by rolling 0.020-inch thick sheets into two semi-circular cylinders, which were joined by two seam welds. When received from the vendor, the container sleeve was found to be as much as 0.020 inch out-of-round. Nevertheless, it was decided to use this unit for the in-pile test, because it had required five successive trials to produce this one leaktight container.

Although it had originally been planned to EB-weld the W-Re container sleeve¹⁵ to the W-Re emitter flanges¹⁴, it was later decided to employ vacuum brazing, because of the poor fit at these joints. A palladium-nickel-silver alloy (1050°C) was used for this purpose.

No difficulty was encountered in making a leaktight joint at the lower emitter flange, where a step had been machined to receive the secondary container. On the other hand, there was considerable difficulty in sealing the upper joint, where in places the gap between flange and sleeve was almost 0.020 inches wide. Eventually, the joint was sealed by first filling the gap with W-Re shim wires.

After the secondary container¹⁵ was sealed to the emitter flange¹⁴, it was possible to recheck the leaktightness of the joints where the four cover tubes^{36, 37} join the upper flange. Although these EB-self-brazed joints had all been leaktight after fabrication, one of the four was now found to have developed a small leak. Since the joint was not accessible to inspection, the nature and

cause of this leak could not be determined. Most likely, it happened when the affected cover tube or its long extension was accidentally jostled during handling.

Repair of this diode was complicated by three factors: the impossibility of heating the region at the base of the cover tube without simultaneously heating and remelting the nearby braze joint between the upper flange and the secondary container; the impossibility of properly leakchecking the cover tube joint once the secondary container joint had opened up; and the inaccessibility of the cover tube joint at the bottom of the cup formed by the upper molybdenum skirt³¹, which made it impossible to properly clean and prepare the area at the base of the cover tube.

After repeated, unsuccessful repair attempts, it was reluctantly decided to cut away the molybdenum skirt³¹ to gain access to the affected area. The leak area was then cleaned thoroughly by filing down to base metal, after which the cover tube joint and secondary container joint were readily sealed by vacuum brazing. Finally, a new molybdenum skirt was EB-welded to the upper emitter flange. This, too, was quite difficult, particularly because of the proximity of the previous braze joints to the cover tube and the secondary container. Fortunately, both of these joints remained leaktight.

The outside of the converter assembly was then thermally insulated, using 50 layers of thoria-coated tungsten foil. The thermal insulation sleeve had been previously tested to determine the emergent heat flux with a hot-side temperature of 1900°C. This is described in Section A 2.2 of the Appendix.

Figure 18 presents a photograph of the completed converter assembly, after installation of the emitter thermocouples, the secondary container¹⁵, and the thermal insulation³⁵.

8.3 Discussion

Although the various repair efforts described above were eventually successful, they consumed an inordinate and totally unexpected amount of time and effort. In retrospect, it would have been very desirable, wherever

possible, to back-braze all tungsten weld joints, as was done in the joints between emitter end caps¹² and flanges¹⁴. Such a braze not only serves as a back-up seal, but also makes for a more reliable weld joint by reducing the mechanical and thermal stresses. This was not done on the emitter flanges because testing showed that one or two of the braze rings would invariably melt before the others, resulting in attack on the niobium tubes by the molten palladium-base braze. However, in retrospect, further testing of alternative heating methods or braze materials would have been justified.

In addition, the decision to instrument the fuel element with six thermocouples appears to have been over-ambitious. Flashlight-type thermionic fuel elements are tested in-pile without any thermocouples on the fuel-emitters. By contrast, the external-fuel design lends itself to such instrumentation. However, in view of the difficulty introduced by the requirement for double containment, it appears that the use of only one or two thermocouples would have been a wiser choice for the first in-pile test.

A still more basic lesson derived from this program concerns the choice of materials. It would have been much wiser to confine the use of tungsten or tungsten alloy to the high-temperature emitter body¹ and its end caps¹⁰, and to employ columbium for all other components, including the emitter flanges¹⁴, the thermal chokes³¹, and the secondary containment sleeve¹⁵. This had been recommended early in the program, but was overruled mainly because of concern about thermal stresses on the emitter lead. All columbium welds in the converter were made with consistent success and maintained perfect reliability, even the thirty welds in the thin-walled (0.005") collector bellows¹⁹.

8.4 Fission Gas Collection Assembly

The design of the fission gas collection assembly was described earlier, in Section 3.5. The principal problem in implementing the plan concerned the selection and construction of a suitable pressure transducer, with the required degree of radiation resistance.

A survey of the radiation effects literature was conducted in order to determine which types of pressure transducers might be used to monitor the pressure of accumulated fission gases. In order to limit the length of the fission gas vent tube which must be doubly contained, it was preferred that the accumulator be located as close to the fuel as practical, limited by the radiation damage sensitivity of the monitoring transducer. The other requirements of the transducer were good low pressure sensitivity, large range, and low drift. Fast response time or shock insensitivity were not deemed significant factors in this application.

From the available literature (5, 6, 7) and from consultation with personnel at nuclear reactor facilities as well as with transducer manufacturers it was determined that either potentiometer or LVDT (linear variable differential transformer) type transducers would be most suitable for our application. In both cases, the electric coil insulation limits the nuclear hardness of the system. In the potentiometer transducer a miniature wiper arm traverses the coil in proportion to the displacement of the pressure-sensitive bellows to which it is attached. In the LVDT-type the bellows displaces a magnetic slug inside a nulled pair of transformer coils. In both cases the translating instrumentation can be remotely located and connected with wiring to the transducers.

The LVDT-type appeared superior in low pressure sensitivity and reproducibility due to the absence of mechanical contact, and also offered a wider potential range of operation. Furthermore, it was available in a nuclear-hardened configuration, as a special order but with materials of known characteristics. The core was wound on a ceramic bobbin and made of polyimide (ML)-insulated magnet wire. In this configuration the units are rated to withstand a minimum of 10^{13} nvt and 10^9 rads of neutron and gamma dose, respectively.

Based on the data of Figure 8 of Appendix C, a transducer lifetime of 10,000 hours would be expected at a height of 60 inches above the grid plate of the BRR, which would locate the accumulator a reasonable 30 to 36 inches above the diode.

LVDT transducers with full-scale rating as low as one-half psia are available, limited only by the softness of the bellows. However, because in our experiment the transducers must be subjected to one atmosphere pressure differential prior to final installation and pumpdown, permanent deformation of such soft bellows would result, leading to a loss of calibration data. Consequently, units rated for full-scale deflection of 10 psia were procured. The manufacturer claims a maximum resolution of 0.1 percent full scale, or .01 psia, approximately 0.5 torr. Maximum hysteresis is 0.25 percent, and linearity from zero to full-scale is rated at 1 to 2 percent.

The nuclear hardened configuration is also a high-temperature configuration, rated to 450 F. The translator unit will also automatically compensate for temperature variation of electrical properties of the wire up to 300 F with an accuracy of 1 percent per hundred degrees Fahrenheit.

The six-conductor leadwire was similarly hardened by the specification of polyimide (kapton) insulation.

Following delivery, the units were assembled and tested. Translator gain was arbitrarily set to yield full scale output at 250 torr, using an accurate Bourdon tube pressure gauge as a standard. Linearity was seen to be well within specifications yielding maximum low-pressure error of 1.5 torr. Sensitivity and reproducibility were at least as good as the Bourdon gauge, and so could not be determined. However, low-pressure sensitivity appears to be well below one torr.

Fabrication of the fission gas collection assembly was straightforward. Except for the brazes at the pressure transducer diaphragms, all joints were made by EB-welding, without any difficulties. Figure 19 shows a photograph of the completed assembly, ready for joining to the vent tube and cover tube of the converter and for the subsequent vacuum pumpdown and pinch-off of the primary and secondary containment volumes.

The photograph also shows the accumulator cooling coil and heating coil. The cooling coil is needed to prevent excessive temperatures in the fission gas collector as the result of gamma heating. The heater coil would only be used in

the event of a leak between the diode and the fuel chamber. In that case, the heater could be used to raise the temperature of the fission gas accumulator above the condensation point of cesium, thus permitting continued operation of the converter.

8.5 Assembly Plate

Figure 20 presents a photograph of the assembly plate, which is at the top of the test capsule, approximately 8 feet above the top of the reactor core (see Figure 4). As can be seen, the assembly plate contains nine electrically insulated high-vacuum feedthroughs, using ceramic insulators. The six large (0.375-inch O.D.) copper lines carry cooling water to and from the collector and the upper and lower emitter power take-offs. The smaller tubes serve to cool the cesium reservoir and the fission gas accumulator assembly, and to connect to the helium volume for collector temperature adjustment.

The bottom of the assembly plate also contains three blind holes, tapped to receive 8-32 stainless steel threaded hanger rods, which support the fission gas collection assembly. That assembly in turn supports the converter assembly by three hanger rods. The latter supports employ alumina bushings for electrical insulation. The converter hangs in a position approximately 1/8-inch off the centerline of the test chamber. This eccentricity provides greater clearance between the chamber wall and the thermal insulation, to allow more room for the ceramically insulated coolant lines going to the bottom of the converter.

As shown by Figure 20, all coolant lines contain hydroformed stainless steel bellows, to minimize axial stresses. In addition, high-conductance by-pass straps were made for the six current-carrying lines. Each of these straps, which are not shown in the photograph, consists of five 0.005-inch thick copper strips, 0.5-inch wide and 3.5 inch long. They are clamped onto the copper tubes, above and below the stainless steel bellows.

All feedthroughs were joined to the assembly plates by EB-welding to its underside. In addition to the various coolant line feedthroughs, the assembly plate

also contains two 37-pin hermetic connectors for thermocouple leads, voltage probes, pressure transducer leads, and auxiliary heater leads. One of these is made with Chromel-Alumel paired feedthrough pins; the other has nickel pins. Altogether, the experiment is instrumented with 21 thermocouples. Of these, 16 are chromel-alumel, which go through the matching connector. Above the assembly plate, insulated thermocouple extension wire is used.

Each feedthrough pin is electrically insulated by means of a glass compression seal, and is designed for a maximum current of 7.5 amperes. The outer cesium reservoir heater will be doubled up, because it requires up to 10A heater current.

To test the radiation resistance of the 37-pin connector, an identical unit was exposed in the BRR to decay gammas in excess of 10^{10} ergs/gm. It was subsequently helium-leakchecked, with no indication of a leak. It appeared visually unchanged in appearance.

Figure 20 shows a seal band (1/16" high by 1/8" wide) machined into the top of the stainless steel assembly plate, which mates with a 1"-thick aluminum flange on the bottom of the instrumentation tube leading to the top of the reactor pool. The mating surfaces are sealed by means of a 0.0015"-thick tempered aluminum foil gasket, compressed by twelve 7/16-inch bolts torqued to approximately 150 in-lb. An identical arrangement seals the bottom of the assembly plate to the top of the test capsule. Metal foil gaskets are used because radiation-effects data indicates that elastomer seals would not have adequate radiation resistance for this application.

8.6 In-Pile Test Chamber and Vacuum System

As illustrated in Figure 4, the diode hangs in the interior of a stainless steel test section, which is 2.635" I.D. x 2.75" O.D. x 26-1/4" long. The bottom of the test section is seal-welded to the small end of a 2.5" by 6" eccentric stainless steel reducer. A 30" length of 6" Schedule-10 stainless steel pipe is welded to the large end of the reducer. A stainless steel flange of a special design is welded to the open end of the 6" pipe. A total length of this stainless steel portion of the test chamber is 61-13/16 inches. The distance between the centerlines of the two pipe sections is 1.862 inch.

The upper portion of the test chamber is fabricated from a 26-11/16" length of 6" Schedule-40 aluminum pipe and a 6 x 6 x 6-inch Schedule-40 aluminum tee. The length of pipe is welded to the bottom of the tee; an aluminum flange to mate with the flange on the top of the stainless steel section is welded to the bottom end of the pipe. A similar flange is welded to the top of the tee. A standard 6" flange with an O-ring groove is welded to the side arm of the tee. The test section is assembled by bolting the two sections together; the 2-1/2-inch diameter test section is located so that it is turned 45 degrees to the right of the approach line of the vacuum system to the core. The inside length of the assembled test chamber is 99-11/16 inches. The assembly plate is located approximately 103 inches above the reactor grid plate.

The leads from the assembly plate to above the pool surface are enclosed but not sealed in a lead tube fabricated from 6" Schedule-40 aluminum pipe. A 1-ft long section of this pipe is welded to the flange that is sealed to the top of the assembly plate. The lead tube extension pieces consist of a 40" length of pipe, cut on a 12-degree bias, and another piece 9-1/2 ft long. The bias piece is welded between the two straight sections to obtain an offset, which does not allow a line of sight through the lead tube; thus, radiation streaming to the surface of the pool is minimized.

The vacuum system consists of two major 8-inch pipe sections connected to the out-of-pile pumping system. The upper section is fabricated from 8-inch Schedule-1- stainless steel pipe; it has a 9.5 ft vertical drop from the flange joint at the upper end to the centerline of an 8-inch 90-degree elbow at its lower end. The horizontal distance from the vertical centerline to the surface of the flange on the elbow is 12-1/2 inches. This flange is mated to a flange welded to a 90 degree elbow on the top of the lower pipe section, which is fabricated from 8-inch Schedule-40 aluminum. This flange joint is the location of the last vacuum seal to be established when the pipe system is assembled. The vertical drop in the lower section is 10 feet -7 inches. A 90-degree elbow is welded to the bottom end of the vertical pipe, and an 8 x 8 x 6-inch tee is welded to the elbow.

The vacuum system was modified on the downstream side of this tee to accept the test chamber. A standard 6-inch flange is welded to the 6-inch side arm of the tee; two ion gauges are mounted on a flange and enclosed in a housing-lead tube arrangement, which is sealed to the tee flange, in order to monitor system pressure at the bottom of the pipe. In addition, a bare ion-gauge is mounted within the main experiment volume, near the fission gas accumulator system.

The following elements were installed to attach the vacuum system to the test chamber.

- (a) An 8 x 6-inch concentric reducer
- (b) A 6-inch vacuum gate valve
- (c) A water-cooled 6-inch chevron baffle.

The large end of the 8 x 6-inch reducer was welded to the open end of the vacuum piping tee; a standard 6-inch flange was welded to the other end of the reducer. The flange was bolted to one side of the gate valve and the baffle and gate valve were bolted together. The other flange on the baffle was bolted to the side arm flange on the test chamber. A cross brace to strengthen the structure was installed between the lead tube and vertical piece of the lower pipe section. The horizontal distance between vertical center lines of the lower vacuum pipe and the test section is 50-1/2 inches.

To provide isolation of the test chamber in the event radioactive products were released and detected in the vacuum system, an air-activated gate valve was acquired and modified for underwater operation. In addition, a baffle was installed to condense cesium vapor in the event radio-cesium is released into the system. At the conclusion of the irradiation, the gate valve will be closed and the test chamber with baffle and valve attached will be unbolted from the vacuum piping for shipment to the BRR hot cell building. The gate valve and baffle will be recovered for use with subsequent experiments.

The vacuum pumping system consists of:

- (a) A 1000-liter/sec titanium sublimator
- (b) Two 350 liter/sec triode-type ion pumps
- (c) A double-wall liquid-nitrogen cold trap
- (d) A Rootes blower pump
- (e) A KC-30 roughing pump

The ion pumps and sublimator are mounted on a framework which can be pivoted laterally and raised or lowered. The entire pump and vacuum system assembly is located on a movable bridge above the reactor or pool, which allows movement toward and away from the reactor core. Two ion gauges are located in the upper section of the vacuum piping, immediately below the sublimator, for pressure measurement. Direct readings of pressures in the ion pumps are obtained from their power supplies. It is expected that the sublimator will be used for short times during high-outgassing periods, which will occur during the initial reactor startup.

The entire vacuum system with test chamber assembled was evacuated to checkout its leaktightness and operation. A dummy assembly plate with rubber gasket seals was installed to seal the test chamber and the bottom of the lead tube. Pumping was continuous for 5-1/2 weeks, and a pressure of 5×10^{-7} torr was achieved at the top of the vacuum piping. Pressure at the ion gauge station at the bottom of the vacuum piping was estimated to be less than 3×10^{-6} torr; ion gauges at this location were inoperable, owing to a water leak in the lead tube enclosing the ion gauge cables. The test chamber was not instrumented with pressure gauges, and thus the influence of the baffle and the smaller pipe diameter on pressure levels could not be assessed.

It would be desirable that the diode experiment remain in the core position during reactor shutdown, and be moved as few times as possible. However, the experiment must be raised vertically on alternate reactor shutdown, to allow refueling of the reactor core. Even this movement of the experiment would not be necessary if the small-diameter section of the test chamber could

have been made longer, to move the eccentric reducer away from the core so as not to interfere with reloading operations. However, this was not done, since lengthening of this part of the test chamber would have crowded the diode accessory system in the 6-inch portion of the test section, and would have decreased the conductance of the vacuum system.

A 20-inch long, 1/2-inch diameter centering pin was attached to the bottom center of the test chamber. This pin will be inserted through a hole in the top of a grid plug in the test facility. A long centering pin was used, to hold the capsule in line with the core facility during reloading operations, and to facilitate relocation of the test chamber in the core position. The grid plug contains a series of holes to allow the reactor water flowing through the facility to exit from the core. The positioning of the test chamber in the core facility has been checked, and minor adjustments in the vertical alignment of components of the vacuum system will be necessary when the diode is installed, to straighten up the test chamber in the core position.

8.7 External Controls and Instrumentation

The following out-of-pile systems were installed:

- (a) A water flow and control system for diode cooling
- (b) A helium pressure control system for adjusting the collector temperature
- (c) Diode-performance monitoring instrumentation
- (d) An experiment safety and alarm system.

Complete descriptions of their elements, functions, and locations are presented in the experiment safety report and addenda. The instrumentation requirements were reviewed periodically and the following listing represent the final instrument specifications:

| <u>Instrument</u> | <u>Function</u> |
|---------------------------------------|--|
| 4-channel voltage recorder | Diode voltage |
| 3 strip chart single-pen TC recorders | Emitter, collector, and cesium temperature |
| 24-point TC recorder | Other thermocouples |
| 5 Ion gauges | Pressure measurement |
| 2 Ion gauge readouts | Pressure monitors |
| 4 Rotometers | Water flow measurement |
| 0-10 V recorder | Transducer output |
| 0-760 torr pressure gauge | Helium pressure |
| Millivolt chart recorder | Helium pressure recorder |
| Voltmeters and ammeters | Cesium heater power |
| Variable transformers | Cesium heater power |
| Step-down transformer | Cesium heater power |
| Calibrated shunts | Diode amperage |
| 1000-amp power supply | Diode load |
| LVDT translator and switch | Transducer output |
| Pump | Water supply |
| Gauges and pressure switches | Water system |
| Vacuum System | Experiment system |
| Gamma meter | Radiation Alarm |
| Safety circuits | Alarms and scrams |

Installation of all systems is essentially complete, except for those portions of the external systems to be connected after the diode is installed.

8.8 Final Assembly

Originally it had been planned that the converter, after completion of the out-of-pile test, encapsulation in the secondary container and thermal shields, and installation of the thermocouples, would be joined to the fission gas collector and the assembly plate at Fairchild, to be shipped as a single package to Battelle for installation in the test capsule and in-pile testing in their Research Reactor.

Subsequently, it was decided to ship these three subassemblies as separate packages, with final joining between them to be carried out by Battelle. Primarily, this involves torch-brazing of interconnecting tubes, pumpdown and pinch-off, and installation of thermocouples other than those on the emitter body.

The revised procedure is considered much safer than the original plan, which would have required the shipment of a very unwieldy 12-ft high package. Moreover, it would have been quite difficult to provide adequate support to the many long and thin tubes within this package. To minimize bending moments, the tall package would have had to be shipped in an upright position. Even then, vibrations and shocks during shipment could have endangered the joints at the base of these tubes.

The three subassemblies, together with the required accessories, were shipped to Battelle on July 30, 1971, two years and nine months after inception of this program. The major conclusions derived from the program are summarized in Section 2.

SECTION 9

DESIGN ALTERNATIVES

9.1 Introduction

Throughout the course of this program, various alternatives or modifications of the present design had been considered. Some of these modifications were directed towards somewhat different reactor design concepts; others were designed to simplify the experimental arrangement for in-pile testing the converter; while still others were motivated by a desire for easier fabrication and greater reliability, based on the results of the present program.

Unfortunately, the scope of that program did not permit the construction of converters incorporating these design changes. However, to illustrate a number of these possible modifications, Figure 21 presents an advanced design for an in-pile test converter. Before proceeding to a more detailed discussion of that design and its rationale, it should be emphasized that the design is intended to illustrate various conceptual features that are largely independent of each other. In other words, it is possible to adopt some of these concepts without the others.

Figure 21 depicts the illustrative design by an exploded view, showing the three major subassemblies: the fuel-emitter subassembly (center), the collector-heatpipe subassembly (right), and the nuclear containment (left).

9.2 Heatpipe-Cooled Converter Module

One major change illustrated in Figure 21 is the use of a single-ended heatpipe-cooled converter, with its active (fueled) region extending over half the core height. This contrasts with the double-ended full-core-height converter, using forced-circulation cooling, built under the present program.

The heatpipe cooling concept permits complete modularization of the thermionic fuel element. Each thermionic fuel module, including its heat rejection system, can be fabricated and pre-tested as a separate entity. The

reactor core would then be built up from these performance-proven thermionic fuel modules, by inserting the condenser sections of their collector-heatpipes into mounting holes on a liquid-metal-cooled heat exchanger, with redundant coolant loops. Each heat exchanger with mounted thermionic fuel modules constitutes half of the reactor core. The reactor is then assembled by inserting the two core halves into a side frame, which provides structural support, neutron reflection, and reflector control.

A discussion of the pros and cons of this design alternative from the viewpoint of the thermionic reactor has been presented in other reports (8, 9) and will not be repeated here. From the viewpoint of building an experimental converter and testing it in-pile, there appears to be one major complication, i. e., the need for a high-performance heatpipe, and numerous offsetting simplifications, or reliability improvements, as discussed below:

9.3 Single-Ended Converter

The use of a single-ended half-length converter would essentially cut the size of the experimental device in half. It would not only halve the requirement for most components (e. g., ceramic seals, fuel pellets, etc.) but would eliminate the need for certain components entirely.

Since the emitter, collector, and containment shells could independently expand at the free end of the converter, there would be no need for any bellows in the converter. This would eliminate the columbium bellows, with its 30 EB-welds. The single-ended construction would also serve to reduce thermal stresses.

Another component that can be eliminated in a single-ended converter is the emitter end cap. This can be done because the 4-inch-long fuel chambers can be electric-discharge machined as blind holes from the free end of the converter. Thus, the need for failure-prone tungsten welds can be avoided completely.

In the design shown, neither the cesium enclosure nor the fuel enclosure depends on the integrity of any tungsten welds. The cesium enclosure has no tungsten welds because the emitter cavity is electric-discharge-machined as a blind hole from the terminal end of the emitter body. And the fuel enclosure does not depend on tungsten welds because the emitter body does not serve as the primary container in the illustrated design. The cover disk at the free end of each fuel chamber merely serves as a mechanical constraint. Primary containment is provided by a separate cup, similar to the secondary container. These are discussed later.

9.4 Emitter Body Geometry

The features discussed above are all compatible with a cylindrical revolver cross-section, as in our present converters. Although that geometry can yield fairly high fuel volume fractions, it does waste a good deal of potential fuel volume, not only in the cusps between the cylindrical modules but also in the high metal fraction within the revolver itself.

To meet the need for the very high fuel volume fractions required for low-power reactors, alternative fuel element geometries should be investigated. For example, the fabrication of a cylindrical emitter body with thin radial metal webs between fuel chambers is under active investigation. Such an emitter body is, of course, more difficult to fabricate than the cylindrical revolvers used in the present program. Moreover, it still wastes the space in the cusps between converter modules. And it leads to non-cylindrical fuel chambers.

Such wedge-shaped fuel chambers would be more difficult to load, and may lead to distortion and stress failure at the corners of the fuel chambers, as the result of thermal stresses and fuel swelling.

One way of increasing the fuel volume fraction of the revolver, as mentioned in Section 3.1, is to hexagonalize its outer boundary; this permits closer packing of adjacent modules. An even more efficient way, which still retains the circular fuel chamber cross-sections and cylindrical UO_2 pellets is

to employ the scalloped revolver geometry illustrated in Figure 21. An emitter body of this geometry could be made from a single tungsten billet by electric-discharge machining, after which its cylindrical fuel chamber walls could be finished by standard honing techniques.

In a sense, the configuration shown approximates a cylindrical diode surrounded by six clad fuel cylinders. As illustrated in Figure 22, neighboring elements can be nested together, so that the volume lost in inter-element cusps is negligible. The design results in a much lower metal volume fraction than the cylindrical revolver, yet retains the cylindrical fuel pellet geometry to minimize stresses.

9.5 Axial Reflector

Another design concept illustrated in Figure 21 is the inclusion of a neutron reflector right within the thermionic fuel module. This would be located between the fuel region and the ceramic seal.

Extended irradiation of ceramics by neutrons with energies greater than 0.1 Mev can lead to swelling and eventual loss of vacuum integrity (10). This is a particular problem in applications with very long lifetimes, e.g., 5 years.

The external-fuel converter, extending over the half or full core height, offers the distinct advantage that its ceramic seal is located outside the reactor core, where the fast neutron flux is significantly lower than at the core center.

An even greater reduction of the neutron flux at the seals can be achieved by interposing an axial reflector layer between the fuel region and the seals. In the design shown in Figure 21, the reflector layer is approximately 2.5 inches thick, and is formed by extensions of the columbium collector and the tungsten emitter body. Previous studies have shown that refractory metals are very effective reflectors of fast neutrons.

The use of metallic reflectors makes it practical to pass the high currents generated in the diode through the axial reflector, without excessive voltage drop. In spite of its unusual length, the emitter lead has more than enough cross-sectional area to achieve its optimum resistance.

Finally, the rather massive metal layer, located right next to the reactor core, should also serve as a very effective primary gamma shield.

9.6 Emitter Flange

In addition to the tungsten emitter body discussed above, the emitter assembly includes a columbium double flange, machined from a single billet. As in the present design, it serves several functions. It is an electrical conductor, a thermal conductor, part of the cesium envelope, and part of the containment envelope. A double-flange is used, to mate with both the primary and secondary containment cups. Both of these can be made of columbium, provided thermal insulation is inserted to reduce their temperatures. There are no thermal stresses due to differences in an axial expansion, since the two containment cups are free to expand independently.

The flange assembly contains an integral thermal baffle, terminating in a water cooling channel, which serves as the emitter power take-off. Emitter thermocouple leads and fission gases are brought out through coaxial columbium tubes EB-welded to the columbium flanges.

9.7 Collector Assembly

As shown in Figure 21 the collector assembly consists of the collector-heatpipe, the centering guide, the cesium reservoir, and the ceramic seal which joins it to the emitter assembly. All metal components are made of columbium.

The collector-heatpipe uses an annular condensate channel, which is separated from the central vapor duct by a fine-pore cylinder, formed by swaging multiple layers of fine screening. The preferred heatpipe working fluid is potassium, which yields a significantly higher maximum axial heat flux than does sodium.

The collector centering arrangement shown in Figure 21 differs considerably from the design used in our present diode. Instead, it resembles the emitter centering guides used in flashlight fuel elements. The use of a thin-walled Belleville spring offers two advantages: it reduces the maximum temperature of the ceramic insulator bushing; and it accommodates difference in axial expansion of the emitter and collector, without requiring any sliding motion at the centering guide.

The cesium reservoir shown in Figure 21 has a re-entrant geometry. This is because the converter would be tested in-pile in an upside-down position, i.e., with the cesium reservoir at the top of the diode. Thus, the converter hangs from the emitter flange, and all electrical and coolant lines emerge from the upper end. The cesium reservoir is connected to the interelectrode gap by means of a small-diameter tube along the center of the heatpipe.

The required columbium-alumina-columbium seal could be made by a number of different fabrication techniques. For example, the graded planar seals described in the present report exhibited good reliability, but rather poor production yields. The design illustrated in Figure 21 is based on the use of an annular seal made by hot isotatic compaction of alumina-coated columbium microspheres. This is a technique pioneered at NASA's Lewis Research Center where seals of this type have exhibited excellent reliability under severe testing (11).

9.8 Converter Assembly

After the collector assembly is fabricated and charged with potassium, the heatpipe can be subjected to an extensive performance test. Once this is completed, the collector with centering guide is inserted into the emitter cavity, and the ceramic seal lip is EB-welded to the emitter flange. After the electrically heated out-of-pile test of the converter, the primary and secondary containment cups would be EB-welded to their respective emitter flange lips.

Note that, with but one exception, all hermetic joints in the converter are between columbium and columbium. Such joints have demonstrated consistent ease of fabrication and operational reliability. The one exception is the joint between the

tungsten emitter body and the columbium emitter flange. Fortunately, this joint operates at only a moderate temperature. The joint could be made either by EB-selfbrazeing the columbium lip to the tungsten, followed by a lower-temperature backup braze; or by diffusion bonding coaxial sleeves under elevated temperature and pressure. The particularly vulnerable weld joint between the thin tungsten vent tube and the high-temperature fuel chamber end cap has been eliminated. There are no tungsten-to-tungsten seals required in this design.

Finally, it should be noted that, if desired, the fission gas accumulator could be completely eliminated. This would be done by adding enough length to the containment cups so as to provide sufficient volume for fission gas accumulation (without excessive pressure buildup) directly within the primary container. With that arrangement, the differential pressure transducers could be connected near the top of the thermocouple cover tubes.

REFERENCES

1. M. J. Abbate, C. L. Eisen, B. Raab, and A. Schock; "External-Fuel Thermionic Reactors"; Second International Conference on Thermionic Electrical Power Generation, Stresa, Italy, p. 221 (1968).
2. J. P. Davis and H. G. Gronroos; "Uninsulated In-Core Thermionic Diode Concept"; Second International Conference on Thermionic Electrical Power Generation; Stresa, Italy, p. 237 (1968).
3. A. Schock; "Analysis and Optimization of Full-Length Diodes"; Second International Conference on Thermionic Electrical Power Generation; Stresa, Italy, p. 865 (1968).
4. D. R. Wilkins; "SIMCON, A Digital Computer Program for Computing Thermionic Converter Performance Characteristics"; GESR-2109, General Electric Company, Nuclear Thermionic Power Operation, Pleasanton, California (1968).
5. W. E. Chapin, J. E. Drennan, D. J. Hamman, "The Effect of Nuclear Radiation on Transducer; REIC Report No. 43, TIC Report No. 3, October 31, 1966.
6. C. L. Hauks and D. J. Hamman, "The Effect of Radiation on Electrical Insulating Material, REIC Report No. 46, June 16, 1969.
7. W. E. Chapin, D. J. Hamman, E. N. Wyler, "The Effect of Nuclear Radiation on Transducers, REIC Report No. 25, April 19, 1963.
8. A. Schock et al, "300-ekw Thermionic Reactor Design Study," Final Report, September 30, 1968, NYO-3873-1, FHR 3428-2 (CRD)
9. A. Schock, M. J. Abbate, C. L. Eisen, "Thermionic Reactor Design Studies," Final Report, May, 1970, NYO-3873-2, FHR 3428-3 (CRD)
10. W. H. Reichelt et al, "Radiation-Induced Damage to Ceramics in the EBR-II Reactor", Proceedings of the 1970 IEEE Thermionic Conversion Specialist Conference, P. 39.
11. W. Kaufman, R. Tischler, R. Breitwieser, "Cermet Seal Having High Strength and Thermal Conductance," Proceedings of the 1967 IEEE Thermionic Conversion Specialists Conference, p. 268.

Appendix

APPENDIX A

PREDICTED THERMIONIC PERFORMANCE AND ESTIMATE OF REQUIRED THERMAL POWER

A.1 Converter Operating Parameters

The determination of thermal power required for performance of the experiment required a prediction of the operating parameters of the long double-ended diode, as well as calculations of the expected parasitic losses.

The diode calculation was based on a modification of the previously developed TET program for the thermal, electrical, and thermionic analysis of long external-fuel converters. As explained in Reference A1, TET computes simultaneous solutions for two Laplacian equations, for emitter temperature and interelectrode potential. It takes account of non-uniform nuclear heat generation, internal electrical resistance of the electrodes, and axial heat conduction. At each axial position, the current density and emitter heat flux is determined by multi-dimensional interpolation of thermionic performance data previously computed by the SIMCON program (A2).

The TETREV modification was specifically designed for the revolver fuel element. It can automatically account for fuel redistribution, as the result of UO_2 vapor transport, by computing the shape of the isothermal cavity at the center of each fuel chamber.

Both TET and TETREV can optimize the emitter lead dimensions to maximize output power; alternatively, the diode can be analyzed for a prescribed off-optimum lead conductance. As will be seen, this alternative was an important option.

The input nuclear profile used was based on the results of the first mock-up experiment (aluminum-cadmium) conducted in the BRR (Appendix C, Figure C3).

A series of TETREV calculations was run with thermal input power as a parameter, based on the available fuel volume fraction. Because the flux profile measured in the mock-up experiment was not exactly symmetric around the mid-plane of the cylinder (Figure C3), two different flux profiles were programmed into this series. However, the differences between the two were not significant.

For each value of thermal input power, TETREV performs a sub-series set of calculations for various net output voltages, permitting the construction of the set of constant-input-power I-V curves shown in Figure A1. Each calculation results in a slightly different maximum emitter temperature. It was stipulated that the reference design point be selected for a maximum emitter temperature of 2000°K. The 2000°K line is shown on Figure A1, as interpolated from the various calculated cases. This reveals that the stipulated emitter temperature can be achieved over a fairly large range of thermal input power by an adjustment of load resistance. This adjustment, therefore, can be used as a final tuning of the emitter temperature without adjustment of the reactor power level.

For selection of the reference design point, some compromise was sought between maximum power output and maximum efficiency (and minimum fuel cost). It was decided that the range between 0.5 and 0.6V net output voltage would be the region of greatest desirability. TETREV predicted optimum cylindrical emitter lead thickness/length ratio of 0.0825 in this region.

Because the entire fuel-emitter structure is supported by the emitter lead and because the emitter lead is part of the diode cesium envelope this ratio was judged to be too small for complete reliability. Consequently a series of TETREV studies was made for off-optimum emitter lead ratios, resulting in the selection of 0.125 for this ratio. As expected, the major change resulting from the off-optimum emitter lead selection was a reduction in predicted efficiency, from approximately 13 to 12 percent in the region of interest. This was thought to be a worthwhile price to pay in order to permit increasing the emitter lead wall thickness from .033 to .050-inch for the design length of 0.4 inch.

The nominal design point selected calls for operation at a diode current of 1000 amps and a terminal voltage of 0.58. As shown on Figure A1, this corresponds to a thermal power input of 4600 watt. Figure A2 shows the axial variation of emitter and fuel temperature, interelectrode potential, and electric power density for the reference design point, as calculated by TETREV.

A.2 Parasitic Losses

Three significant sources of parasitic heat loss were identified.

- (1) Heat radiated from the fuel body outer surface to the secondary containment sleeve and thence conducted to the emitter flanges at each end,
- (2) Heat radiated through the multifoil insulation surrounding the secondary containment sleeve,
- (3) Heat radiated from the ends of the fuel body to the emitter flanges.

These will be discussed separately below:

A.2.1 Conduction in Containment Sleeve

This source of heat loss is the most significant of those identified, both in magnitude and because it limits the thickness of the secondary containment sleeve. The differential heat input, dQ , along the tubular sleeve in the axial (z) direction can be expressed as:

$$\frac{dQ}{dz} = \frac{2 \pi \sigma (T_f^4 - T^4)}{\frac{1}{r_1 \epsilon_1} + \frac{1}{r_2} \left(\frac{1}{\epsilon_2} - 1 \right)} \quad (1)$$

where T_f is the fuel body temperature (assumed constant over its length) and T is the sleeve temperature (function of z). The symbols r_1 , ϵ_1 , and r_2 , ϵ_2 refer to the radii and emissivities of the fuel body and inner surface of the sleeve, respectively.

The heat conduction along the sleeve can be expressed as:

$$Q = -2\pi r_2 wK \frac{dT}{dz} \quad (2)$$

where w is the thickness of the sleeve ($w \ll r_2$). Differentiating equation (2) with respect to z and combining with (1) yields a non-linear second-order differential equation in temperature T . This can be integrated once to reduce it to a first-order equation. Inserting the resultant expression for dT/dz in (2) yields:

$$Q = 2\pi wKr_2 \left[\frac{-2(\sigma/K)(T_f^4 T - T^5/5)}{(r_2/r_1 \epsilon_1) + (1/\epsilon_2) - 1} - 1 \right]^{1/2} \quad (3)$$

For boundary conditions, we note that at the mid-plane of the fuel body $z=0$, $T=T_o$, and $Q=0$, while at the end of the fuel body $z = z_1$, $T = T_1$, and $Q = Q_1$. Applying these to Equation (3), we obtain:

$$Q_1^2 = \left[\frac{8\pi^2 r_2 wK \sigma}{(r_2/r_1 \epsilon_1) + (1/\epsilon_2) - 1} \right] \left[T_f^4 (T_o - T_1) - \frac{1}{5} (T_o^5 - T_1^5) \right] \quad (4)$$

Next, we define α by $T_o = (1-\alpha)T_f$, and note that when $w/z_1 \ll 1$, i.e., in the case of a long thin-walled sleeve, $\alpha \ll 1$. Therefore,

$$T_f^4 T_o - \frac{1}{5} T_o^5 \approx T_f^5 (1-\alpha) - \frac{1}{5} T_f^5 (1-5\alpha) = \frac{4}{5} T_f^5 \quad (5)$$

Further, assuming no significant heat input for $z > z_1$, the heat flow Q_1 must also satisfy the conduction equation

$$Q_1 = 2\pi r_2 wK (T_1 - T_2)/(z_2 - z_1), \quad (6)$$

where T_2 is the temperature of the emitter flange, and z_2 its distance from the mid-plane of the fuel element.

Finally, combining equations (4), (5), and (6) results in an expression for Q_1 in terms of known parameters:

$$Q_1 = 2\pi r_2 \left(\frac{2 w K \sigma}{\frac{r_2}{r_1 \epsilon_1} + \frac{1}{\epsilon_2} - 1} \right)^{1/2} \left\{ \frac{4}{5} T_f^5 - T_f^4 \left[\frac{(z_2 - z_1) Q_1}{2\pi r_2 w K} + T_2 \right] + \frac{1}{5} \left[\frac{(z_2 - z_1) Q_1}{2\pi r_2 w K} + T_2 \right]^5 \right\}^{1/2} \quad (7)$$

Figure A3 shows a solution of Q_1 as a function of T_2 , based on what was considered to be the minimum practical thickness of container sleeve, 0.05 cm. Other parameters, corresponding to the reference design were:

$$r_1 = 1.9 \text{ cm}, \quad r_2 = 2.4 \text{ cm}, \quad \epsilon_1 = \epsilon_2 = .25, \quad K = 1 \text{ W/cm-deg. K},$$

$$T_f = 2000 \text{ K}, \quad z_2 - z_1 = 1.25 \text{ cm}.$$

Therefore, from the design value of emitter flange temperature of 650°C, $Q_1 = 275 \text{ W}$, each end.

A.2.2 Losses Through Insulation

The multi-foil thermal insulation was of the thoria-on-tungsten type. A minimum of 50 layers was specified, which the manufacturer claimed would result in a radiation loss of 1/2 watt per square centimeter or less, for a hot-side temperature of 1900°C.

This was subsequently verified following receipt of the insulation. A tungsten wire heater was inserted into the central cavity of the shield package and the ends were carefully insulated with zirconia felt. With the central cavity forming a near black body, its temperature was accurately monitored through a small penetration in the zirconia cover. At 1900°C in the interior the outer surface was too cool for accurate pyrometry. Thermocouples on the outer surface read 640°C near the end and 675°C near the center, although the latter reading was erratic. With a

tungsten emissivity of 0.10 at a temperature of 650°C, radiation loss through the foil insulation would be 0.41 W/cm^2 , for total heat lost in this manner of approximately 65 watts. This had been previously estimated at 75 watts.

In addition, a heat balance applied to the experiment, taking account of heat conduction along the heater leads, indicated an additional heat loss rate of 120 watts due to edge streaming, i.e., radiation around the edges of the thermal shielding. This correlated well with prior experience of the manufacturer of this insulation.

Total loss through the thermal insulation was therefore estimated at 185 watts.

A.2.3 Radiation From Fuel to Emitter Flange

This source of heat loss was treated by a simplified model of radiation between parallel discs, one at 2000°K and the other a 1000°K. Effective emissivity was determined from earlier work (A3) to be 0.2, resulting in an estimated heat loss of 125 W at each end.

Total parasitic heat loss was thus estimated a 985 W. However, gamma heating will occur within the secondary containment sleeve and tungsten-foil thermal insulation, which will partially make up for this loss. The gamma heating experiment performed on the tungsten fuel body (Appendix C) indicated a heating rate of 1/2 watt per gram of tungsten at this location. It can readily be shown that for a large number of foil layers ($\gg 1$), approximately half the deposited heat can be subtracted from the parasitic heat loss. Thus, for a total weight of insulation and secondary containment of 900 grams, net parasitic heat loss $Q_{\text{PNET}} = 985 - 225 = 760$ watts. Consequently total thermal power requirement is:

$$Q_{\text{net}} = Q_e + Q_{\text{PNET}} = 5360 \text{ W.}$$

Based on the gamma heating experiment (Appendix C) some 1010 watts will be provided by gamma heating within the fuel and tungsten fuel body, so that the total fission heat requirement was estimated at:

$$Q_{\text{fission}} = Q_{\text{net}} - Q_{\gamma} = 4350 \text{ W.}$$

This combined with the data of Appendix C, Figure C7 resulted in a fuel enrichment specification of 9.0 percent.

REFERENCES

- A1. A.Schock, "Analysis and Optimization of 'Full-Length' Diodes", Second International Conference on Thermionic Electrical Power Generation, Stresa, Italy, p. 865.
- A2. D.R. Wilkins, "An Improved Theoretical Description of Thermionic Converter Performance Characteristics," Report on Twenty-Seventh Annual Physical Electronics Conference, Cambridge, Massachusetts March, 1967.
- A3. A.Schock, M.J. Abbate, "Comparison of Methods for Calculating Radiative Heat Transfer," Second International Conference on Thermionic Electrical Power Generation, Stresa, Italy, p. 813.

APPENDIX B

NUCLEAR ANALYSIS

The code THERMØS was used to determine the flux and power distribution within the fuel element.

The dimensions and compositions assumed for the capsule are summarized below.

| <u>THERMØS Region</u> | <u>Region</u> | <u>OD, in.</u> | <u>Thickness, in.</u> | <u>Composition</u> |
|---------------------------|---------------|----------------|---------------------------|---------------------------|
| A | 1 | 0.5 | 0.5 | Nb-H ₂ O-SS |
| | 2 | 0.6 | 0.05 | Tungsten |
| B | 3 | 1.4 | 0.4 | UO ₂ -tungsten |
| | 4 | 1.5 | 0.05 | Tungsten |
| C | 5 | 1.7 | 0.10 | Void (He) |
| | 6 | 1.74 | 0.02 | W-Re alloy |
| | 7 | 1.83 | 0.045 | Thoriated-tungsten foil |
| D | 8 | 2.67 | 0.42 | Void |
| | 9 | 2.75 | 0.04 | Stainless steel |

In THERMØS, a one-dimensional, 30 energy group integral transport code, the capsule was represented by five different concentric regions and a sixth annular region represented the BRR reactor. The innermost region of the capsule, containing stainless steel, water, helium, argon, niobium, and cesium, was homogenized with the 0.05-in.-thick tungsten ring surrounding the cesium to form the first mock-up region. Cesium and the helium-argon gas mixture were treated as void, and stainless steel as iron, for calculational purposes. A 1.016-cm thick ring containing the fuel and tungsten represented the second region. Rings of tungsten (0.127 cm thick), helium-argon (0.254 cm thick), tungsten/rhenium (0.0508 cm thick), and tungsten (0.1143 cm thick) make up the third region. Void and stainless steel (iron) were homogenized to form the fourth ring, and water (the unoccupied volume of the reactor grid) made up the fifth shell. As stated, the reactor materials made up the outer ring.

In homogenizing the tungsten with the fuel material, the different surface-to-average fluxes seen by the two materials (tungsten diluent and UO₂ fuel) were considered in order not to overestimate the fission rate in the fuel. In other words, a simple volume-fraction homogenization of these materials is not adequate. Values for the surface-to-average fluxes for cylindrical rods for different enrichments were calculated on the basis of the concept of capture fractions, and the results are indicated in Table 1.

TABLE 1. FLUX DEPRESSIONS IN FUEL CYLINDER BASED ON CAPTURE-FRACTION CALCULATIONS

| Enrichment, percent | $\bar{\phi}_s / \bar{\phi}$ |
|---------------------|-----------------------------|
| 10 | 1.18 |
| 20 | 1.39 |
| 30 | 1.72 |

The total reaction rate in a homogeneous mixture of fuel and diluent, $V_T \bar{\Sigma} \bar{\phi}$, can be related to the reaction rate of each of the components by

$$V_T \bar{\Sigma} \bar{\phi} = V_f \bar{\Sigma}_f \bar{\phi}_f + V_m \bar{\Sigma}_m \bar{\phi}_m \quad (1)$$

where V_T , V_f , and V_m refer to total, fuel, and tungsten volumes, respectively. Equation (1) can be interpreted as a defining equation for proper homogenization using the assumption that

$$V_T \bar{\phi} = V_f \bar{\phi}_f + V_m \bar{\phi}_m \quad (2)$$

Using Equations (1) and (2), the homogenized number densities, N , are then defined as

$$N(\text{fuel}) = \frac{V_f' N^o(\text{fuel})}{V_f' + V_w' \frac{\bar{\phi}_s}{\bar{\phi}}} \quad (3)$$

and

$$N(\text{tungsten}) = \frac{V_w' N^{\circ}(W)}{V_f' \frac{S}{\bar{\Phi}} + V_w'} \quad , \quad (4)$$

where primes indicate volume fractions and N° are the true number densities of fuel and tungsten. The effect of Equations (3) and (4) is to decrease the simple volume-weighted number density of the fuel and to increase that of the tungsten, as expected.

THERMØS yields results for the average flux and the average fission cross section in a region. The averages being defined by

$$\bar{\Phi} = \frac{1}{V_k} \int_k d\bar{r} \int_{v_1}^{v_{30}} v N(\bar{r}, v) dv \quad n / (\text{cm}^2)(\text{sec}) \quad (5)$$

and

$$\bar{\Sigma}_f = \frac{\int_k d\bar{r} \int_{v_1}^{v_{30}} v N(\bar{r}, v) \Sigma_f(\bar{r}, v) dv}{\int_k d\bar{r} \int_{v_1}^{v_{30}} v N(\bar{r}, v) dv} \quad \text{cm}^{-1} \quad , \quad (6)$$

where V_k is the volume of a region (shell) k , \bar{r} is the spatial position of points in the region, and v represents the thermal velocities (1 to 30 groups).

For the fuel region, the average values defined above are given in Table 2 as a function of fuel enrichment. The values are normalized by the code to a total source strength of unity (1 n per sec slows down into the thermal region).

TABLE 2. VALUES OF $\bar{\Sigma}_f$ and $\bar{\Phi}$ IN THE FUEL REGION NORMALIZED TO A SOURCE STRENGTH OF 1 AS GIVEN BY THERMØS

| Fuel Enrichment, percent | $\bar{\Sigma}_f$ | $\bar{\Phi}$ |
|-----------------------------|------------------|--------------|
| 10 | 0.4157 | 0.004089 |
| 20 | 0.7415 | 0.003050 |
| 30 | 0.9763 | 0.002503 |

In order to obtain meaningful fission rates, the values of Table 2 must be renormalized to a source strength corresponding to a power level of 2 Mw for the BRR. Since the thermal-neutron profile on the axis of a water-filled test cell (CP-44) of the BRR was measured to define the actual location of the vertical flux peak, as part of the experimental studies for the proposed thermionic diode, it was convenient to use some of these results for normalization purposes. The measured value of the peak thermal-neutron flux in the water-filled test cell was

$$\bar{\phi} = 4.9 \times 10^{13} \text{ n}/(\text{cm}^2)(\text{sec}) \quad .$$

It should be understood that experimental thermal-flux measurements are made through the use of reaction rates and the assumption of $1/v$ absorber. That is,

$$\text{Reaction Rate} = \int \sigma(v) v N(v) dv \quad . \quad (7)$$

Assuming that

$$\sigma(v) = \frac{\sigma_0 v_0}{v} \quad ,$$

where σ_0 and v_0 refer to values at 0.025 ev, the reaction rate, R, is given by

$$R = \sigma_0 v_0 \int N(v) dv = \sigma_0 v_0 \bar{N} \quad , \quad (8)$$

$v_0 \bar{N}$ being defined as the thermal flux and clearly given by the measured reaction rate divided by the detector's absorption cross section at 0.025 ev. This prescription, although usually applied in experimental work, is inconsistent with the THERMØS flux definition. The THERMØS-consistent flux is given by

$$\bar{\phi}_{\text{th}} = \frac{R}{\bar{\sigma}} \quad , \quad (9)$$

where $\bar{\sigma}$ is a spectrum weighted cross section. That is,

$$\frac{\text{THERMØS Consistent Flux}}{\text{Experimental Thermal Flux}} = \frac{\sigma_0}{\bar{\sigma}} = \frac{\bar{v}}{v_0} \quad . \quad (10)$$

As part of the renormalization scheme, a THERMØS run was made mocking up the water filled test cell of the BRR. From the run and Equation (10) above, it was determined that $\sigma_0/\bar{\sigma} = 1.26$. Therefore, the peak flux of the water-filled cell was taken to be

$$\Phi = 6.174 \times 10^{13} \text{ n/(cm}^2\text{)(sec)} \quad .$$

To relate this value to a THERMØS value at that point, an axial correction due to the nonuniform spatial distribution of the flux had to be considered, owing to the one dimensionality of the code. From the experimental results at was estimated that

$$\bar{\Phi} = 0.95 \Phi_{\text{peak}} \quad .$$

The experimental value of the flux, averaged axially at the test cell center was then taken as

$$\bar{\Phi} = 5.85 \times 10^{13} \text{ n/(cm}^2\text{)(sec)} \quad .$$

The THERMØS value of this flux was 0.103 (source strength of unity).

Since the values of the flux at the cell's reflecting boundary were the same for both the water-filled test cell and the test cell with the diode in place, the value of $5.85 \times 10^{13} \bar{\Phi}_N$ can be used as a norm. It follows then that the renormalized value of the flux, $\bar{\Phi}^N$, is related to the THERMØS flux value by

$$\bar{\Phi}^N = \frac{(5.85 \times 10^{13}) \times \bar{\Phi}}{(0.103)} \text{ n/(cm}^2\text{)(sec)} \quad .$$

The total fission rate in the fuel region is given by,

$$\text{Fission Rate} = \sum_f \bar{\Phi}^N V_f \text{ fissions/sec} \quad .$$

APPENDIX C

NUCLEAR MOCK-UP EXPERIMENTS

C.1 Overall Approach

In order to assist in the accurate analysis of required fuel loading for the thermionic diode irradiation, a number of nuclear mock-up experiments were conducted. The tentative assignment in the BRR of Core Position-44 (CP-44), Figure C1, was made for the experiment. Following flux measurements in the water-filled test cell to assist in the renormalization of the THERMOS calculations (Appendix B), the first mock-up experiment was run. This consisted of an aluminum cylinder wrapped in cadmium foil, to approximately simulate the neutron absorption of the actual thermionic fuel element. This permitted the first estimate of the flux profile, both axially and radially, which would be encountered in the irradiation, thus providing important data for the fuel body thermal calculations.

Because THERMOS is a one-dimensional calculation and the revolver fuel element has three-dimensional details, it was considered necessary to evaluate the accuracy of the calculation with a more sophisticated mock-up of the actual revolver fuel body. To do this the fuel body mock-up shown in Figure C2 was used with appropriate absorbers and flux monitors to obtain the desired data. This fuel body was also used to evaluate the expected gamma-heating rate of the fueled revolver in the reactor. These various experiments and results are described in this Appendix.

C.2 Aluminum-Cadmium Mock-up Experiment

For this irradiation a very simple mock-up experiment capsule was used. The nuclear mock-up consisted of a 1-1/2-inch diameter Aluminum cylinder, 8-inches in length, and completely encased in 0.010 inch thick Cadmium sheet. The cylinder was centered within a 2-3/4 inch O.D. stainless steel can with 0.050-inch wall thickness. The center of the cylinder was positioned on the peak of the vertical neutron flux profile, i.e., at 13.5 inches above the grid plate. Flux wires were wrapped around the circumference of the outer can at the 11.5-, 13.5-, and 15.5-inch levels, for a total of three circumferential wires. Two axial

surface wires were also activated, located at 45 and at 225 degrees, relative to the zero reference shown in Figure C1. In addition, a circumferential wire was positioned at the mid-plane of the interior cylinder, directly on the Cd cover.

All aluminum-cobalt dosimetry wire used in these experiments was removed from the same spool of wire. The 0.68 w/o cobalt content was verified by comparison with data from cobalt and gold (bare and cadmium covered) wires irradiated simultaneously in the BRR core. All results from the aluminum/cobalt dosimetry were then corrected by the ratio of the mean of the aluminum/cobalt, cobalt, and gold activities, to the cobalt-aluminum activity only. This ratio was 0.93.

The following data are presented:

- (1) Three peripheral distributions on the outer surface of the 2-3/4-inch O.D. mock-up capsule at vertical positions of 11.5, 13.5, and 15.5 inch above the grid plate (Figure C3).
- (2) One peripheral distribution on the surface of a cadmium-covered aluminum cylinder (8 inch by 1.5 inch in diameter) (Figure C3).
- (3) Three axial distributions in the water-filled test cell, with the control rod in CP 35 withdrawn to 100 percent, 0 percent, and 75 percent. (Figure C4).
- (4) Two axial distributions on the outer surface on the capsule at radial positions of 45 and 225 degrees (Figure C4).

The shapes of the neutron distributions in Figure C3 were not easily interpreted. The curves at the 11.5 - and 13.5- inch positions were quite similar, but the curve at the 15.5-inch position was not similar to either of the other two. These three curves all showed the flux between 315 degrees and 135 degrees to be greater than that between 135 degrees and 315 degrees, as expected. This was not apparent in the distribution around the cylindrical mock-up

of the diode. The orientation of the cylinder in the capsule was not certain and the data may be displaced by some unknown angle. Also, resolution was not good since only five sections could be cut from the peripheral dosimeter wire.

Note in Figure C3 that three extra data points are included at the 45-degree and the 225-degree positions. These are interpolations of the two axial distributions on the surface of the capsule, taken from Figure C4, and represent intersections of the peripheral and axial wires. Five of the six points fall exactly on their respective curves.

The ratios of maxima to minima for the four peripheral distributions of Figure C3 were less than 1.30. For each distribution, the average flux was determined and the deviations of the maximum and minimum points from the average were found. The mean deviation was 13 percent. Therefore, it can be said that the neutron flux incident on the diode capsule will vary no more than ± 13 percent from the radial average at any axial position.

Figure C4 suggests only slight depressions in the flux peak, both in position and in magnitude, as the control rod in CP 35 is driven from the 100 percent to the 75 percent position. The ratios of maxima to minima for the two axial distributions on the capsule, Figure C4, are less than 1.25. The mean deviations of the maximum and minimum points from the average was 10 percent. Therefore the flux will vary no more than ± 10 percent from the axial average at any radial position.

Figure C5 indicates the flux distribution in the cell as predicted by THERMOS, for three relative values of enrichment. (Absolute magnitudes are not available for this calculation due to an error in the program).

C.3 Revolver Mock-Up Experiment

The basic plan for this experiment was to use the first tungsten revolver to be machined together with suitable absorbers and flux monitors within the fuel holes. The revolver had been made deliberately oversized in the outer diameter with the intention of finish-grinding the O.D. after the experiment.

This would be a closer simulation of the converter with tungsten-rhenium secondary container and tungsten-foil thermal shielding in place.

It was originally planned to line the fuel holes with thin foil of depleted and enriched uranium, so that the relative volume of each could be well controlled. The enriched foils would then be monitored after irradiation, for the most direct and accurate measure of actual fission density. This approach, however, was found to be too costly, as was the use of UO_2 powder.

The approach finally adopted used mixtures of boron carbide and graphite in various proportions as the absorbing materials. The dosimetry was done by locating small fully-enriched uranium foils at the midplane of each of the six columns of powder in the fuel holes.

Remote handling was required for unloading and reloading between runs owing to the fairly high gamma dose rates from the short half-life tungsten isotopes

Similar uranium foils were irradiated simultaneously in the thermal column in a known thermal-neutron flux to normalize the count rates from the mock-up foils to an absolute fission rate. In addition, two axial flux monitors were attached to the outside diameter of the tungsten body.

The tungsten body was centered in the stainless steel can used for previous dosimetry experiments. Plugs were provided to hold the column of powder in place.

Powder mixtures to simulate fuel enrichments of approximately 5, 10, and 15 percent were used. One uranium foil (0.375-inch O.D. x 0.001-inch thick, 93 percent enriched) was loaded at the center of each of the six fuel columns in the body. The plane of these foils was located 13.5 inch above the reactor grid plate. The fuel simulation irradiations were conducted in Test Cell 44 of Core 70 (which also included Test Cells 17 and 47).

Control Rod 4 (CP 35) was positioned at 75 percent during the irradiations to match the most likely of the three conditions shown in Figure C4. Using the same reference orientation as shown in Figure C1, the six fuel columns were numbered one through six, starting with one at the zero reference and proceeding counterclockwise.

Reactor power levels were determined from the $^{17}\text{N}/\text{BF}_3$ power monitor, from gold normalizing foils, and from an RSN-202 self-powered neutron detector. Agreement was generally within 5 percent. The fission rates in the foils were determined by comparative gamma-counting techniques, using a foil irradiated in the thermal column as a standard. The fission rate in the standard foil was calculated from the thermal neutron flow reduced by a self-shielding factor calculated for the foil. The fission rate in the standard foil obtained through an independent radio-cesium determination agreed within 5 percent with that calculated from the measured neutron flux.

Table 1 lists the specific fission rates in each of the six uranium foils for each of the simulations, and also the effective thermal neutron flux seen by each foil.

Table 1. Fission Rates and Effective Fluxes Measured by Uranium Foils

| Fuel Column | Nominal Fuel Enrichment Simulation | | |
|-------------|---|------|------|
| | 5% | 10% | 15% |
| | Fission Rate, 10^{-10} f/(sec)(atom) ^{235}U | | |
| 1 | 11.3 | 8.79 | 6.95 |
| 2 | 10.8 | 7.65 | 6.43 |
| 3 | 9.39 | 7.21 | 6.06 |
| 4 | 9.10 | 8.16 | 6.62 |
| 5 | 9.99 | 8.98 | 7.63 |
| 6 | 11.0 | 9.67 | 7.98 |
| | Effective Flux, 10^{12} n/(cm ²)(sec) | | |
| 1 | 1.95 | 1.51 | 1.20 |
| 2 | 1.85 | 1.31 | 1.10 |
| 3 | 1.61 | 1.24 | 1.04 |
| 4 | 1.56 | 1.40 | 1.14 |
| 5 | 1.72 | 1.54 | 1.31 |
| 6 | 1.89 | 1.66 | 1.37 |

Figure C6 shows the following data:

- (1) The thermal-neutron-flux profile on the axis of the water-filled Test Cell 44, using one cobalt wire (Control Rod 4, in CP 35, was at 47 percent for this irradiation).
- (2) The thermal neutron flux on the surface of the tungsten, using five peripheral cobalt wires during the irradiation of the 10 percent fuel simulation.
- (3) The thermal-neutron-flux profile on the axis of the tungsten, using one central cobalt wire during the 10 percent irradiation.
- (4) The thermal neutron flux on the periphery of the stainless steel capsule at 13.5 inch during the 5 and 15 percent irradiations, using one peripheral cobalt wire for each case.
- (5) The fast neutron flux (> 0.1 Mev) profile on the axis of the tungsten, using one central nickel wire during the 10 percent irradiation.

In the mock-up tests, the six "fuel" cylinders in the capsule were filled with different mixtures of B_4C and graphite to simulate certain UO_2 enrichments. The loadings corresponded to 4.5, 9.4, and 16.2 percent enrichments, respectively, based on a 0.025-ev absorption-cross-section equivalence. Six thin foils of ^{235}U were placed at the midplanes of the "fuel" columns. Fission rates per atom of ^{235}U were then obtained for each of the B_4C loadings.

The mock-up experiment was simulated by the use of the THERMOS code. The fission powers computed by THERMOS were based on the assumption of (1) 180 MeV per fission, (2) an experimental flux at the center of the water-filled test cell of 4.4×10^{13} n/(cm²) (sec), and (3) an average-to-centerline flux in the capsule of 1.1. The latter two values were measured during the mock-up run.

The experimental results and the calculated results are compared in Table 2 and are shown in Figure C7. A maximum difference of less than 5 percent between the THERMOS predicted fission power and the experimental one is indicated for the B_4C mock-up cases.

| ^{235}U % Enrichment (B_4C , Mock-up) | Experimental Fission Rate, ^(a) $10^{-10} \text{ f / (sec) (atom)}^{235}\text{U}$ | THERMOS Fission Rate, $10^{-10} \text{ f / (sec) (atom)}^{235}\text{U}$ |
|--|--|--|
| 4.5 | 10.26 | 9.95 |
| 9.4 | 8.41 | 8.1 |
| 16.2 | 6.93 | 6.657 |

(a) The experimental fission rates were averaged over the six fuel columns.

These results lent confidence to the use of the THERMOS code for the revolver configuration, therefore, THERMOS runs were also made for the actual uranium-fueled thermionic device and capsule, both for an all-tungsten cylinder and for a tungsten-rhenium cylinder. The difference in fission power calculated for the B_4C mock-up and the actual fueled case can be attributed mostly to the fact that the tungsten cylinder used in the mock-up was larger in diameter (by 1/4 inch) than that to be used in the actual test. The substitution of B_4C for UO_2 fuel also contributed to the difference.

It may be seen from Figure C7 that for a tungsten cylinder, an 8.0 percent enriched fuel should be adequate to give the desired fission power of 4350 watts (assuming that THERMOS underpredicts the fission power by about a maximum of 5 percent, as was shown experimentally). The gamma power was estimated at 1010 watts, giving a total power of about 5360 watts for the capsule (see Appendix A). (Use of a tungsten-rhenium cylinder requires an enrichment of about 25 percent for the same power generation.) A final adjustment to the enrichment was made based on the actual fuel loading. The THERMOS calculation was based on a smear fuel density of 70 percent of theoretical, including all voids in the fuel holes. Actual smear density was 57 percent of theoretical UO_2 density. To maintain the same total U-235 inventory, an enrichment of 9.0 percent was finally specified.

C.4 Neutron Flux Profiles

A nickel wire dosimeter was used for the fast-neutron-flux (neutron energy above 0.1 Mev) distribution in the same facility at 2MW. The integral flux measured by the $^{58}\text{Ni}(n,p)$ threshold reaction was corrected to total integral flux above 0.1 Mev

by the Cranberg energy spectrum of fission neutrons. The maximum flux is 1.8×10^{13} n/(cm²)(sec), unperturbed. The observed ratio of perturbed to unperturbed fast flux is 0.67. The fast flux at 100 inches above the grid plate is 3×10^8 n/(cm²)(sec).

The thermal-neutron-flux distribution was not measured, but the thermal flux is estimated to be 1.5×10^{13} n/(cm²)(sec) at the peak and 1×10^9 n/(cm²)(sec) 100 inches above the grid plate. The thermal-flux distribution will be very sensitive to components of the experiment assembly during an in-pile operation.

This information coupled with available data on radiation effects on materials was adequate to permit the selection of materials and components for the in-pile experiment.

C.5 Gamma Flux Profile Experiment

The gamma-flux profile from the core centerline to a distance of 100 inches above the grid plate was determined, to serve as a basis for the selection of the required materials for instrumentation lead-out insulation and vacuum seals for a 10,000-hour irradiation. The gamma-flux distribution was measured in an aluminum mock-up of the proposed test section for the diode irradiation. The mock-up capsule was irradiated in CP-33 to determine two axial distributions: the residual (i. e., fission product) gamma at zero reactor power, and the gamma at full reactor power (2MW). These data are shown in Figure C8.

A 10-cm³ graphite-wall ionization chamber was used for the gamma measurements. This chamber had been calibrated in a gamma irradiation facility using chemical dosimeters. The chamber was maintained at a 500-volt potential with one atm of CO₂ fill gas. The gamma exposure rate up to 40 inches above the grid plate was too intense for measurement at full power. These data were obtained at 40 KW as determined from reactor instrumentation, and extrapolated to 2 MW; data above the 40-inch position were obtained during 2-MW operation. The reactor was operated at both of these power levels for about one hour to allow short-lived fission products to approach saturation. The maximum gamma exposure rate is 1.4×10^8 rads (carbon)/hr at 14 in. above the reactor grid plate.

The residual gamma data were normalized to the 2MW data at 16 inches above the grid plate for a comparison of the distributions. The more rapid rate of decrease of the residual gamma may be due to a difference in the energy spectra of the residual- and prompt-gamma sources. It was estimated that the residual gamma is 3×10^7 R/hr 14 inches above the grid plate immediately after reactor shutdown, and that it averages 1.5×10^6 R/hr during a 3-day BRR cycle shutdown. Therefore the gamma dose accumulated during reactor shutdown is 0.2 percent of that accumulated during full-power operation. The external gamma radiation (i.e., the gamma penetrating the water shield and incident on the capsule wall) is estimated to account for 50 percent of the total gamma observed at 85 inches above the grid plate and 25 percent at 100 inches. The experimental assembly in the final capsule design will tend to increase these fractions because of greater shielding of the direct component of the total gamma radiation.

From the data obtained, the gamma energy deposited at the assembly plate will total 10^{10} ergs/g (carbon). Therefore, instrumentation and thermocouple leads will have to be sleeved with ceramic tubing for most of the distance to the assembly plate. Above this point it should be possible to use standard PVC insulation.

C. 6 Tungsten-Emitter Gamma Heating Experiment

The heat generated in the tungsten emitter by the gamma flux during the irradiation is a significant fraction of the total heat which must be removed from the diode and will strongly influence the operating temperatures of the emitter. Therefore, the total gamma heat had to be defined more accurately. However, owing to the complex geometry of the revolver, the heating rate could not be calculated reliably.

Consequently, an in-pile experiment was conducted in the BRR to evaluate the gamma heating rate. The O.D. of the tungsten revolver employed in the nuclear mock-up experiment was ground to 1-1/2 inch diameter and was instrumented with Chromel-Alumel thermocouples. It was suspended on a 1/16-inch stainless steel rod and was centered within the stainless steel can

used for the nuclear mock-up experiment. The fuel-bearing holes were filled with a mixture of metal powders simulating the smear density of the UO_2 fuel. The thermocouples extended to above the surface of the pool through the lead tube. The container and lead tube were evacuated and sealed.

The experimental data were obtained by inserting the experiment in the CP-44 facility 48 hours after the start of the reactor shutdown period; the rate of temperature rise with time owing to the predetermined residual gamma flux was monitored. The thermocouples were connected to a high-speed multi-channel chart recorder. The temperature was expected to rise to about 900°F in a gamma flux of 2.5×10^6 R/hr.

The gamma heating experiment, as described, did not yield satisfactory results owing to the long time required for the small heat addition to raise the temperature of the body. The experiment was rerun with the following revisions: (1) the revolver was exposed to an air environment, (2) a small heater was axially aligned within the centerline hole, and (3) Chromel-Alumel thermocouples were attached to the O.D. of the revolver at the axial center in three azimuthal positions. The experiment was placed in CP-44 of the BRR and the revolver surface temperature equilibrated at 320°F . All thermocouples indicated temperatures within 2 degrees of each other. Figure C2 is a photograph of the gamma-heating experiment as it finally evolved.

The experiment was then removed from the core position and the heater was employed to heat the revolver. Equilibrium temperature data points at heater power inputs between 15 and 45 watts were obtained. The curve through these data points indicated that the 320°F surface temperature was obtained with a heat generation of 27 watts. The gamma flux in the facility was measured immediately after the heating experiment was removed. Using the ratio of the full-power gamma flux to the measured residual gamma flux, the predicted gamma heat-generation rate for the fuel and tungsten revolver is 1010 watts. This is equivalent to the value used in the computer-program evaluation to determine the required fuel enrichment. Thus, it appears that the calculated gamma heat generation was reasonably accurate and no change was required in the fuel enrichment.

APPENDIX D

THERMAL STRESS ANALYSIS BY THE BOUNDARY POINT LEAST SQUARES APPROACH

The stresses for the emitter body based on the temperature distribution shown in Figure 12, assuming all heat generation occurred in the fuel, were evaluated by computer-program techniques. The boundary-point least-squares approach was used. This method was developed for the computer solution of types of problems for which formal solutions are developed in series form. Battelle had developed computer programs utilizing this method for analyzing stresses in various types of bodies under both thermal and mechanical loads. To calculate stresses in structures with circular holes, it was desirable to use a series of polar harmonic and biharmonic functions. Harmonic functions were used for the temperature solutions, while both harmonic and biharmonic functions were used to obtain solutions for the stresses.* Such functions were most conveniently obtained as the real and imaginary parts of the complex power series in z . Thus, the general harmonic series for the temperature was obtained as the real part of the series,

$$F(z) = A_0 \log z + \sum_{n=1}^{\infty} \left[A_n z^n + A_{-n} z^{-n} \right]$$

where the complex constants are written as $A_n = a_n + ib_n$ and $A_{-n} = a_{-n} - ib_{-n}$, so that in real notation

* Although the temperature distributions were already known from a finite-difference calculation, application of the current technique for thermal stresses is most convenient when the temperatures are obtained in series form.

$$T(r, \theta) = A_0 \log r + \sum_{n=1}^{\infty} (a_n r^n + a_{-n} r^{-n}) \cos \theta + \sum_{n=1}^{\infty} (b_n r^n + b_{-n} r^{-n}) \sin \theta.$$

The corresponding stress-function series is somewhat more complicated. It may be found in most elasticity books (e.g., Timoshenko, S., and Goodier, S., Theory of Elasticity). The complex form is written as

$$\begin{aligned} \Phi(r, \theta) = & A_0 \log z + \bar{z} (B_0 z \log z + C_0 z) + A_1 z \log z + A_{-1} \bar{z} z^{-1} \\ & + \sum_{n=2}^{\infty} [(A_n + \bar{z} C_n) z^n + (A_{-n} + \bar{z} C_{-n}) z^{-n}] \end{aligned}$$

To solve for the temperature and stress in a multiholed region it is necessary to use one series expanded about the center of each hole. The coefficients of all of these series must then be determined so that the boundary conditions on the hole and on the outside boundary are all satisfied.

The boundary-point least-squares technique provides a numerical procedure for satisfying all of the boundary conditions simultaneously. Truncated series forms are used in which the infinite upper limits on the sums are replaced by finite numbers. The boundary conditions are approximately (but accurately) satisfied.

The boundary-point least squares technique consists of choosing a set of points distributed on the boundary of the region and requiring that the solution meet the boundary conditions in the least squares sense at all of the selected boundary points. This leads to a system of simultaneous equations which is solved for the coefficients of the series. Knowing the series then permits calculation of the temperatures and stresses everywhere.

The transverse temperature distribution in the revolver fuel element was first calculated by a finite-difference thermal analysis program, using $r-\theta$ geometry. The resultant temperature profile of the emitter hole and fuel hole boundaries is shown in Figure D1. To carry out the thermal stress

analysis, it is first necessary to match these boundary temperatures with a series expression for the temperature field. By using a specially combined series form, it is possible to create a series solution with sixfold symmetry about the center of the emitter hole, so that boundary conditions need only be matched over the basic 30-degree symmetry element shown in Figure D2.

The temperature boundary conditions were matched everywhere on the holes to within less than 0.1°C, and the zero gradient condition on the outer edge was matched with a maximum error of 3.5×10^{-3} C/in. compared to a gradient on the center hole of $2.8 \times 10^{+2}$ C/in. Thus, it is evident that the temperature solution was obtained with sufficient accuracy.

The Battelle thermal stress computer program automatically calculates the thermal stresses using the series solution for the temperature as input. To make this calculation, material properties were evaluated at 1760°C.

Poisson's Ratio (ν) = 0.3

Young's Modulus (E) = 2.7×10^7 psi

Thermal Expansion Coefficient (α) = 6.84×10^{-6} /C

It was assumed that the region had no external loads acting on it. Thus, the boundary conditions assumed for the holes and the exterior boundary were $\sigma_n = \tau_{nt} = 0$, where σ_n is the normal boundary stress and τ_{nt} is the tangential boundary shear stress. These boundary conditions were satisfied with a maximum error of 18 psi in σ_n and 10 psi in τ_{nt} .

The maximum tensile hoop stress σ_θ on the boundary of the center hole was found to be 8440 psi. The maximum hoop stresses on the off-center holes were 16,100 psi compression and 5900 psi tension. The stresses on the outside edge varied from 7800 psi compression to 3400 psi tension. On the basis of experience in performing many similar analyses it is believed that these values are accurate to within 50 psi if the assumed material constants are accurate.

The tangential stress distributions on the center hole and outside edge are shown in Figure D3 as functions of the central angle θ_1 . The tangential stresses on the off-center hole are shown in Figure D4 as a function of the angle θ_2 measured from the hole center (see Figure D2).

The combined effects of the variation in temperature and hole interactions are easily seen. The large compressive stresses in the thin outer web and the corresponding tensile stresses in the inner web are the result of the temperature variations. The seemingly anomalous variation in stress on the boundary of the eccentric hole is a result of stress interaction with the neighboring holes.

The stresses arising from the temperature differences will be quickly relieved by creep at the operating temperature. For the temperature distributions considered here the deformations are probably 0.0001 inch or less (particularly in the central hole, the region of greatest concern for dimensional stability). Choice of alternative materials will not reduce this deformation since the creep strengths of other tungsten alloys is not markedly greater than that of tungsten. Data (2, 3, 4) on the creep rate of tungsten, tungsten-1 percent thoria and tungsten-7 percent rhenium are shown in Figure D5. It can be seen from this plot that little improvement in creep strength can be achieved even by selecting the most creep-resistant tungsten alloys known.

Since the very small deformations noted above will be experienced during each temperature cycle from room temperature to the operating temperature and back, it appears that, if possible, heaters should be incorporated into the design to reduce the thermal cycling to a minimum. This will tend to keep the total distortion of the refractory fuel-containing body within reasonable limits even during long-term operation.

REFERENCES

1. "The Engineering Properties of Tungsten and Tungsten Alloys", DMIC Report 191, September 27, 1963.
2. Klopp, W.D., et al., "Mechanical Properties of Ductile Tungsten-Rhenium Alloys", NASA TN D-3483 (September 1966).
3. Flagella, P.N., "High Temperature Creep-Rupture Behavior of Unalloyed Tungsten", GEMP-543 (September 1967).
4. Sell, H.G., et al., "Physical Metallurgy of Tungsten and Tungsten Base Alloys", Progress Report to USAF ASD on Contract AF33(657)-8247 (February 1964).

APPENDIX E

HYDRAULIC-ELECTRIC DESIGN DETAILS

E.1 Introduction

Because the water coolant lines to the converter also serve as the current-carrying conductors for the diode electrical load, both the hydraulic and electric requirements must be simultaneously satisfied. Fortunately, these are not in conflict, since in general both are improved as sizes are increased. However, in the diode region of the capsule, the fixed diode and capsule dimensions, all basically limited by the size of the core test position, required a number of design compromises.

Originally, three cooling loops were provided: diode collector, upper emitter flange and lower emitter flange. (The emitter flanges act as emitter power take-offs in this double-ended design). The cesium reservoir was to be cooled by the collector coolant. However, out-of-pile testing of the converter showed the necessity for a separate insulated coolant line for the cesium reservoir (Section E.4). When it was subsequently decided to cool the fission gas accumulator as well, these two functions were combined into a fourth cooling loop.

The assembly plate and, therefore, the entire test capsule assembly is set at the potential of the upper end of the fuel body, via the fission gas vent tube and the fission gas accumulator. Therefore, all other conductors must be insulated from all parts of the test capsule.

Each of the coolant tubes is electrically insulated throughout the system. In the diode region this is accomplished by ceramic sheath tubes; at the vacuum interface the assembly plate is fitted with ceramic-metal tube adapters; above the assembly plate the coolant tubes are sheathed in polyolefin shrink tubing. Where the tubes are unsheathed, they are separated by insulated stand-offs.

E.2 Hydraulic Design

The hydraulic design was governed by four somewhat conflicting constraints:

- (1) Keeping the flow velocity low enough to insure long-term tube integrity
- (2) Keeping the flow rate low enough to avoid excessive pressure drops
- (3) Having a high enough flow velocity in the heated regions to reduce the film temperature drop and avoid film boiling.
- (4) Having a high enough flow rate to keep the outlet temperature of the coolant significantly below its boiling point.

Generally, because the heat transfer regions are short compared to the total length of coolant lines, the approach which suggests itself is to reduce the film drop by increasing flow velocity in the heat transfer regions, while keeping total pressure drop within reason by reducing flow velocity elsewhere. This is accomplished simply by enlarging the flow area wherever possible outside the active diode regions and by providing enough driving pressure head to produce the desired flow rate within the active regions.

The most critical region for film temperature drop is the diode collector coolant tube. This must conduct the main diode reject heat, approximately 3500 watts, more than 100 watts per cm^2 of tube surface area. For long term reliability it was decided that flow velocity within the diode should be limited to a maximum of 20 feet per second, although in the 3/16-inch riser tube alongside the diode the flow area is somewhat smaller and the flow rate is 24 feet per second. This leads to a Reynolds number of approximately 20,000, and a Fanning friction factor of 0.007 (average for commercial tubing), yielding a heat transfer coefficient of 3500 BTU/hr-ft-°F and a film temperature drop of 67°C.

This is an acceptable film drop. In tests conducted on a simulated collector-cooling system at a collector temperature of 700°C, a heat transfer rate of 4300 watts was achieved at a flow velocity of only 8 ft/sec, corresponding to a computed film temperature drop of 120°C. Even at this high film drop, the coolant flow was stable, with no evidence of boiling.

Based on the friction factor previously noted, the pressure gradient in the diode region is calculated at 6.0 psi per foot of length. Above the diode region, transition to 3/8 x .042 (O.D. x wall thickness, in inches) tubing reduces the pressure gradient to 0.41 psi/ft. Therefore, total pressure drop in the collector loop for lengths of 3.5 and 60 feet of 3/16- and 3/8-inch tubing, respectively, is 46 psi.

The emitter cooling circuits must conduct the emitter flange heat load, which is estimated at 750 watts. Although the coolant tubes are 1/8-inch O.D. in the active region and, therefore, the heat transfer area is small, the heat transferred per unit area is less than that of the diode collector, and hence the film drop is also less. At a flow rate of 10 ft/sec the $\Delta T_{\text{film}} = 50^\circ\text{C}$.

Within the 1/8-inch tubes the pressure gradient at a flow rate of 20 ft/sec is calculated at 13 psi/ft. For the lower emitter, the 1/8-inch tubes extend downward for an additional one-foot below the upper emitter flange, or a total of two feet of additional circuit length. Therefore, the pressure drops for the upper and lower circuits is calculated at 34 and 60 psi respectively, again assuming transition to 3/8 x .042 tubing a few inches above the diode. During the in-pile test, proper flow distribution will be regulated by throttle valves.

E.3 Electric Design

The electric limitations on the coolant lines result from the desire to keep power dissipation within the conductors low, in order to minimize:

- (1) Power supply size and cost
- (2) Total heat which must be transferred to a heat exchanger
- (3) Temperature rise of the coolant water.

This dictated that all current-carrying water tubes be made of copper, preferably high-purity high-conductivity copper, and that the tube wall thickness be maximized within the limitations of reasonable cost and weight. The basic decision was to use the 3/8 x .042 Oxygen Free High Conductivity (OFHC) copper tubing above the diode region, with a calculated resistance of 0.19 milliohm per foot of length.

Adding the resistances of all tubes leads to the predicted voltage drops shown in Table 1. Since the two ends of the converter are connected to a common power supply, additional lead resistance (outside the vacuum chamber) will have to be added to the upper circuit for balancing the two terminal voltages.

Table 1. Calculated Voltage Drops in Water-Cooled Conductors
(I = 500A, each end)

| | Top | Bottom |
|-----------|-------|--------|
| Collector | 3.0 | 3.9 |
| Emitter | 1.6 | 2.0 |
| Total | 4.6 V | 5.9 V |

The power supply must be capable of producing the total power dissipated in the coolant lines, less the power generated by the diode. The power supply was specified as 0-10 volts, 1000 A total current. The total temperature rise in each coolant loop is determined by adding the diode-supplied heat and the heat dissipated throughout the conductor lengths as a result of the voltage drop shown in Table 1. At the design flow rates, this is approximately 20° C for each loop. Table 2 summarizes the thermal-hydraulic data discussed above.

Table 2. Summary of Coolant Data

| | | Collector | Emitter Flange (upper) | Emitter Flange (lower) |
|----------------------------|--------------------|-----------|---------------------------|---------------------------|
| Water Flow Rate | GPM | 1.30 | 0.35 | 0.35 |
| Water Δp (two way) | PSI | 46 | 33 | 60 |
| Heat Load | | | | |
| through diode | watts | 3300 | 1000 | 1000 |
| distributed | watts | 3500 | 825 | 1000 |
| Total | watts | 6800 | 1825 | 2000 |
| Water ΔT (Total) | $^{\circ}\text{C}$ | 20 | 20 | 22 |

E.4 Cesium Reservoir Cooling

In the original design, the cesium reservoir was to be cooled by a rigid clamp connecting it with the incoming collector coolant line through a calibrated conductor strap. As a result, the cesium reservoir appendage provided a parallel current path to the lower collector. It was calculated that at 500 amperes lower collector current this would produce an additional 60 watts of heat, of which half, a maximum of 30 watts, would be conducted to the reservoir cooling strap. The conduction heat load from the end of the collector was calculated at only 7 watts, but some 40 watts were expected from gamma heating in-pile. Therefore the cooling strap was sized for 100 watts, in order to produce the desired slightly over-cooled condition which would permit precise temperature control of the cesium reservoir with only small heater power.

During the out-of-pile test it was seen that the reservoir cooling was barely adequate with a diode current of 300- to -400 A, even without the expected gamma heating. This was due in part to a design change which had introduced more thermal and hence electrical resistance into the collector thermal baffle, and in part to poor contact conductance of the cooling clamp. This latter was

improved by a slight redesign of the clamp which permitted greater clamping force on the reservoir, and by specifying that the other end of the clamp be brazed rather than clamped onto the coolant tube. Although the heat transfer was thereby improved, the reservoir temperature would still follow the diode current, introducing a feedback effect on diode performance which made it difficult to optimize parameters and was frequently destabilizing. Therefore, the decision was made to uncouple the reservoir cooling function from the diode cooling-power-take-off system. For this purpose a fourth pair of insulated water feedthroughs was provided at the assembly plate.

It was subsequently determined that, without some form of conduction cooling, the fission gas accumulator and pressure transducers would run too hot, simply from gamma heating estimated at approximately 60 watts for the accumulator. However, fabrication of the assembly plate was already at an advanced stage, and no additional space for water tube feedthroughs was available. Therefore, it was decided to place the accumulator cooling in series with the cesium reservoir cooling, provided some method of electrically insulating the two could be found. Glass-metal tube connections were available but deterioration of the glass in the nuclear field could occur before 10,000 hours. Ceramic metal seals would have to be made to order and could crack on brazing.

As an alternative, it was determined by measurement that a three-foot length of 3/16 O.D. by .020 wall, type 304 stainless steel tubing has a resistance of 120 milliohms. The potential difference between the accumulator (fission gas vent tube) and cesium reservoir (lower collector) is approximately the diode voltage (0.6 volt), so that 5 amperes would flow if the two were joined by an uninterrupted length of such tubing. Although this would produce excessive temperature rise in an electrical connector cooled only by conduction to the ends, the 3 watts so dissipated in a water-cooled tube is entirely trivial. Therefore, this was the approach adopted to cooling both the accumulator and cesium reservoir.

REFERENCES

1. Bonilla, C.F. (ed.), Nuclear Engineering, McGraw Hill, 1957.
2. Etherington, Galbraith (ed.), Reactor Engineering Handbook, 1952.

APPENDIX F

ELECTRON-BEAM WELDING OF REFRACTORY METALS

This appendix presents a paper delivered at the 1970 IEEE Thermionic Conversion Specialist Conference, reviewing the EB-welding experience under this program in greater detail than the description offered in Section 4.3.

ELECTRON BEAM WELDING OF TUNGSTEN TO TUNGSTEN/RHENIUM AND TUNGSTEN/RHENIUM TO NIOBIUM*

B. Raab, A. Schock
Fairchild Hiller Corporation/Republic Aviation Division
Farmingdale, New York 11735

INTRODUCTION

The assembly of an external-fuel revolver fuel element and converter, which is described in another paper¹ of these proceedings, requires a number of refractory-metal weldments to be made. In particular, the tungsten revolver is sealed by tungsten-rhenium end caps, one on each end. These in turn are welded to the niobium-1% zirconium sleeves of ceramic-metal seals. All of the remaining joints enclosing the diode are niobium-to-niobium welds of a more standard nature.

Only limited experience exists in welding to tungsten or tungsten-rhenium, especially in attempting to hermetically seal a fuel body of the size of the tungsten revolver. Also, a reliable transition from the tungsten revolver to the niobium-alumina seal was sought which would not require the introduction of transition materials such as tantalum. Tantalum is more vulnerable to oxidation corrosion than either of the materials to be joined.

Empirical solutions were sought which could be readily incorporated into the assembly procedure and tested in actual service. In general, weld specimens were prepared and examined metallographically for most of the critical joints prior to converter usage.

All welding was performed on a high-voltage Hamilton Standard electron beam welder. The results of these trials, together with the actual converter assembly results are reported here.

TUNGSTEN AND TUNGSTEN/RHENIUM

The tungsten revolver fuel element is sealed by a tungsten/25% rhenium end cap, in the geometry shown in Figure 1. Two welds are needed: an axial weld, i.e., with the electron beam parallel to the axis of the revolver, to seal the inner boundary of the fuel chamber, and a radial weld orthogonal to the first, to seal its outer boundary.

Early trial welds were made with powder-metallurgy wrought tungsten (PM-W) fuel billet specimens (GE-13). These consisted of short (~ 1 inch high) cylinders with the emitter hole and end configuration machined. Prior to receipt of the powder-metallurgy tungsten/rhenium (PM-W/Re) material, a number of trial welds were made with the same powder-metallurgy tungsten used for the end cap as for the fuel body specimen.

The earliest trials confirmed the results of other investigators as to the extensive brittle fracture of such tungsten welds made without any special precautions. Successful hermetically-sealed welds of the same PM-W materials were then made by pre-heating the specimen prior to welding. This was done by heating the specimen with the electron beam of the welder until the entire specimen was brought to a visible color. For this purpose the

* This work was performed for the Jet Propulsion Laboratory, California Institute of Technology, sponsored by the National Aeronautics and Space Administration under contract NAS 7-100.

beam was defocused and electronically swept in a circle at a frequency of 60 hertz and a diameter of approximately 1/2-inch. For the axial weld pre-heat the circular beam was applied interior to the joint, i.e., over the emitter lip and into the emitter hole. For the radial weld the revolver was rotated at four-to-five times the normal welding speed and the beam was applied a short distance from the joint, perhaps 1/2-inch. Following the weld a short period of post-heat was applied in the same manner.

Joints made by this method were still leaktight after 20 and 40 thermal cycles to 1800°C. Upon metallographic examination the joints were seen to contain voids in the weld zone and along the fusion zone boundary, typical of welds with the PM-W material (Figure 2).

Upon receipt of the tungsten-rhenium material, similar weld samples were prepared using the PM-W for the revolver specimen and the PM-W/25Re for the end cap. Sound hermetic welds were made using the electron beam pre-heat technique described previously. In cross-section, however, these joints were seen to contain extensive porosity in the fusion zone boundary, including voids clearly visible to the unaided eye (Figure 3). This could perhaps be attributed to extensive porosity in the tungsten-rhenium as delivered (this is more clearly visible in Figure 5), combined with the inherent nature of the PM-W material to agglomerate voids.

Although sound welds were achieved, the long term reliability of these joints was thought to be compromised by the extensive porosity in the fusion zone boundary. Consequently, the first full size revolver for converter use was fabricated from vacuum arc-cast and hot-extruded tungsten (AC-W) which was known to be more weldable although larger-grained and somewhat more brittle than the PM-W material.

The first welds to the AC-W revolver were made using the same electron beam pre-heat technique which had been successfully applied to the PM-W welds. Although the welds produced in this manner were sound, leaks were detected in the tungsten at the pre-heat zone. The surface appearance of the pre-heat zones was clearly abnormal, appearing either crazed or mottled upon close examination (Figure 4).

Cross-section examination of these joints revealed little to explain the unusual surface appearance (Figure 5). Although grain growth was clearly visible in the radial pre-heat zone, this was not apparent in the axial pre-heat zone. Figure 6 shows another cross-section of this axial weld with an electroetched surface preparation. The cross-section showed that the joint itself was satisfactory, with good alloying and without the extensive void development previously seen in the PM-W to PM-W/Re specimens.

Figure 5 clearly shows the void density in the as-delivered PM-W/Re, and the manner in which it varies within the material. The tungsten-rhenium end cap was fabricated from cylindrical rods 1.5-inches in diameter. Apparently the method of preparing and working these rods results in much higher void density toward the axial center than toward

the outer surface of the rods.

Whatever the reason for the unusual surface appearance of the AC-W and the resultant leaks, for which the authors invite explanation, the cause was clearly the pre-heat electron beam. Subsequent welds, therefore, have been made by pre-heating with a resistance furnace in the electron-beam welder. Although this complicates the set-up and fixturing of the workpieces, and the weld-chamber is tied up for several hours on each weld, all welds made since adoption of the furnace pre-heat method have been satisfactory. A total of eleven joints have been made; most have undergone extensive thermal cycling and some aging in converter application without a single failure to date.

The resistance furnace pre-heat has also been employed for PM-W/Re to PMW/Re welds in the emitter flange to end cap joint¹ with good success.

Table I summarizes the welding experience with tungsten and tungsten/rhenium as discussed above.

NIOBIUM TO TUNGSTEN RHENIUM

In common with most high-temperature thermionic converters, it was necessary to devise a joint between the tungsten or tungsten alloy emitter lead and the niobium (in this case Nb/1Zr) seal extension.

Because in this case the emitter lead is PM-W/Re, which some reports have indicated to be more weldable than pure tungsten, first attempts were made to weld a niobium tube directly onto the W/Re sleeve. The niobium tube was thin-walled (.015-inch) so that thermal stresses would be relieved by yielding of this ductile member. Figure 7 shows a weld of this type. The weld initially was sound. Although service temperature for this joint is normally 500 to 700°C, because of its critical nature, the specimen was thermally cycled to 1000°C. No leak was detected following five thermal cycles; however, after 20 thermal cycles a leak was detected and a crack was visible in the weld-zone.

The decision was then made to attempt to develop a so-called "self-braze", in which the niobium member is melted by the electron beam without melting of the tungsten/rhenium, thereby retaining the room temperature ductility of the latter.

This required a thicker seal extension to provide for penetration of the electron beam and to enlarge the effective area of the braze seal. Figure 8 shows a typical specimen with the parameters that were ultimately developed for this seal. The 15-degree beam angle was selected so that the base of the melt zone would correspond to the base of the joint, thus providing the largest possible seal area for this type of joint. The double pass was used to increase the size of the seal area at the back of the joint. Note that at the left side of the same cross-section the fusion zone in the niobium is barely detectable, except by the distortion of the outer surface.

This specimen was leaktight and withstood 20 thermal cycles to 800°C without failure.

In actual application this joint is doubly sealed. Following the electron beam self-braze and validation of leaktightness, a vacuum rf-induction braze of a palladium/nickel/silver alloy is applied as shown in Figure 9. This specimen, using an actual seal and end cap, successfully withstood 12 thermal cycles to 800°C and an additional 12 thermal cycles to 1000°C.

An additional four such joints have been made for converters and have undergone numerous thermal cycles, both in qualification testing and in converter testing, without failure. In general, not one failure of such a joint has been experienced to date.

Because of the apparent reliability of this joint, it was decided to attempt to make a similar self-braze seal of the Cb thermocouple cover tubes to the W/Re emitter flange; a tube-to-plate configuration¹. The restricted geometry of this joint, however, makes it difficult to avoid some melting of the W/Re (Figure 10). Therefore, a stress-relief groove was provided in the W/Re, as would be normally done for a direct weld. Without the relief groove, about one-fourth of the joints were not hermetic. Since the introduction of the groove, four tubes have been welded without failure.

Table II summarizes the experience in joining niobium to tungsten/rhenium as discussed above.

REFERENCE

1. Design, Fabrication, and Testing of External-Fuel Converter by A. Schock, B. Raab, F. Giorgio, 1970 Thermionic Conversion Specialists Conference, Miami Beach, Florida.

Table I.

SUMMARY OF WELDING EXPERIENCE INVOLVING TUNGSTEN AND TUNGSTEN/RHENIUM

| MATERIALS | CONFIGURATION | PREHEAT | RESULTS |
|------------------|---------------------------|--------------------|--|
| PM-W: PM-W | END CAP TO REVOLVER* | — | CRACKING THROUGHOUT |
| PM-W: PM-W | END CAP TO REVOLVER* | EB | WELDS OK; 40 TH~ OK; POROSITY |
| PM-W/25 RE: PM-W | END CAP TO REVOLVER* | EB | WELD OK; EXTENSIVE POROSITY |
| PM-W/25 RE: AC-W | END CAP TO REVOLVER | EB | WELDS OK; LEAKS AND MOTTLED SURFACE IN PRE-HEAT ZONES |
| PM-W/25 RE: AC-W | END CAP TO REVOLVER | RESISTANCE FURNACE | ELEVEN JOINTS TO DATE; ALL OK; NUMEROUS TH~ IN CONVERTERS |
| PM-W/RE: PM-W/RE | END CAP TO EMITTER FLANGE | RESISTANCE FURNACE | FOUR JOINTS TO DATE; ALL OK; NUMEROUS TH~ IN CONVERTER APPLICATION |

(*) SPECIMEN

Table II.

SUMMARY OF WELDING EXPERIENCE INVOLVING TUNGSTEN AND TUNGSTEN/RHENIUM TO NIOBIUM

| MATERIALS | CONFIGURATION | RESULTS |
|----------------|-------------------------------------|--|
| NB: PM-W/25 RE | TUBE TO ROD (.015" WALL) (.250 DIA) | WELD OK; 5 TH~ TO 1000°C, OK; 20 TH~, CRACK |
| NB: PM-W/25RE | TUBE TO ROD (.055" WALL) (.250 DIA) | EB BRAZE OK; 20 TH~ TO 800 °C, OK |
| NB: PM-W/25RE | SEAL TO END CAP* | EB BRAZE OK; 12 TH~ TO 800 °C, OK, 12 TH~ TO 1000 °C, OK |
| NB: PM-W/25 RE | SEAL TO END CAP | EB BRAZE OK; (FOUR IN CONVERTER APPLICATION) |
| NB: PM-W/25 RE | TUBE TO EMITTER FL. (.125" x .020") | MODIFIED EB BRAZE, OK |

(*) SPECIMEN

APPENDIX G

FABRICATION AND ASSEMBLY STEPS

This appendix lists the individual fabrication and assembly steps which were required for the manufacture of the external-fuel converters described in this report.

The flow diagram, Figure G1, shows the sequence of assembly and sub-assembly. The parts and joints referred to in each step are identified by step number on the plan-view drawing of Figure G2.

1. Machine or spin Cb cups for graded seals, as per Drawing PC116D0028-15 and -29 (4x).
2. Machine Cb sleeves for graded seals, as per Drawing PC116D0028-13 (2x)
3. EB-weld Cb seal cup to Cb sleeve, Drawing PC116D0028-7 (2x)
4. Fill Cb seal assembly with graded layers of Cb and Al_2O_3 powder including a central Lucalox disk (2x)
5. EB-weld Cb seal cup to upper edge of Cb sleeve, Drawing PC116D0028-7 (2x)
6. Autoclave graded seal assemblies for 3 hours at 1650°C and 15,000 psi
7. Finish-machine graded seals, as per Drawing PC116D0028-5 (2x)
8. Stamp .005-inch thick Cb foil to form bellows convolutions per Drawing PC116D0055-19 (30x)
9. Machine Cb top-ring as per Drawing PC116D0060-13
10. EB-weld inner edge of one Cb convolution to Cb top-ring
11. Machine Cb bellows bottom ring, as per Drawing PC116D0060-13
12. EB-weld inner edge of one Cb convolution to Cb bottom ring
13. EB-weld remaining Cb convolutions along their inner edges, to form pairs, each pair separated by two Mo spacer-rings, Drawing PC116D0055-17 (14x)

14. EB-weld outer edges of the Cb convolutions with intervening Mo spacer-rings to form the bellows assembly, Drawing PC116D0036-11 (15x)
15. Chemically dissolve the Mo spacer rings in 50% HNO₃, 30% H₂SO₄, 20% H₂O
16. EB-weld Cb bellows top-ring to lower seal (Cb)
17. EDM and grind W/Re fuel end caps, as per Drawing PC116D0050-13, -15, and -17 (2x)
18. EDM and grind W/Re lower flange as per Drawing PC116D0068-11 or -13
19. EB-weld W-Re lower flange to W/Re lower fuel cap (Preheat)
20. EB-selfbrazed Cb seal to W/Re lower fuel cap (2460°C)
21. RF-backbrazed W/Re lower flange to W/Re lower fuel cap, using palladium-nickel-silver alloy (1052°C)
22. RF-backbrazed Cb lower seal to W/Re lower fuel cap, using palladium-nickel-silver alloy (1052°C)
23. Machine Mo lower cooling skirt
27. Form helical winding of inconel-sheathed magnesia-insulated nichrome heater, and insert into Mo lower cooling skirt
28. RF-braze inconel-sheathed heater to Mo lower cooling skirt, using palladium-nickel-silver alloy (1052°C)
29. EB-weld Mo cooling skirt assembly to lower W/Re flange
30. EDM arc-cast W billet to form revolver with one emitter hole and six fuel holes as per Drawing PC116D0048-11
31. EDM six slanted thermocouple holes into webs between fuel holes
32. Anneal W revolver for one hour at 1300°C in vacuum
33. Electropolish W revolver body and inspect for microcracks
34. Hone emitter and fuel holes in W revolver to final dimensions

35. EB-weld inner lip of W/Re lower fuel cap to W revolver (Preheat) approximately 1400°F
36. Anneal weld joint for one hour at 1300°C in vacuum
37. EB-weld outer lip of W/Re lower fuel cap to W revolver (Preheat) approximately 1400°F
38. Anneal weld joint for one hour at 1300°C in vacuum
39. Vapor-deposit W snorkel tubes as per Drawing PC116D0034 (6x)
40. EDM 15 perforations in each W snorkel tube and cut to length (6x)
41. EDM and grind six W fuel cover disks, as per Drawing PC116D0034
42. EB-weld W snorkel tubes to W fuel cover disks (Preheat) (6x)
43. Press and sinter 96 UO₂ fuel pellets to 9% enrichment and 92% theoretical density, as per Drawing PC116D0049
44. Load each of the six fuel holes in the W revolver with 16 UO₂ pellets and one snorkel assembly
45. Outgas fueled revolver at 1300°C in vacuum
46. Machine Cb upper seal extension, as per Drawing PC116D0030
47. EB-weld Cb upper seal to Cb seal extension
48. Machine Cb feedthroughs as per Drawing PC116D0069 (4x)
49. Machine Cb cover tube transition, as per Drawing PC116D0057
50. EB-weld Cb cover tube transition to one of the four Cb feedthroughs
51. EDM and grind W/Re top flange, as per Drawing PC116D0069
52. EB-selfbraze Cb feedthroughs to W/Re top flange (4x)
53. EDM vent hole in W/Re upper fuel cap, Drawing PC116D0050
54. EB-selfbraze Cb upper seal to W/Re upper fuel cap, after first inserting the top flange assembly (2460°)

55. EB-weld W/Re top flange to W/Re upper fuel cap with vent hole lined up with proper feedthrough (Preheat)
56. Vapor-deposit W/Re fission gas vent tube as per Drawing PC116D0057
57. Machine Cb fission gas connector, as per Drawing PC116D0057
58. RF-Braze Cb fission gas connector to W/Re vent tube, using palladium-nickel-silver alloy (1052°C)
59. EB-weld W/Re fission gas vent tube to W/Re upper fuel cap (Preheat)
60. Anneal upper assembly for one hour in vacuum, with W/Re parts at 1300°C
61. RF-backbraze W/Re top flange to W/Re upper fuel cap, using palladium-nickel-silver alloy (1052°C)
62. RF-backbraze Cb upper seal to W/Re upper fuel cap, using palladium-nickel-silver alloy (1052°C)
63. Machine Mo upper cooling skirt and cover ring, as per Drawing PC116D0018
67. Form helical winding of inconel-sheathed magnesia-insulated heater, and insert into Mo upper cooling skirt
68. RF-braze inconel-sheathed heater to Mo upper cooling skirt, using palladium-nickel-silver alloy (1052°C)
69. Machine Cu emitter coolant duct (upper) as per Drawing PC116D0018 (2x)
71. EB-weld Mo upper cooling skirt to W/Re top flange (Preheat)
72. EB-weld inner lip of W/Re upper fuel cap to W revolver (Preheat)
73. Anneal weld joint for one hour at 1300°C in vacuum
74. EB-weld outer lip of W/Re upper fuel cap to W revolver (Preheat)
75. Anneal weld joint for one hour at 1300°C in vacuum
76. Machine Cb cesium leg, as per Drawing PC116D0026
77. Machine Cb reservoir cover, as per Drawing PC116D0026

78. EB-weld Cb cesium leg to Cb reservoir cover
79. Machine Cb reservoir, as per Drawing PC116D9026
80. EB-weld Cb reservoir cover to Cb reservoir
81. Machine Cb collector, as per Drawing PC116D9051
82. EB-weld Cb cesium leg to Cb collector hub, using eccentric jig to rotate assembly about cesium leg axis
83. Machine Cb lower collector cap, as per Drawing PC116D0051
- 83a. Braze SS cap over Cb collector cap
84. EB-weld Cb lower collector cap to Cb collector hub
85. Outgas Cb collector assembly in high-vacuum bell jar for four hours at 1200°C
86. Grind alumina split spacer rings, as per Drawing PC116D9053 (3x)
87. Install alumina spacer ring on Cb collector using W/Re retainer rings per Drawing PC116D9052 (3x)
88. Prepare 12 Al_2O_3 spacer balls, 0.040-inch diameter per Drawing PC116D9059
89. Install six Al_2O_3 spacer balls in hemispherical holes in Cb collector
90. Insert collector assembly into lower end of emitter assembly
91. Machine Cb collector extension, as per Drawing PC116D9061
92. Install six Al_2O_3 spacer balls in hemispherical holes in Cb collector extension
93. Insert collector extension into top of emitter assembly
94. EB-weld Cb bottom ring of bellows to Cb collector
95. EB-weld Cb collector extension to Cb collector
96. EB-weld Cb collector extension to Cb upper seal extension
97. Machine SS collector top cap, as per Drawing PC116D9024
98. Machine helium port (SS) as per Drawing PC116D9024

99. EB-weld SS helium port to SS collector top cap
100. Hydroform SS collector coolant bellows, Drawing PC116D0024
101. EB-weld SS collector coolant bellows to SS collector top cap
102. Machine SS collector coolant tube, as per Drawing PC116D0025
103. Machine SS coolant tube extension, Drawing PC116D0025
104. RF-braze SS coolant tube extension to SS coolant tube, using palladium-nickel-silver alloy (1052°C)
105. Machine Cu coolant tube connector
106. RF-braze Cu coolant tube connector to SS coolant tube extension, using palladium-copper-silver alloy (950°C)
107. EB-weld SS collector coolant tube to SS collector coolant bellows
108. Insert collector cooling assembly into collector
109. RF-braze SS collector top cap to Cu collector, using palladium-nickel-silver alloy (1052°C)
110. RF-braze SS coolant tube extension to SS lower collector cap, using palladium-nickel-silver alloy (1052°C)
111. RF-braze Cu coolant outlet tube to SS collector top cap, using palladium-copper-silver alloy (950°C)
112. RF-braze Cu coolant inlet tube to SS coolant tube extension using, palladium-copper-silver alloy (950°C)
113. EB-weld helium feed tube SS to helium port (SS)

116. Machine Cu cesium ampoule container sleeve as per Drawing PC116D0023
117. Machine Cu cesium ampoule container top cap as per Drawing PC116D0023
118. EB-weld Cu cesium ampoule container sleeve to Cu top cap
119. Form Cu cesium transfer tube, as per Drawing PC116D0023

120. RF-braze Cu cesium transfer tube to Cu cesium ampoule container top cap using copper-silver-alloy (780°C)
121. Load glass ampoules containing vacuum-packed cesium into Cu container sleeve.
122. Machine Cu cesium ampoule container bottom cap, as per Drawing PC116D0023
123. EB-weld Cu cesium ampoule container sleeve to Cu bottom cap
124. Machine Cb reservoir heater sleeve Drawing PC116D0067
125. Form double reservoir heater coil from SS inconel-sheathed Al_2O_3 - insulated, nichrome wire and insert in the heater sleeve.
126. RF-braze inconel-sheathed reservoir heaters to heater sleeve, using palladium-nickel-silver alloy (1052°C)
127. RF-braze Cu cesium transfer tube to Cb reservoir using palladium-copper-silver alloy (950°C)
128. Mount heater assembly on reservoir
129. Machine reservoir cooling strap (Ni) as per Drawing PC116D0097
130. Install Ni cooling strap between reservoir and coolant inlet tube
131. Install converter in high-vacuum bell jar with cesium ampoule container outside the bell jar
132. Connect the Cu cesium ampoule container bottom cap to an external ion pump
134. Install heater leads thermocouples, and outgassing heaters
135. Outgas diode and fuel chamber at maximum operating temperature, with cesium appendages above 200°C
137. Pinch off the diode pumpdown leg just below the Cu tee
138. Break glass ampoule, and transfer cesium to diode
139. Pinch off Cb pumpdown leg just below Cs reservoir

140. Pinch off section of Cb tube to form flobule
141. Procure ZrO_2 thermal insulation felt and thread
142. Wrap ZrO_2 felt around emitter body
143. Perform out-of-pile diode tests
144. Roll W/Re sheet for primary container, Drawing PC116D0029
145. EB-seam-weld W/Re primary container
146. Install W/Re thermocouples on fuel element (6x)
147. Braze secondary container to lower W/Re flange
148. Braze primary container to upper W/Re flange
- 148a. Braze copper cooling skirts to Mo flanges
149. Hydroform SS fission gas bellows
- 149a. Hydroform SS secondary containment bellows
150. Machine SS fission gas transition collar
151. Weld SS fission gas transition collar to SS fission gas bellows
152. Machine SS accumulator bottom cap
153. Braze SS bellows to accumulator bottom cap
154. Machine SS fission gas duct
155. Weld SS fission gas duct to SS fission gas transition collar
156. Machine Ni accumulator pinch off tube
157. Weld Ni accumulator pinch off tube to SS accumulator bottom cap
158. Machine SS lower secondary transducer tube
159. Braze SS water cooling tube (159a) to accumulator transducer housing (160a)
160. Weld SS lower secondary transducer tube to accumulator transducer housing (160a)
161. Machine SS accumulator top cap

- 162. Weld transducer diaphragm (162a) to SS accumulator top cap
- 163. Weld SS accumulator transducer housing (160a) to SS accumulator top cap (161)
- 164. Machine SS accumulator side wall
- 165. Weld SS accumulator side wall (164) to accumulator top cap (161)
- 166. Weld SS accumulator side wall (164) to SS accumulator bottom cap (150)
- 167. Machine SS secondary containment transition
- 168. Weld SS fission gas bellows (149a) to SS secondary containment transition (167)
- 169. Machine SS secondary containment tube
- 170. Weld SS secondary containment tube (169) to SS secondary containment transition (167)
- 171. Machine SS secondary containment bottom cap
- 172. Machine SS secondary containment pumpdown tube
- 173. Weld SS secondary containment pumpdown tube (172) to SS secondary containment bottom cap (171)
- 174. Weld SS secondary containment bellows (149a) to SS secondary containment bottom cap (171)
- 175. Machine SS secondary container side wall
- 175a. Braze heater wire to containment side wall
- 176. Weld containment side wall (175) to SS accumulator top cap (161)
- 177. Weld SS secondary containment side wall (175) to SS secondary containment bottom cap (171)
- 178. Machine SS upper secondary transducer tube
- 179. Machine SS lower secondary transducer housing

180. Weld SS lower secondary transducer housing (179) to SS upper secondary transducer tube (178)
181. Weld Secondary transducer diaphragm (181a) to SS lower secondary transducer housing (179)
182. Weld SS transducer upper housing (182a) to SS transducer lower housing (179)
183. Machine SS secondary transducer supports
184. Weld SS secondary transducer supports (183) to secondary transducer housing (182a)
185. Weld SS secondary transducer supports (183) to fission gas transducer housing (160a)
186. Weld SS lower secondary transducer tube (158) to SS upper secondary transducer tube (178)
187. Machine SS fission gas transition tube
188. RF-braze SS fission gas transition tube (187) to Nb fission gas connector (57) using Pd-Ni-Ag alloy (1052°C)
189. Machine SS feed through transition tube
190. Braze SS feed through transition tube (189) to Nb cover tube transition (49) using Pd-Cu-Ag alloy (950°C)
191. Machine SS containment tube connector
192. Slip SS containment tube connector (191) over SS feed through transition tube (189)
193. Braze SS fission gas duct (154) to SS fission gas transition tube (187) using Pd-Ni-Ag alloy (1050°C)

APPENDIX H

NEW TECHNOLOGY

The only item of "new technology" resulting from this program, which may have broad applicability, is the high-voltage, high-rf-power vacuum feedthrough described in Section 5.1 and shown in Figure 7.

Figures

LIST OF FIGURES

Figure

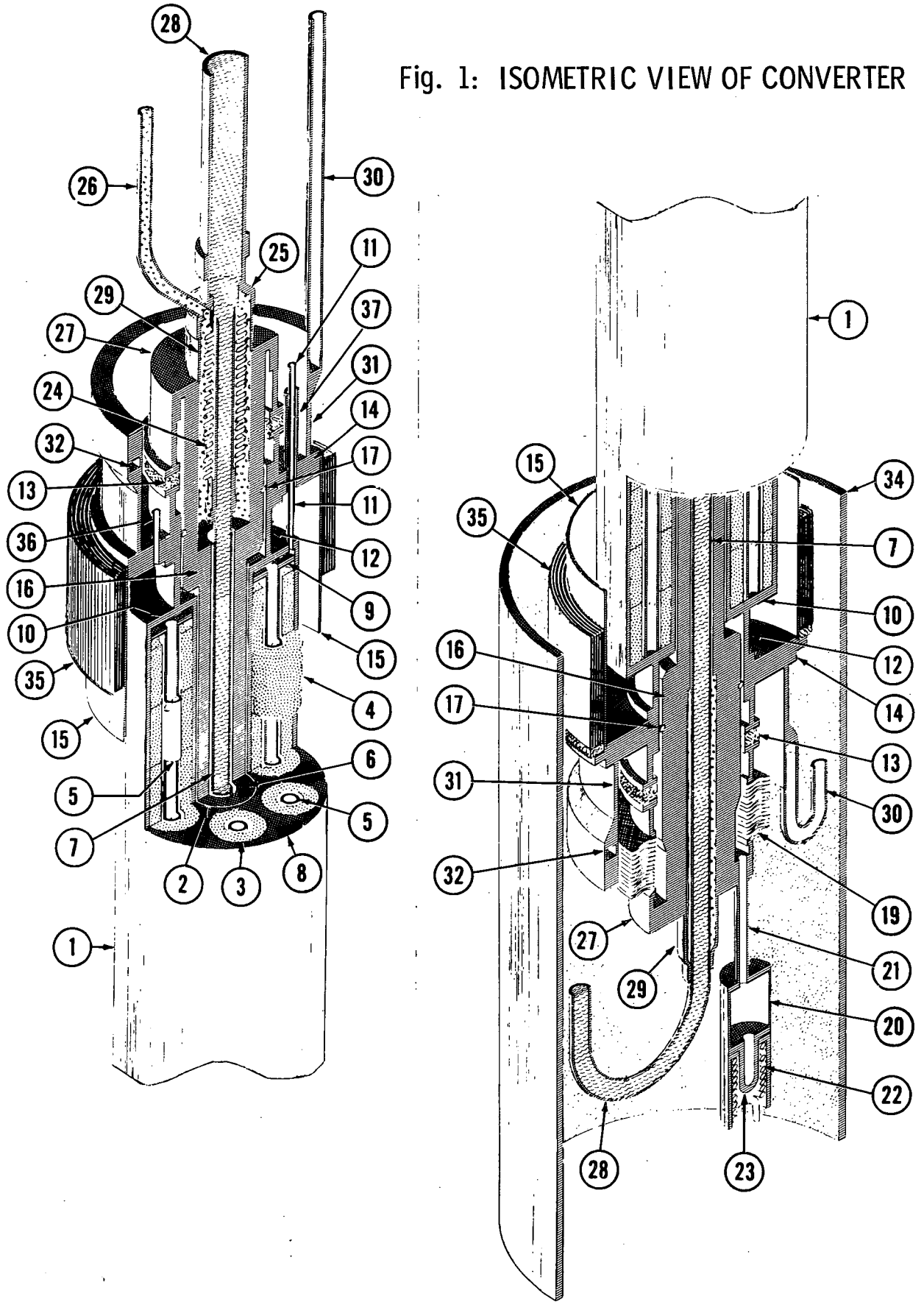
- 1 Isometric View of Converter
- 2 Converter Cross-Section
- 3 Converter Test Capsule
- 4 In-Pile Test Arrangement
- 5 Converter Components and Assembly
- 6 Previous R-F Heating Arrangement
- 7 Coaxial R. F. Power Feedthrough (450 kHz, 75 kW)
- 8 Out-of-Pile Test Station
- 9 Converter Processing and Cesium Charging
- 10 Out-of-Pile Test Arrangement
- 11 Temperature Distribution of R. F. Heated Fuel-Emitter
- 12 Temperature Distribution of Nuclear-Heated Fuel-Emitter
- 13 Remotely Adjustable Liquid Metal Power Load
- 14 Measured Converter Performance
- 15 Comparison of Measured and Predicted Performance
- 16 Revolver Surface After Out-of-Pile Test
- 17 Converter #2 after Out-of-Pile Test and Installation of Fuel-Emitter Thermocouples
- 18 Completed Converter Assembly with Thermocouples, Secondary Container, and Thermal Shields
- 19 Fission Gas Collection Assembly
- 20 Assembly Plate with Insulated Vacuum Feedthroughs
- 21 Converter Design Alternatives
- 22 High Fuel Fraction Converter Nesting Arrangement
- A1 Computed Diode Characteristics
- A2 Axial Profile of Diode
- A3 Secondary Container Heat Loss
- C1 Reactor Core Layout
- C2 Fuel-Emitter Mock-up Experiment
- C3 Thermal Neutron Flux, Azimuthal Profiles
- C4 Thermal Neutron Flux, Axial Profiles
- C5 Computed Radial Flux Profile
- C6 Neutron Flux Profiles at 2-MW Reactor Power

LIST OF FIGURES (Cont'd)

Figure

- C7 Fission Power Versus Fuel Enrichment
- C8 Measured Gamma Distribution in Mock-up Capsule
- D1 Peripheral Temperature Profile of Emitter and Fuel Chamber
- D2 30-Degree Cell for Thermal Stress Analysis
- D3 Tangential Stress at Boundaries of Emitter Body
- D4 Tangential Stress at Fuel Chamber Boundary
- D5 High-Temperature Creep Rates of Tungsten Alloys
- F1 Configuration of End Cap-to-Revolver Welds
- F2 Axial Weld, PM-Tungsten to PM-Tungsten
- F3 Axial Weld, PM-Tungsten to PM-Tungsten/25 Rhenium
- F4 Surface Macrophotographs, PM-W/25 Re End Cap to AC-W Revolver Welds with E-B Preheat
- F5 Cross-Sections Through Welds Showing Preheat Zones
- F6 Enlarged Cross-Section Through Web of Figure F4 Axial Weld
- F7 Niobium Tube to PM-Tungsten/25 Rhenium Sleeve
- F8 E-B "Self-Braze" Joint; Niobium to PM-Tungsten/25 Rhenium
- F9 Niobium Seal to PM-W/25Re End Cap Self-Braze with RF Backbrazes
- F10 Niobium Tube to PM-Tungsten/25 Rhenium Flange Braze Weld
- G1 Converter Fabrication and Assembly Sequence
- G2 Location of Fabrication and Assembly Steps

Fig. 1: ISOMETRIC VIEW OF CONVERTER



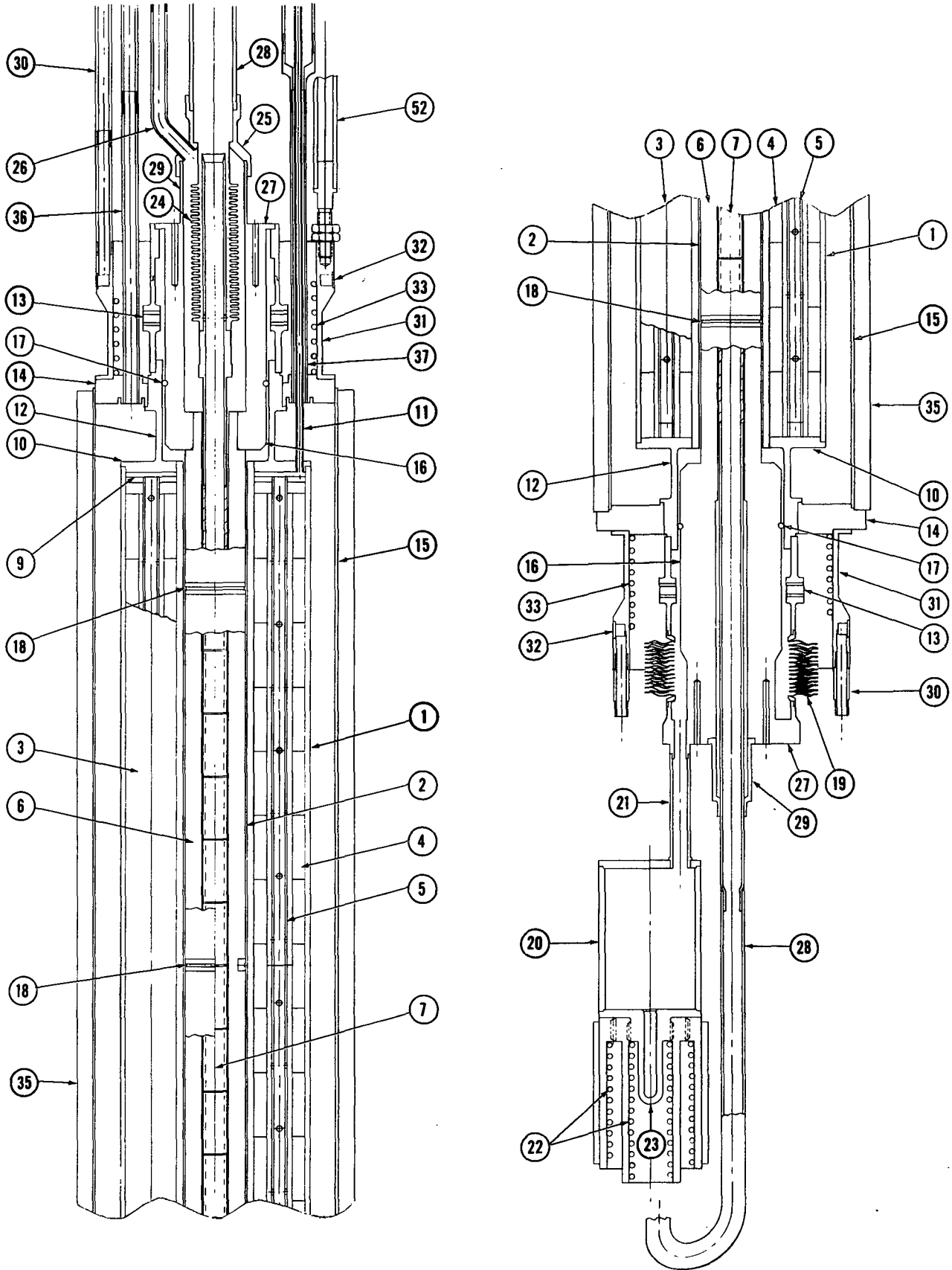


Fig. 2: CONVERTER CROSS-SECTION

Fig. 3: CONVERTER TEST CAPSULE

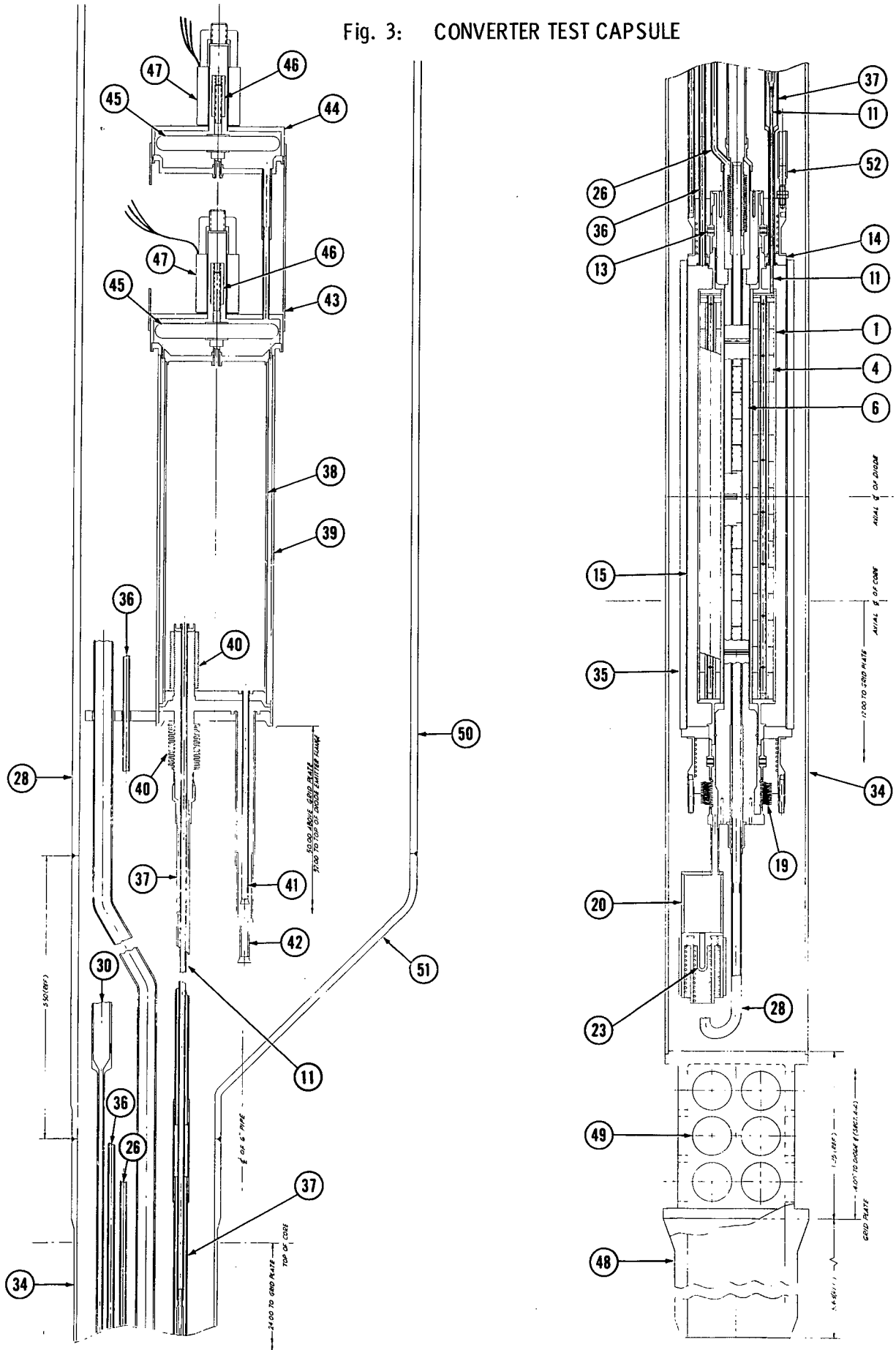


Fig. 4: IN-PILE TEST ARRANGEMENT

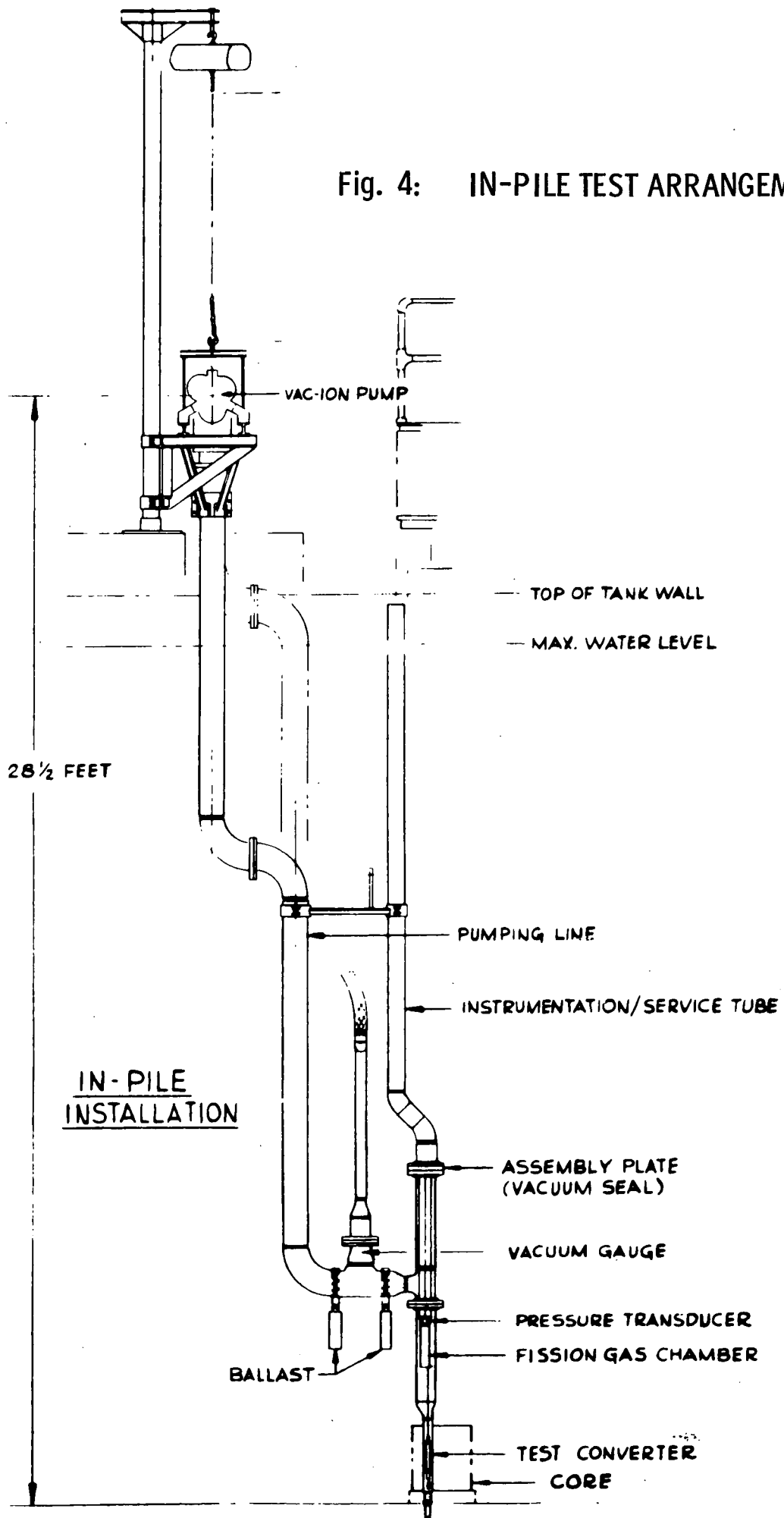


Fig. 5: CONVERTER COMPONENTS AND ASSEMBLY

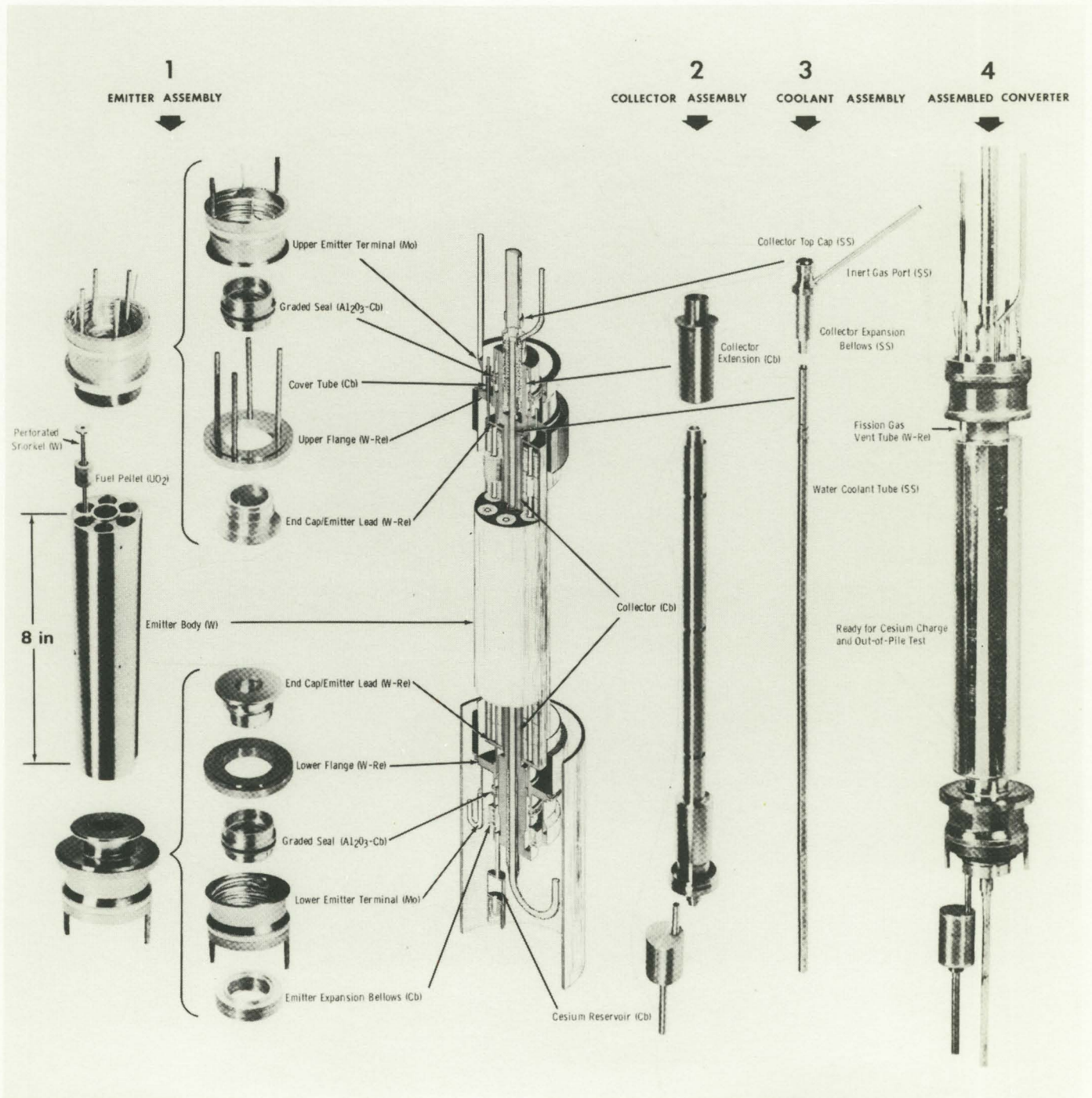




Fig. 6: PREVIOUS RF-HEATING ARRANGEMENT

Fig. 7: COAXIAL R.F. POWER FEEDTHROUGH (450 kHz, 75 kW)

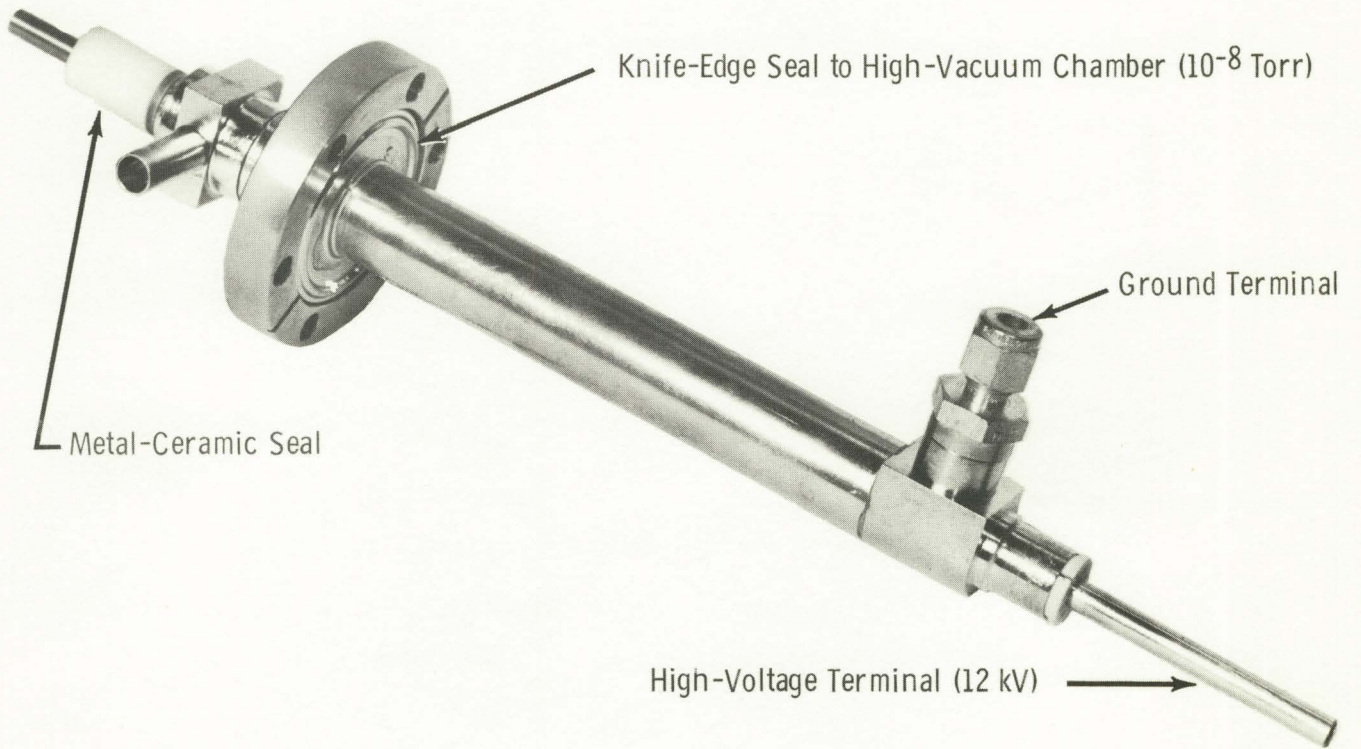
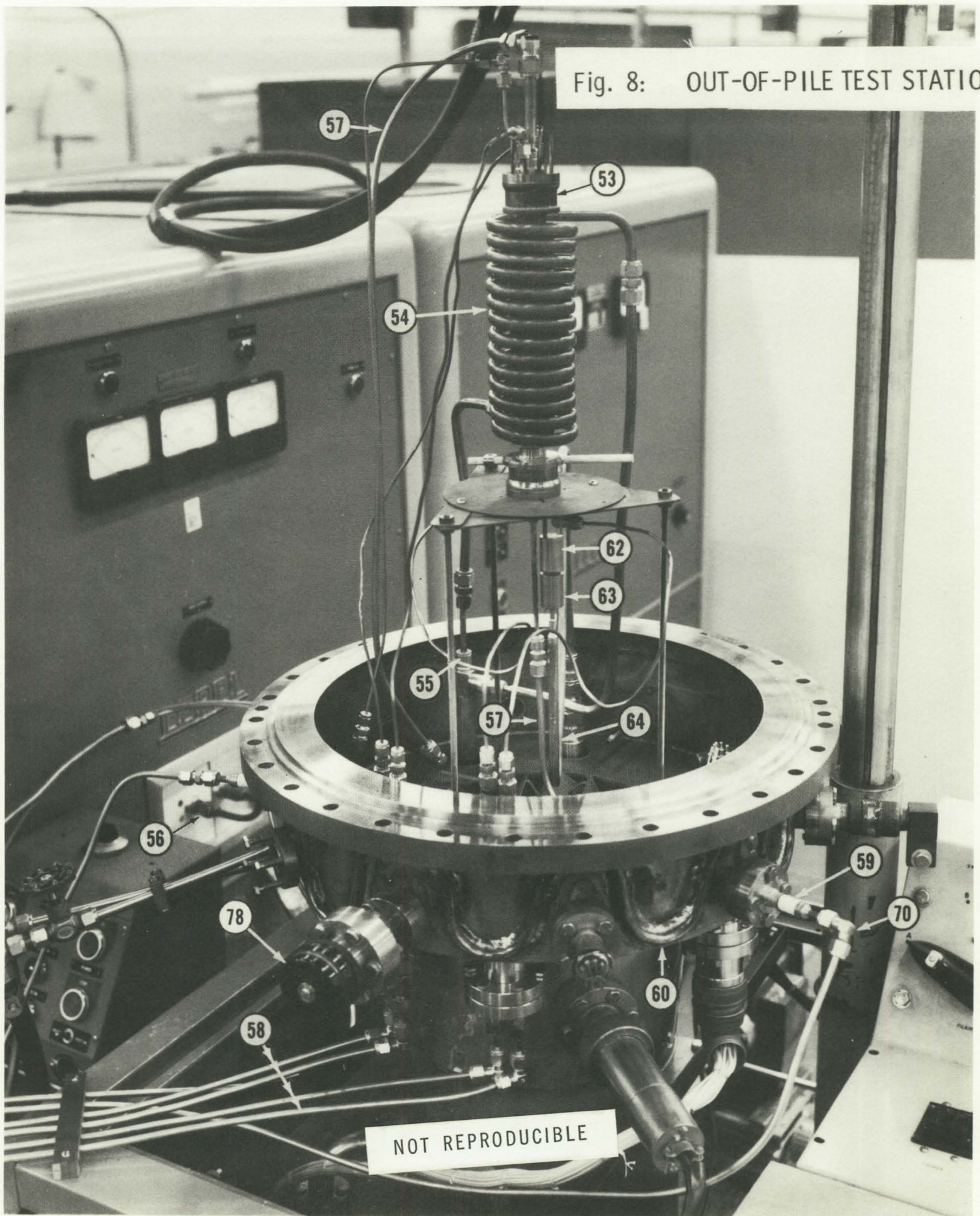


Fig. 8: OUT-OF-PILE TEST STATION



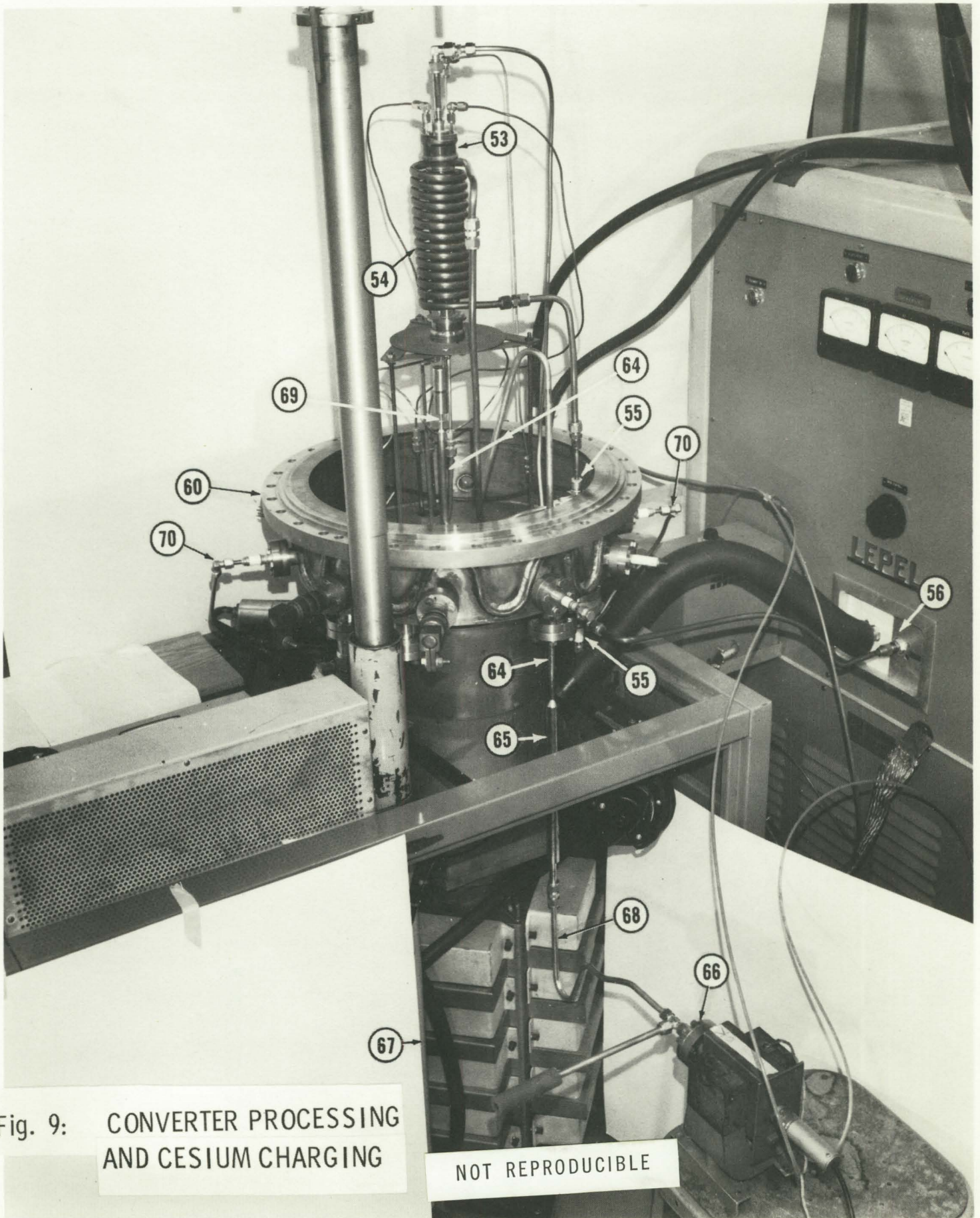
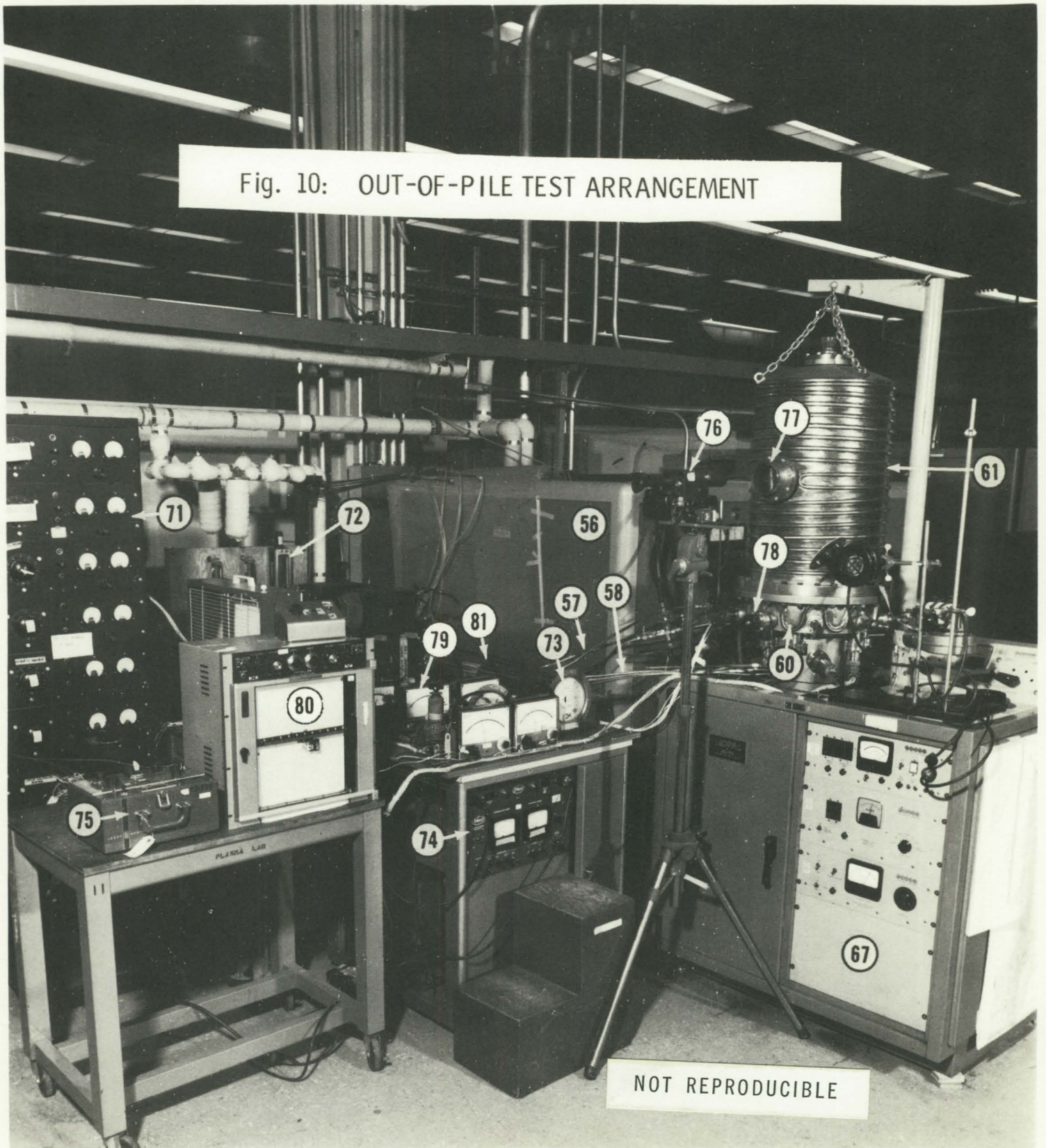


Fig. 9: CONVERTER PROCESSING AND CESIUM CHARGING

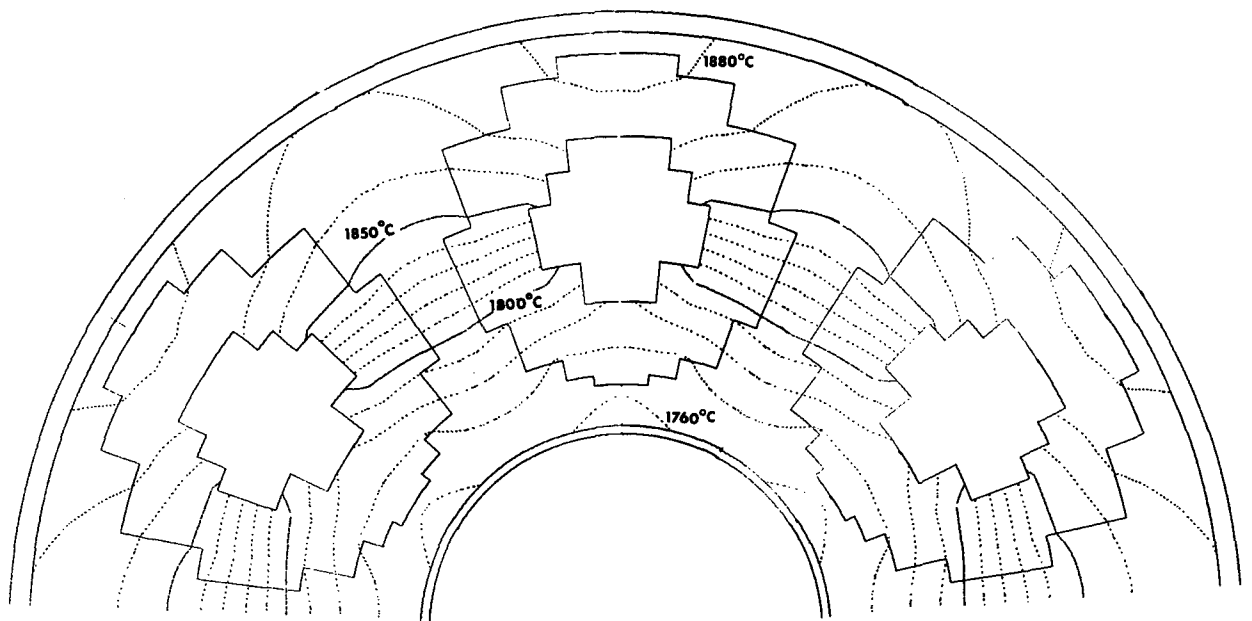
NOT REPRODUCIBLE

Fig. 10: OUT-OF-PILE TEST ARRANGEMENT



NOT REPRODUCIBLE

Fig. 11: TEMPERATURE DISTRIBUTION OF RF-HEATED FUEL-EMITTER



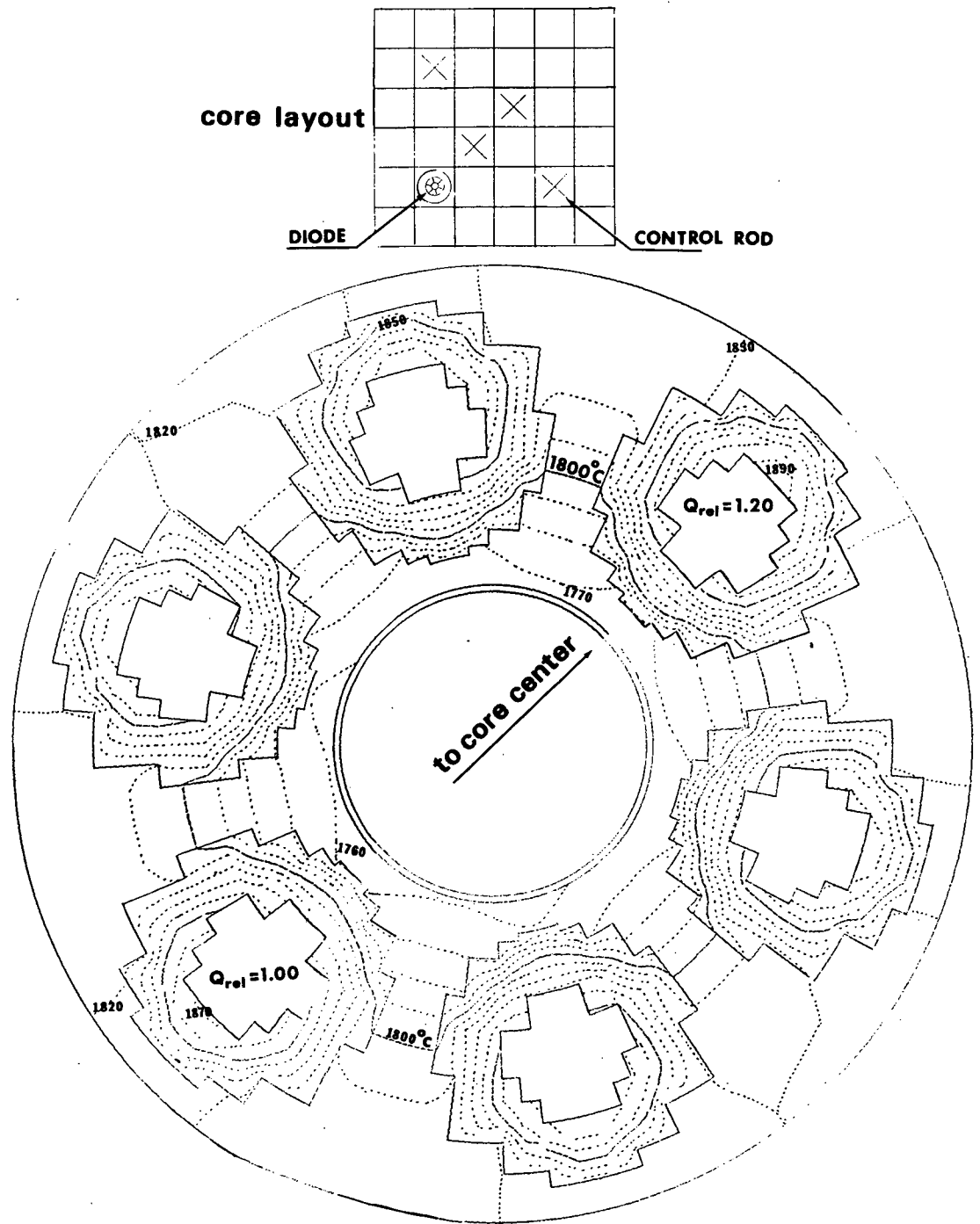


Fig. 12: TEMPERATURE DISTRIBUTION OF NUCLEAR-HEATED FUEL-EMITTER

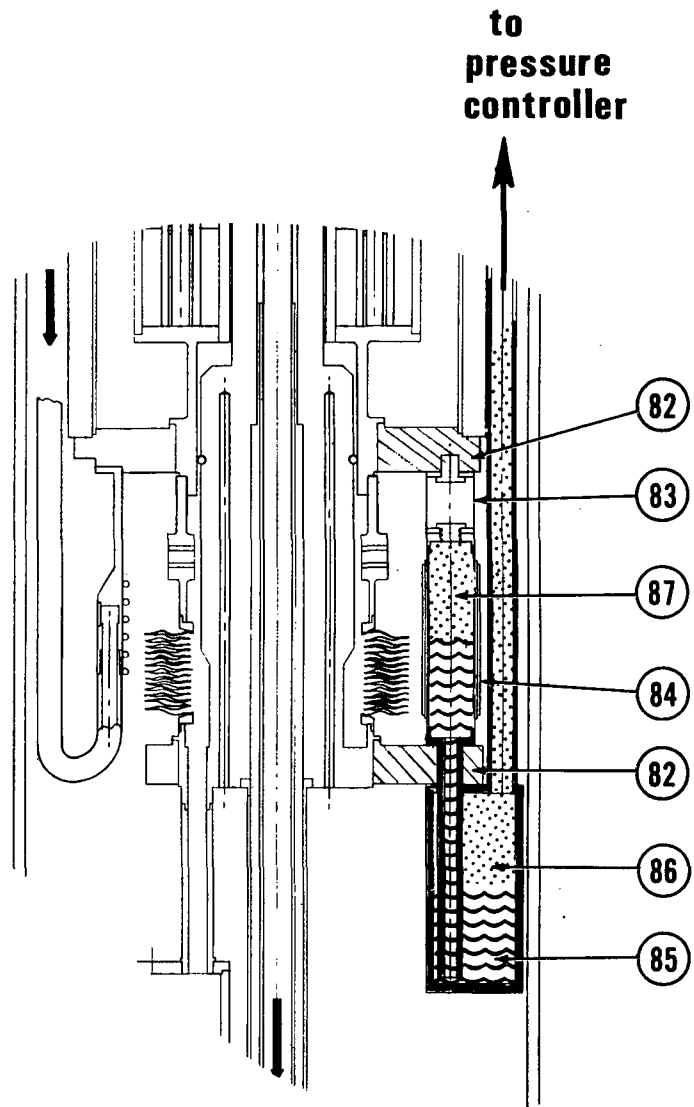


Fig. 13: REMOTELY ADJUSTABLE LIQUID METAL POWER LOAD

Fig. 14: MEASURED CONVERTER PERFORMANCE

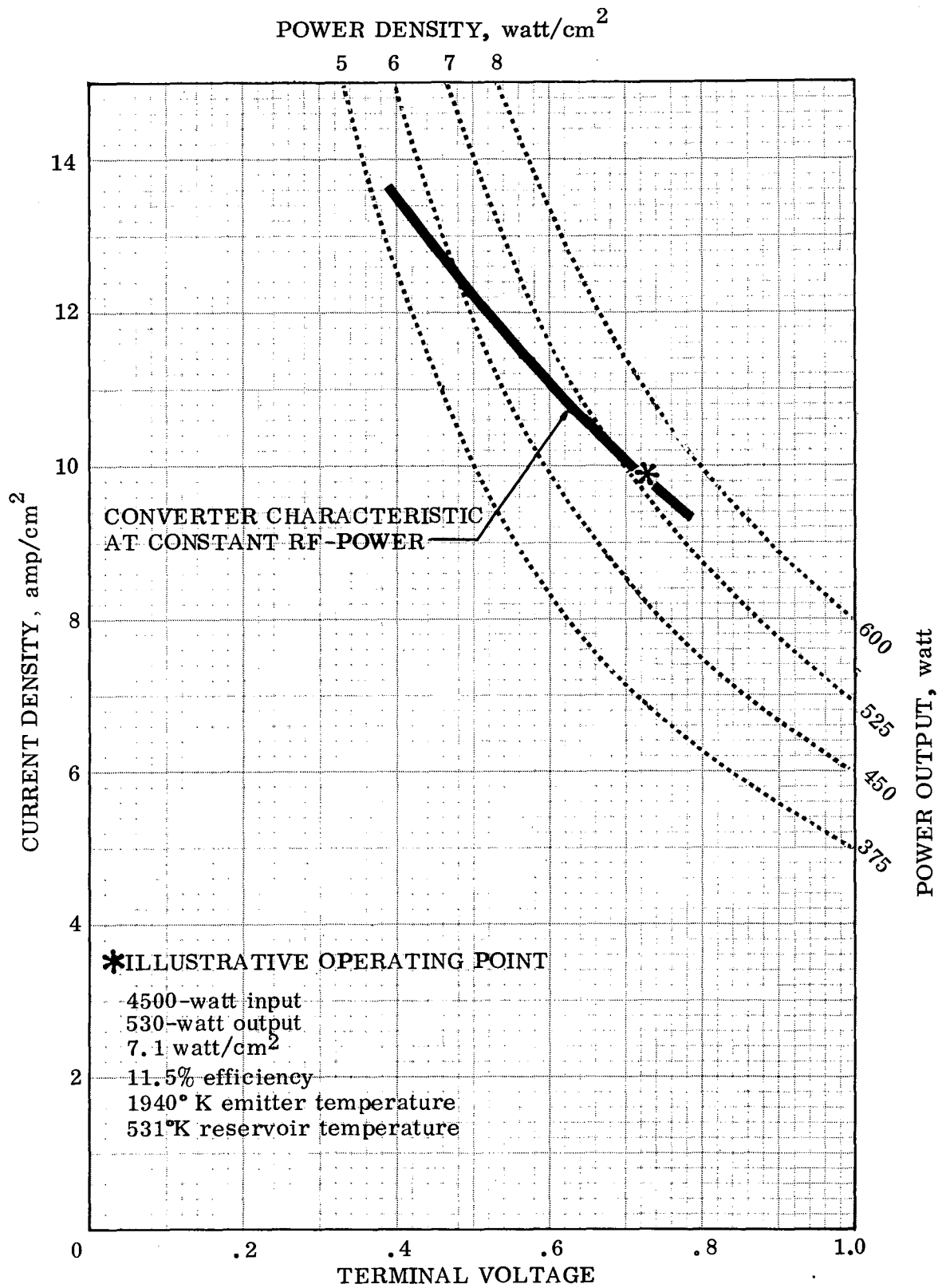
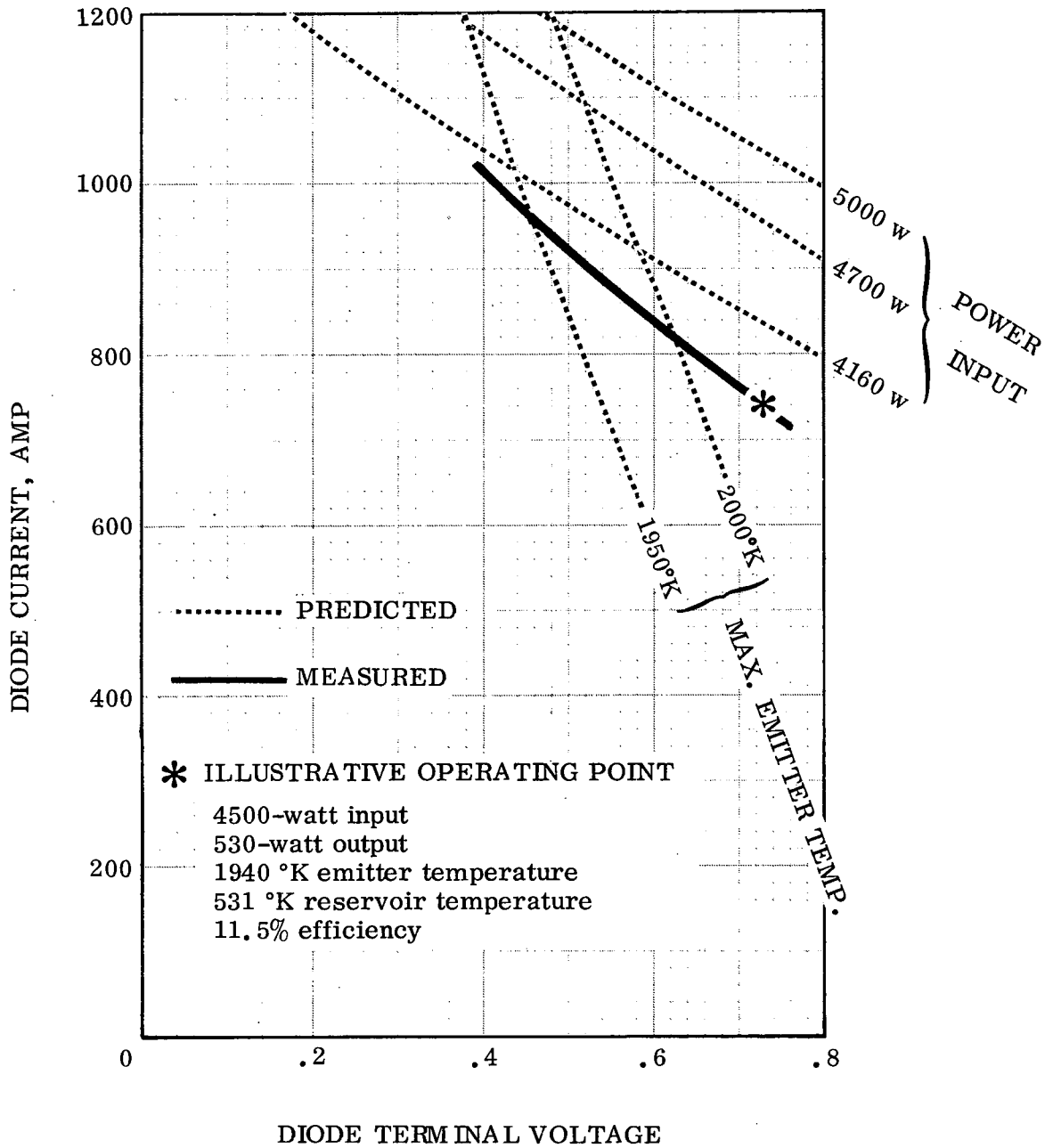


Fig. 15:

COMPARISON OF MEASURED AND PREDICTED PERFORMANCE



Leak

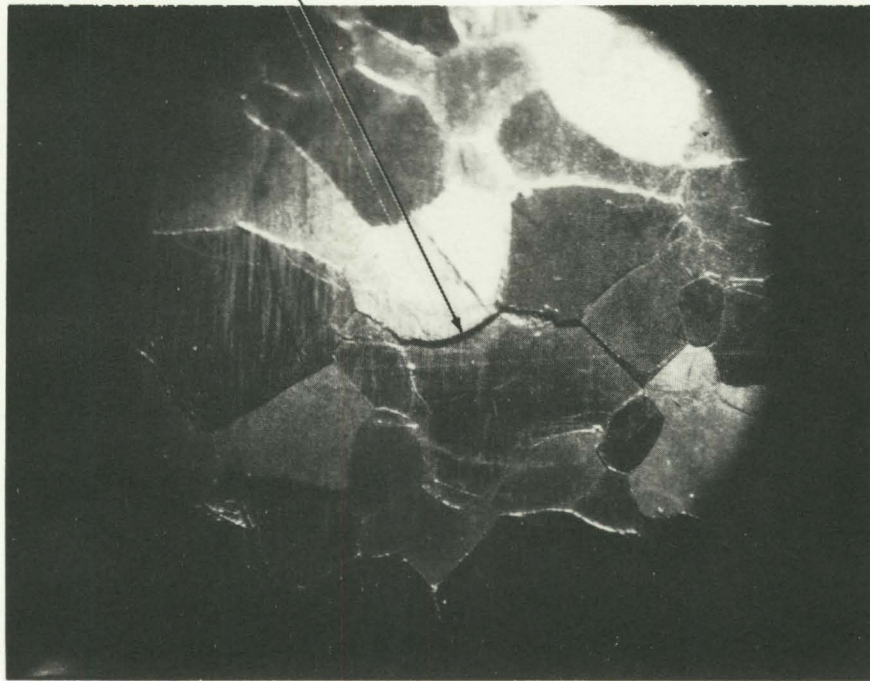


Fig. 16: REVOLVER SURFACE AFTER OUT-OF-PILE TEST

Fig. 17: CONVERTER #2 AFTER OUT-OF-PILE TEST
AND INSTALLATION OF FUEL-EMITTER THERMOCOUPLES



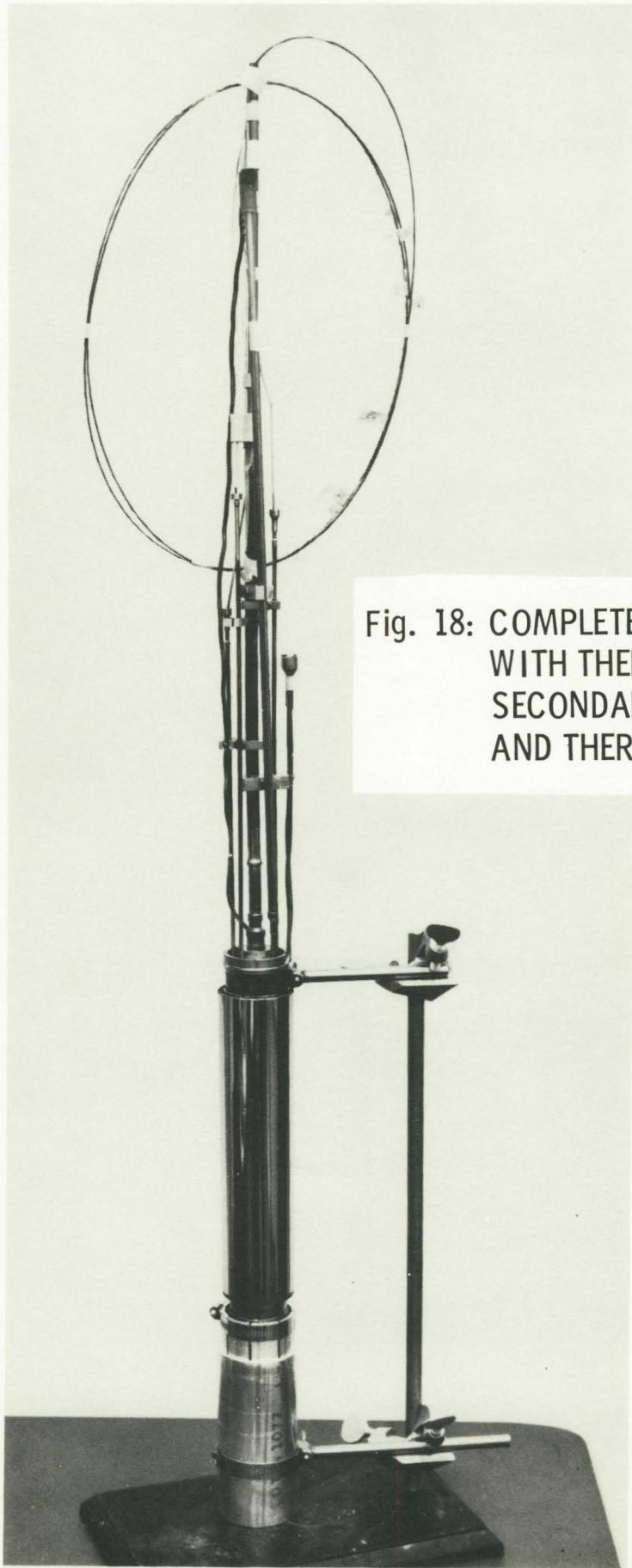
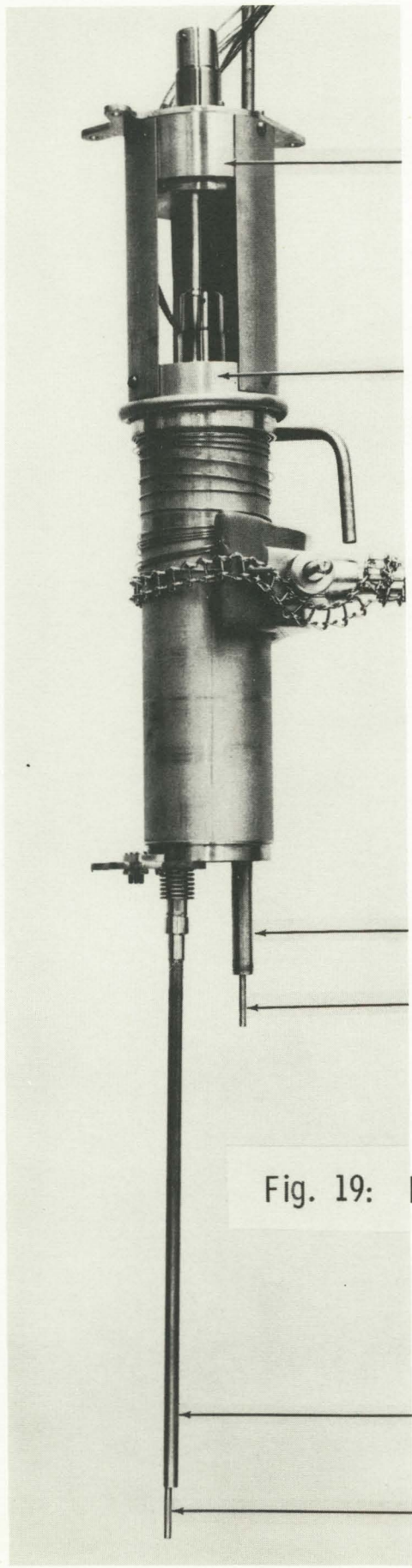


Fig. 18: COMPLETED CONVERTER ASSEMBLY
WITH THERMOCOUPLES,
SECONDARY CONTAINER,
AND THERMAL SHIELDS.



Outer Pressure Transducer

Inner Pressure Transducer

Secondary Container Pumpdown Leg

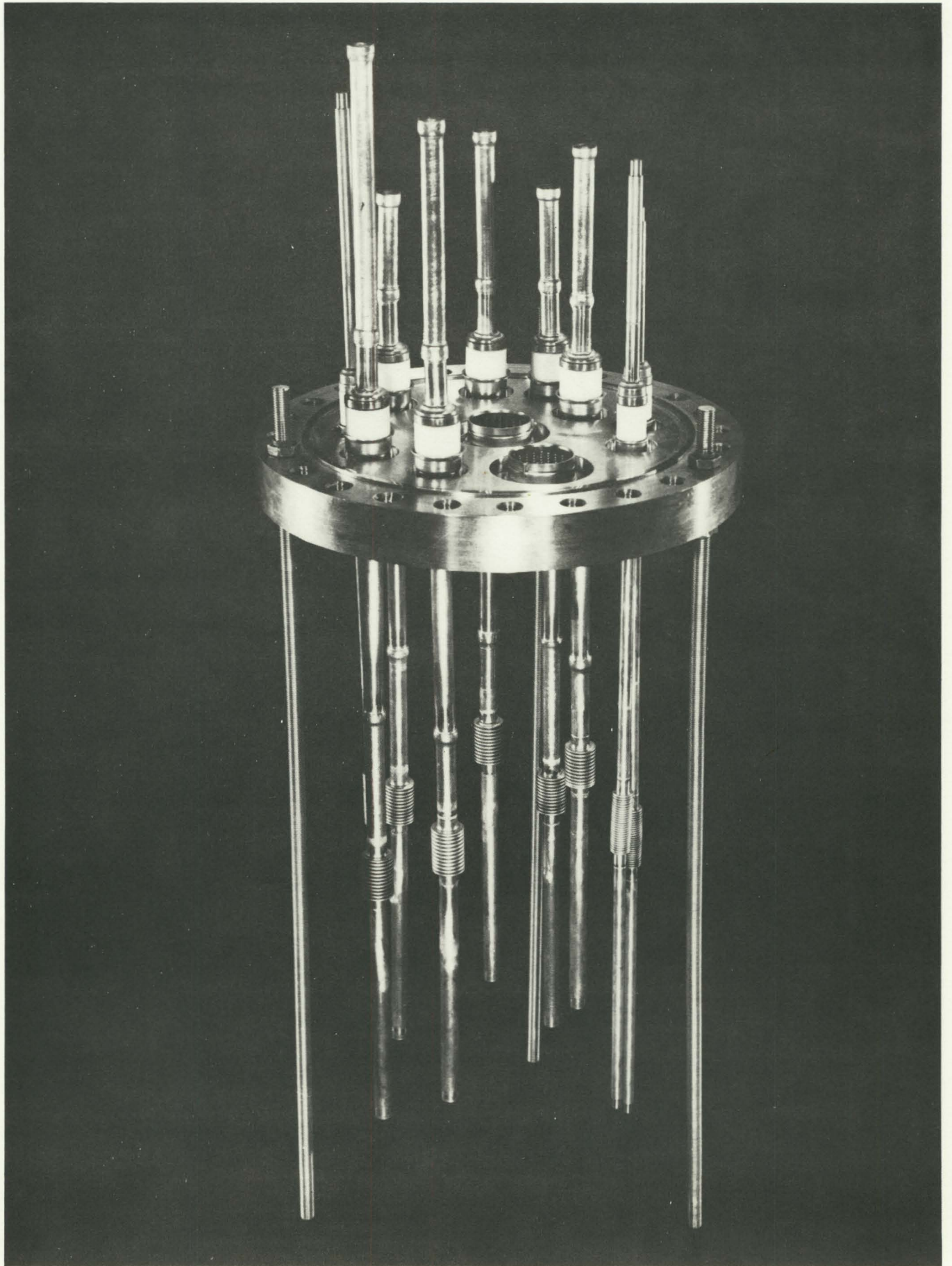
Accumulator Pumpdown Leg

Fig. 19: FISSION GAS COLLECTION ASSEMBLY

Vent Cover Tube

Vent Tube

Fig. 20: ASSEMBLY PLATE WITH INSULATED VACUUM FEEDTHROUGHS



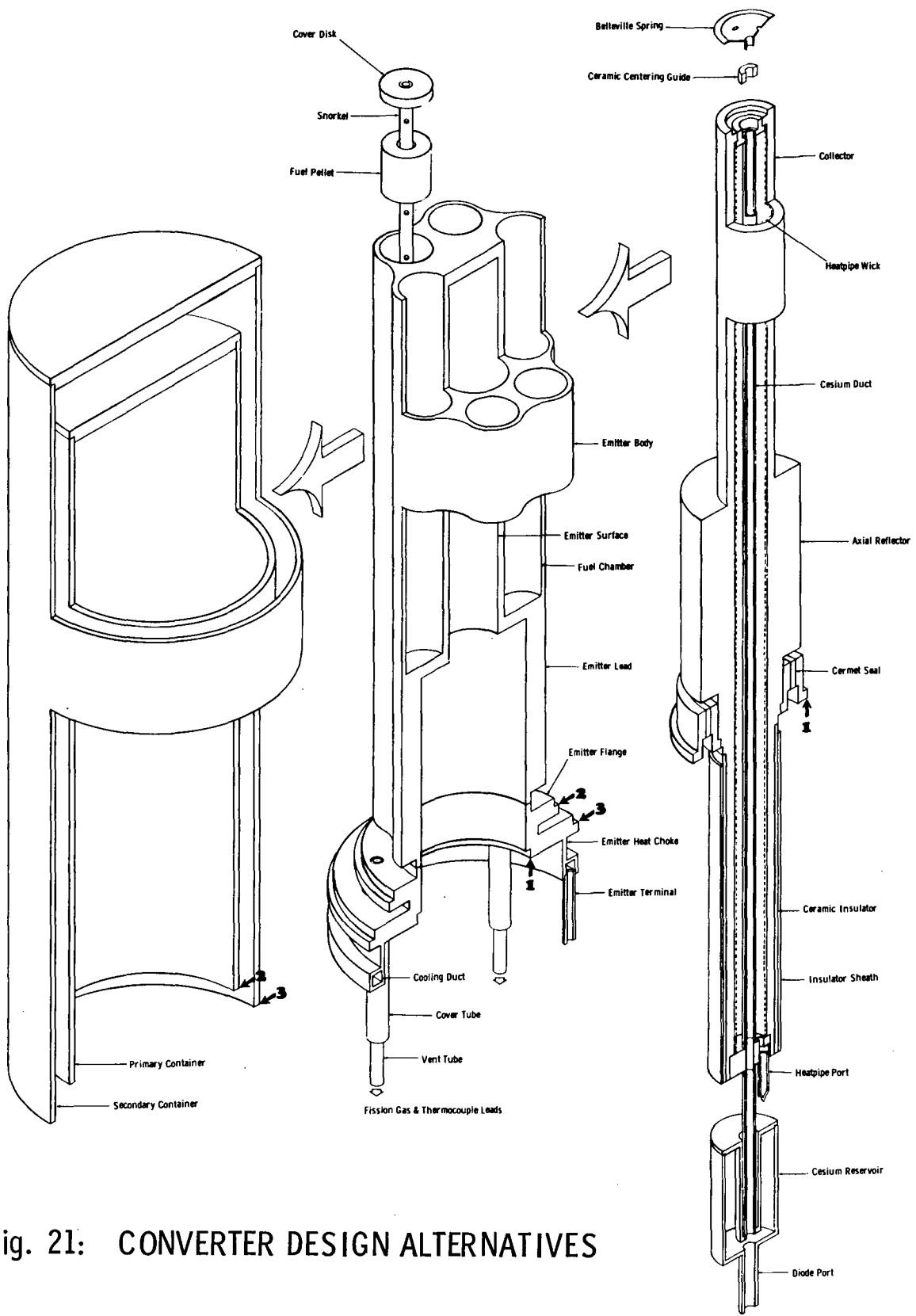


Fig. 21: CONVERTER DESIGN ALTERNATIVES

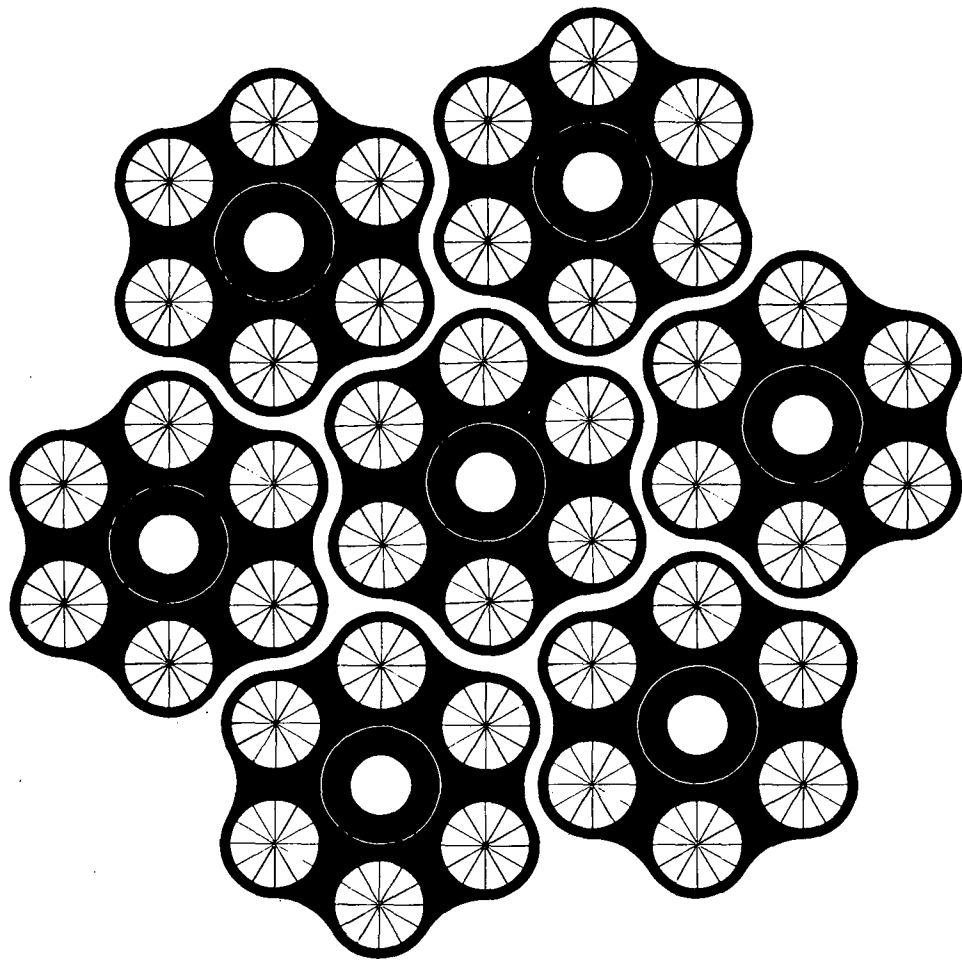


Fig. 22: HIGH FUEL FRACTION CONVERTER NESTING ARRANGEMENT

APPENDIX

Fig. A1: COMPUTED DIODE CHARACTERISTICS

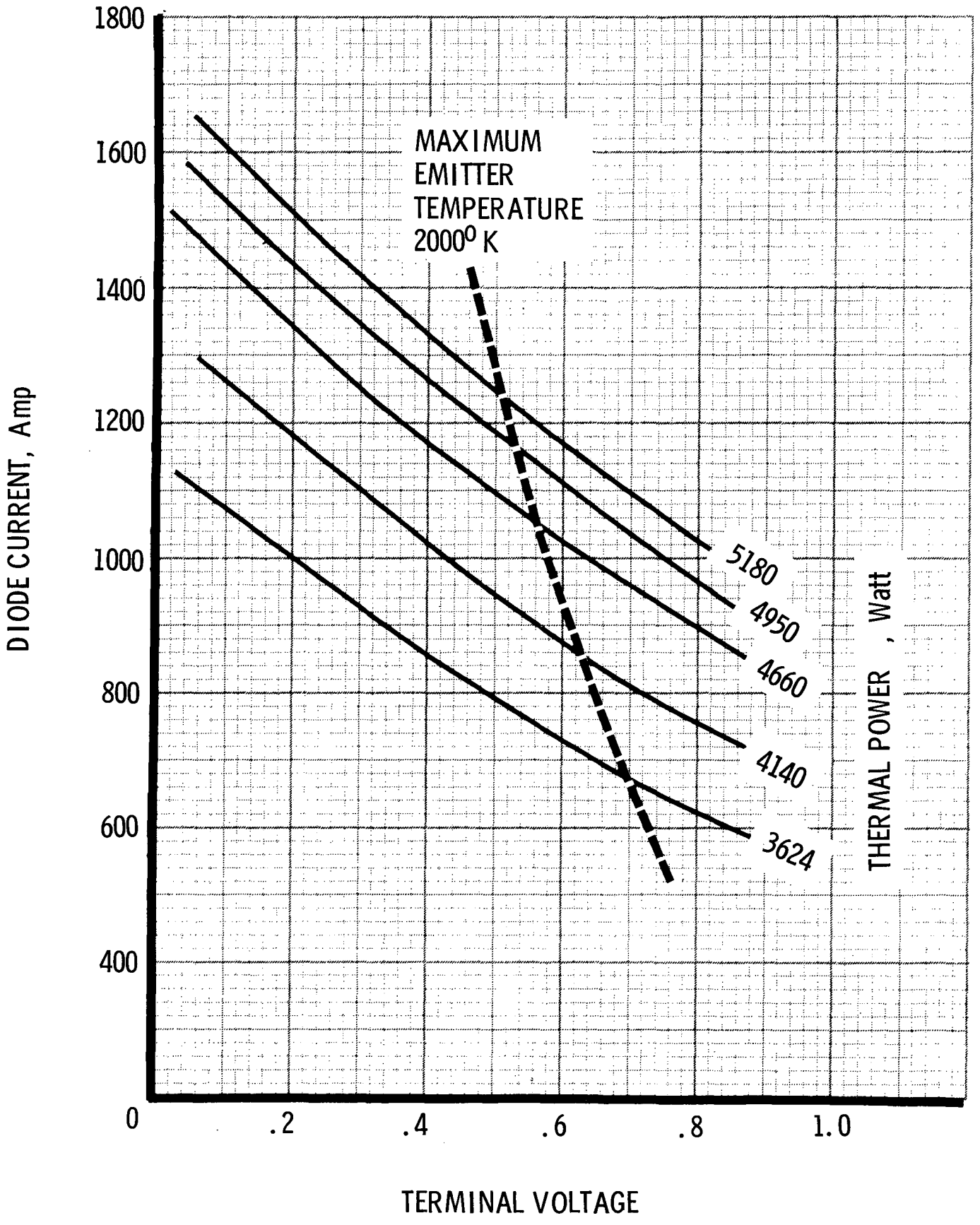


Fig. A2: AXIAL PROFILE OF DIODE

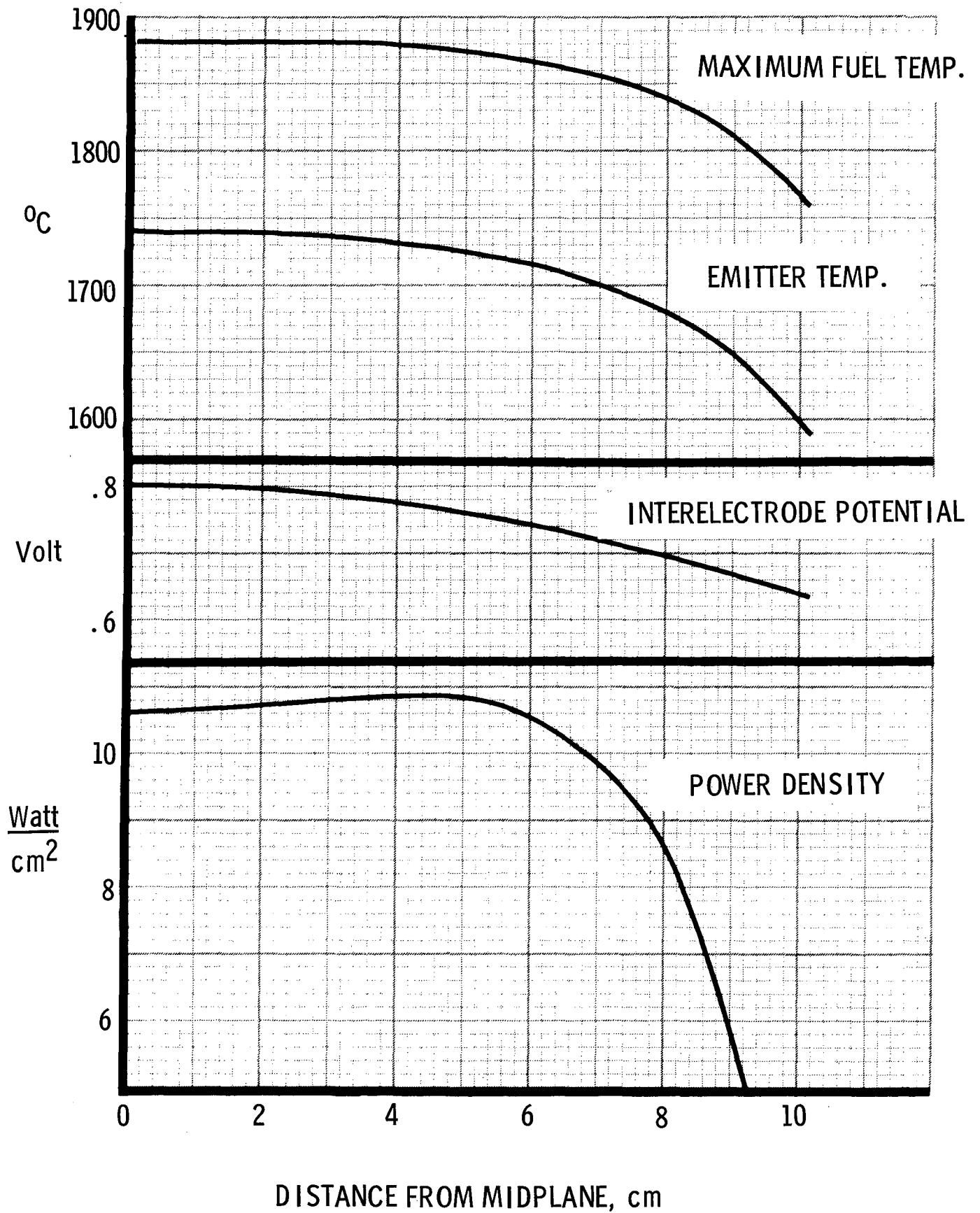


Fig. A3: SECONDARY CONTAINER HEAT LOSS

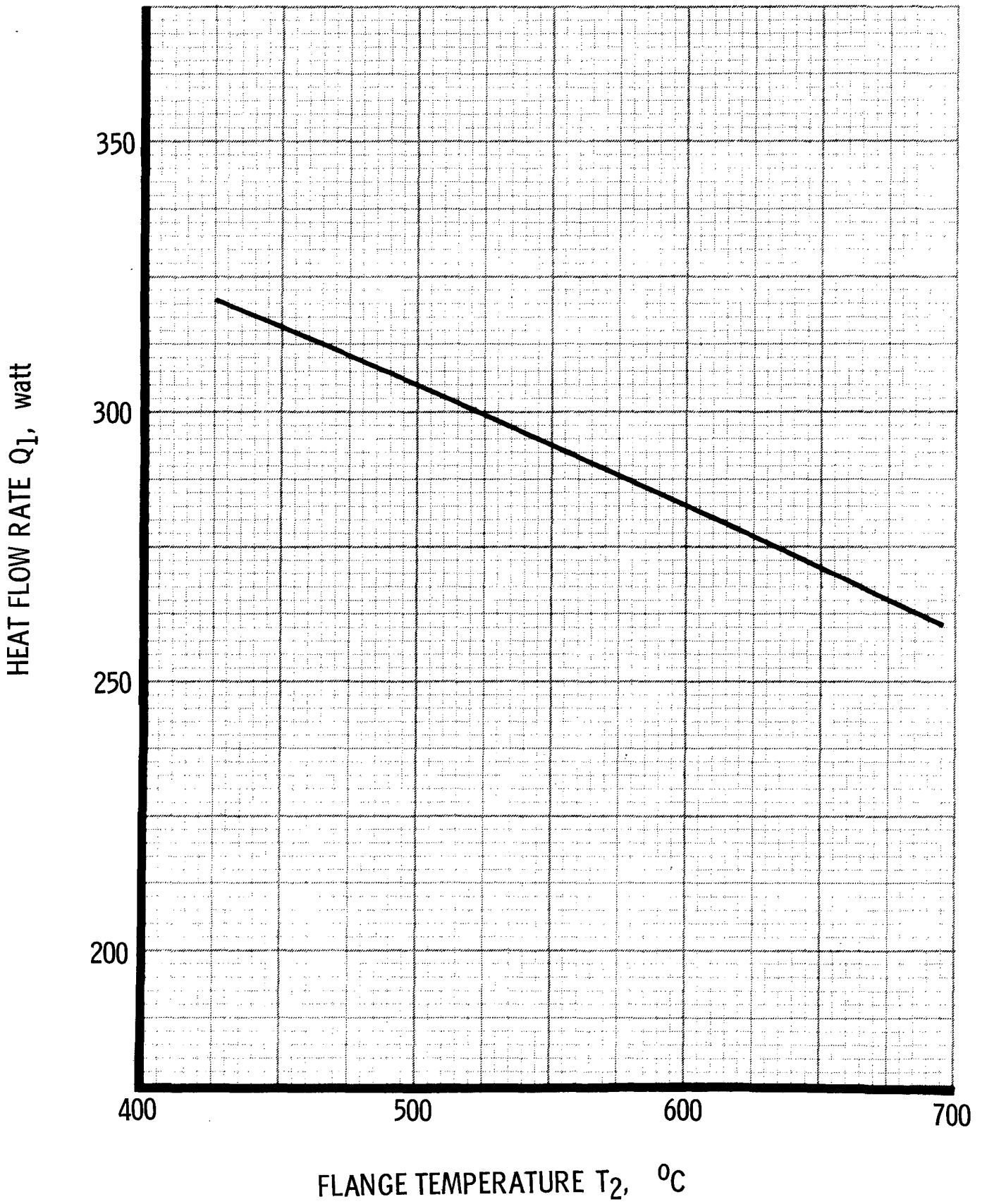
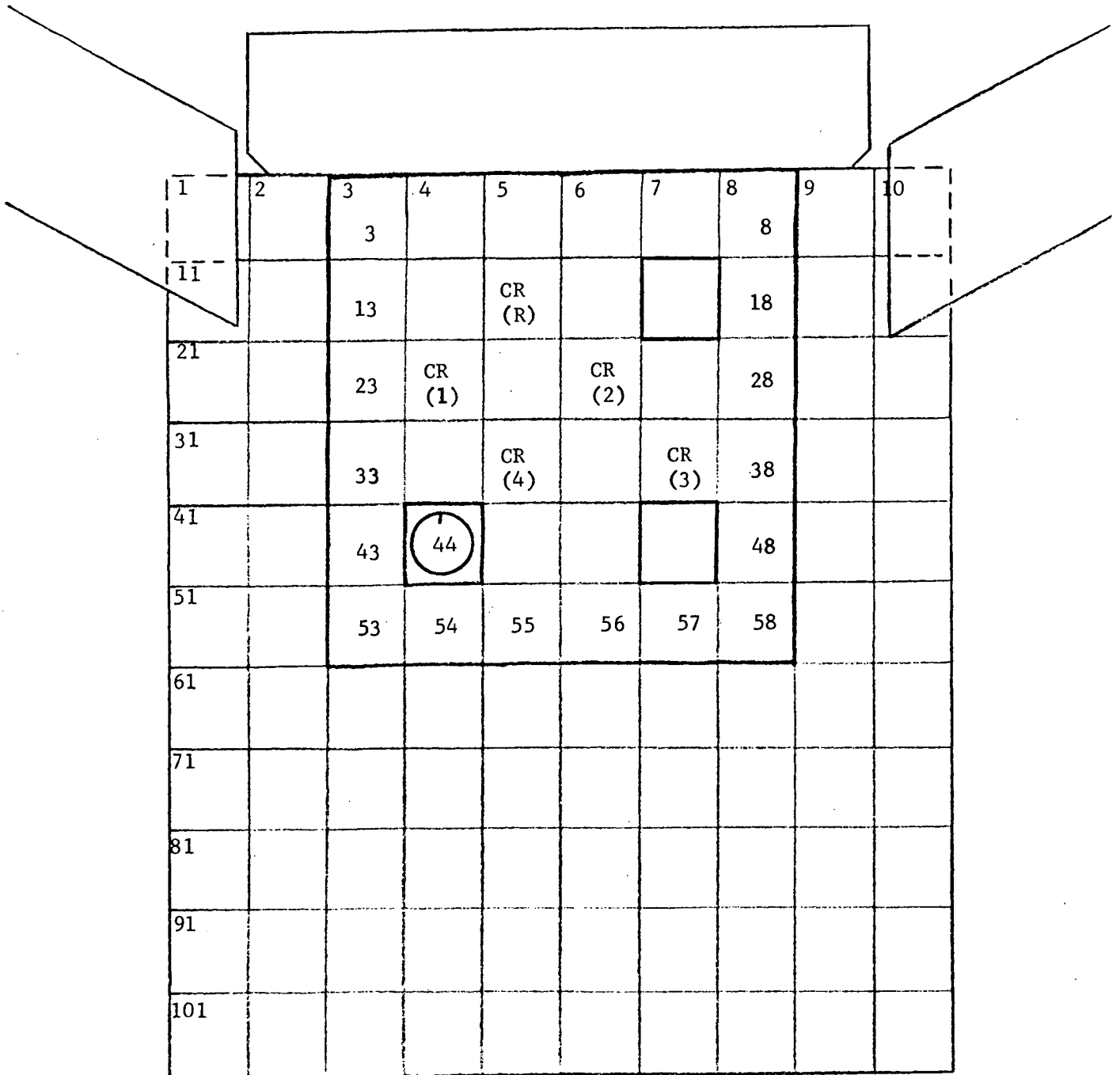


Fig. C1: REACTOR CORE LAYOUT



CR denotes control rod.

Mark on capsule section is 0 degrees; angular positions taken clockwise.



Fig. C2:

FUEL-EMITTER MOCK-UP EXPERIMENT

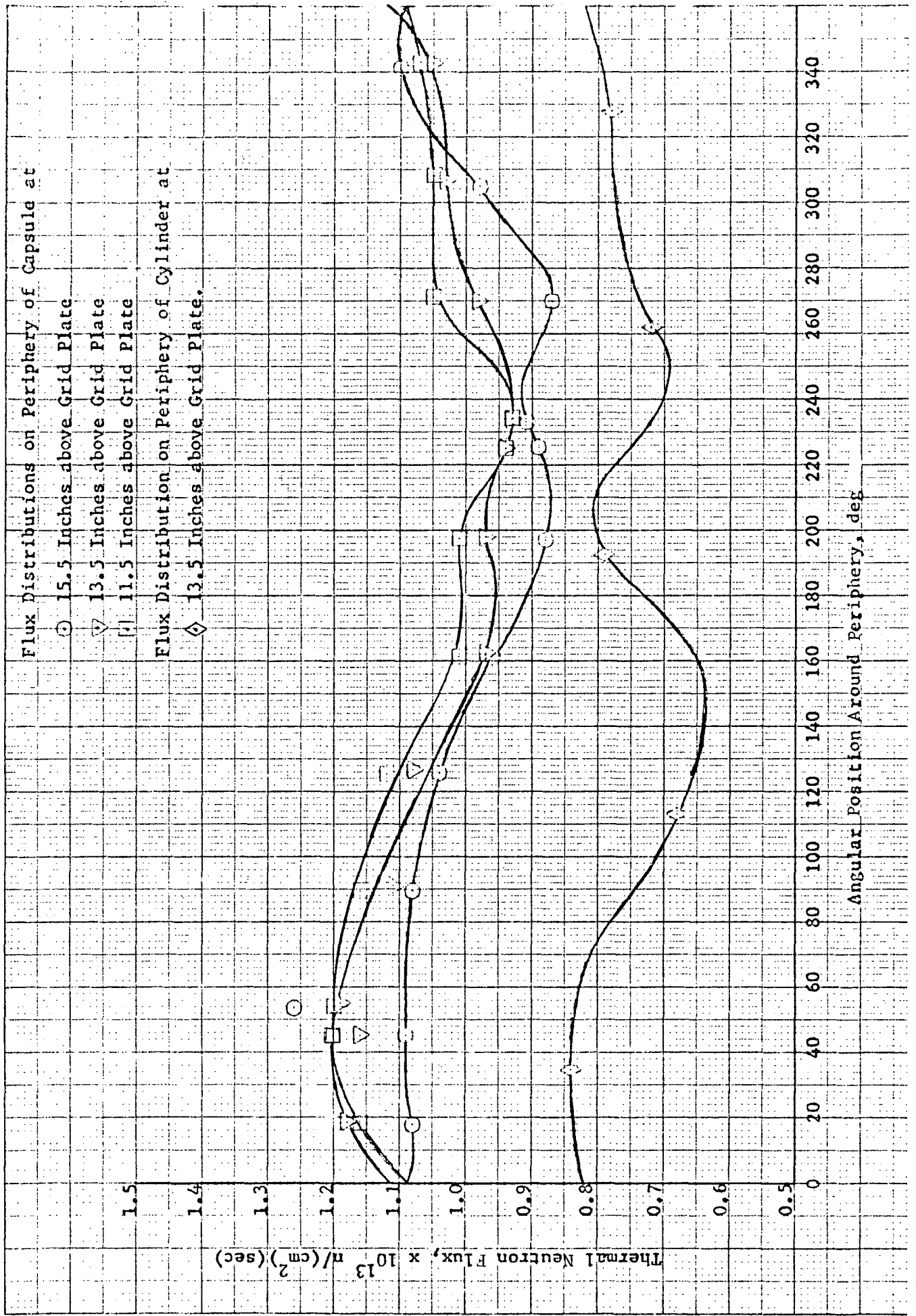


Fig. C3: THERMAL NEUTRON FLUX, AZIMUTHAL PROFILES

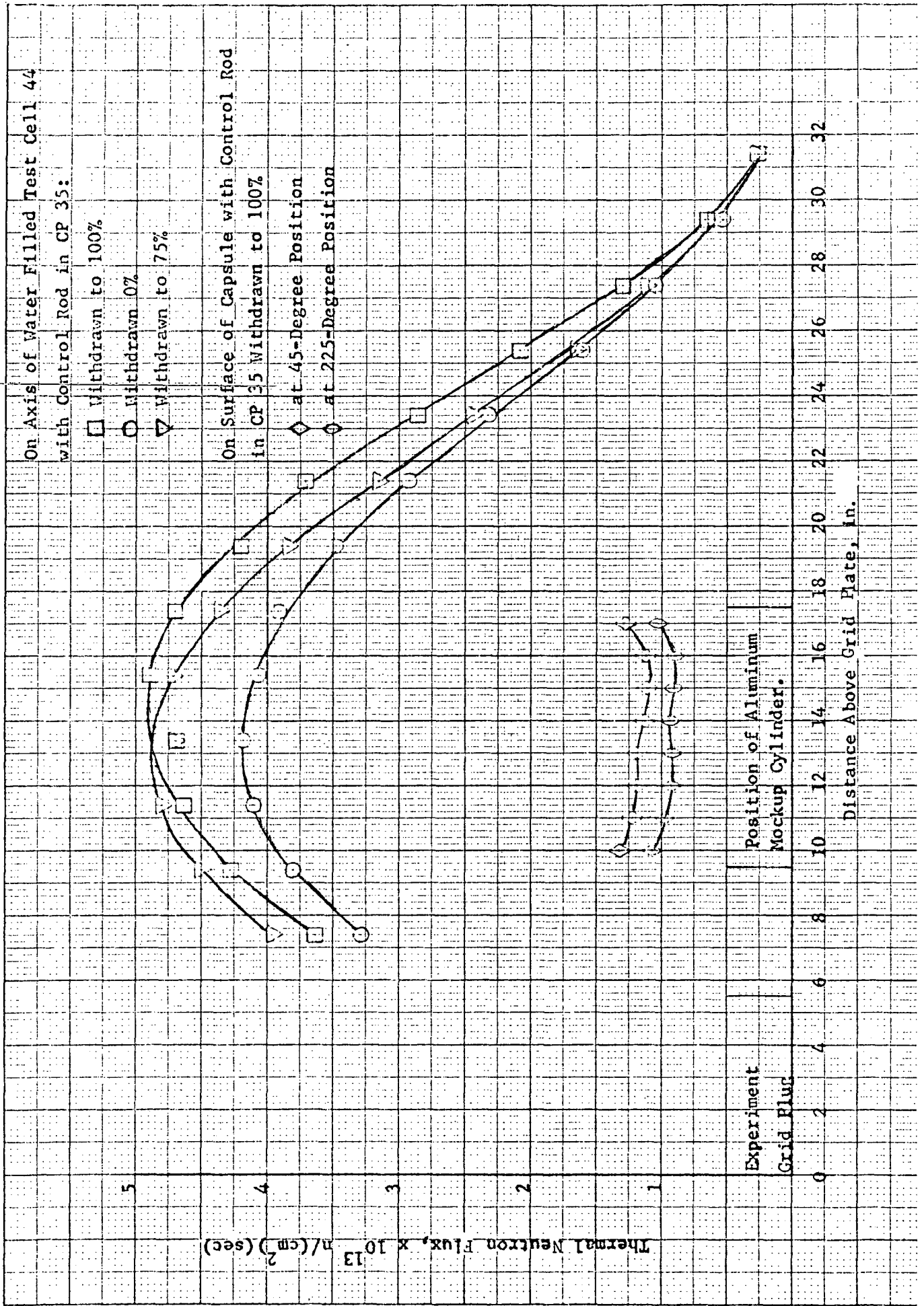


Fig. C4: THERMAL NEUTRON FLUX, AXIAL PROFILES

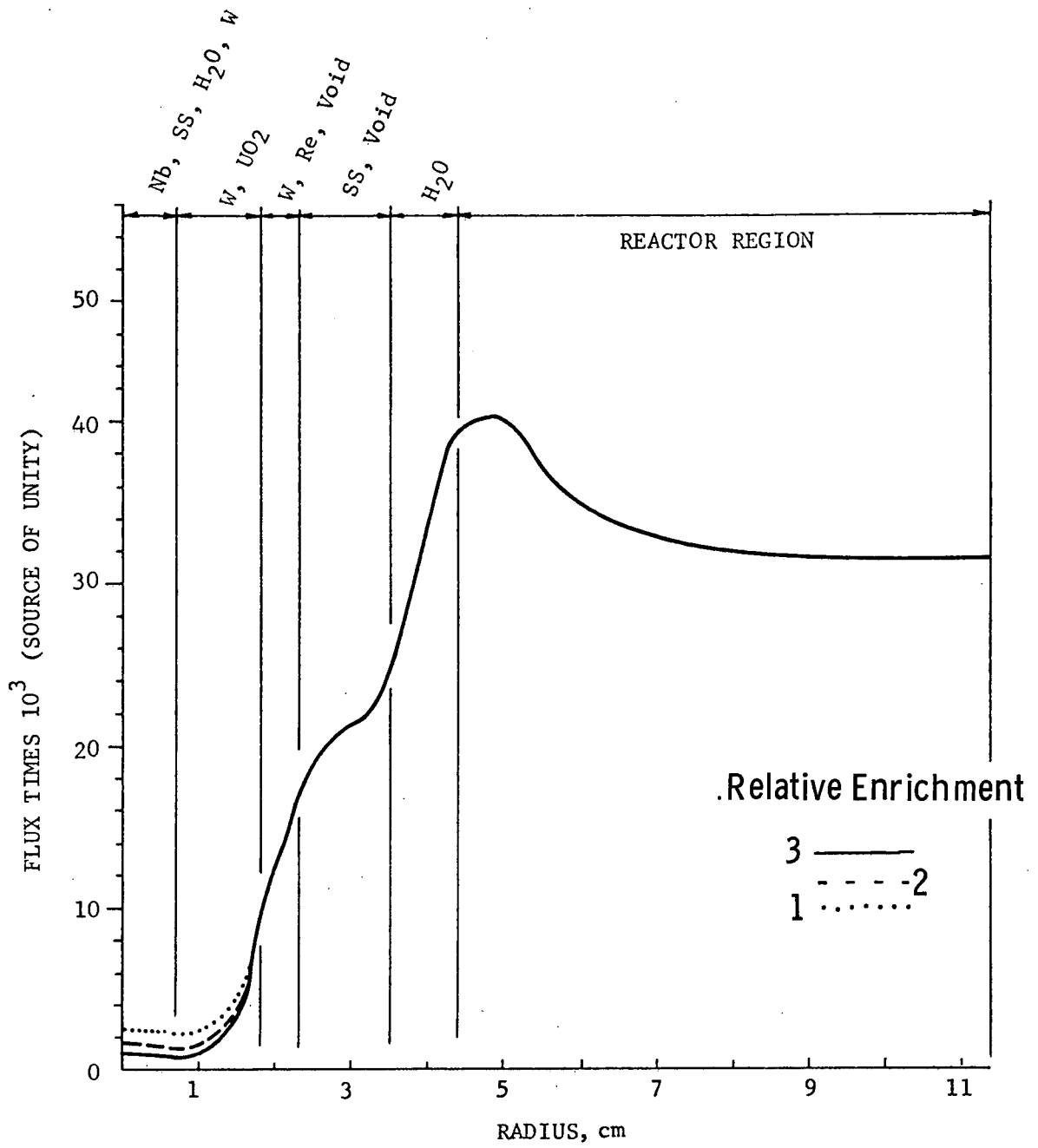


Fig. C5: COMPUTED RADIAL FLUX PROFILE

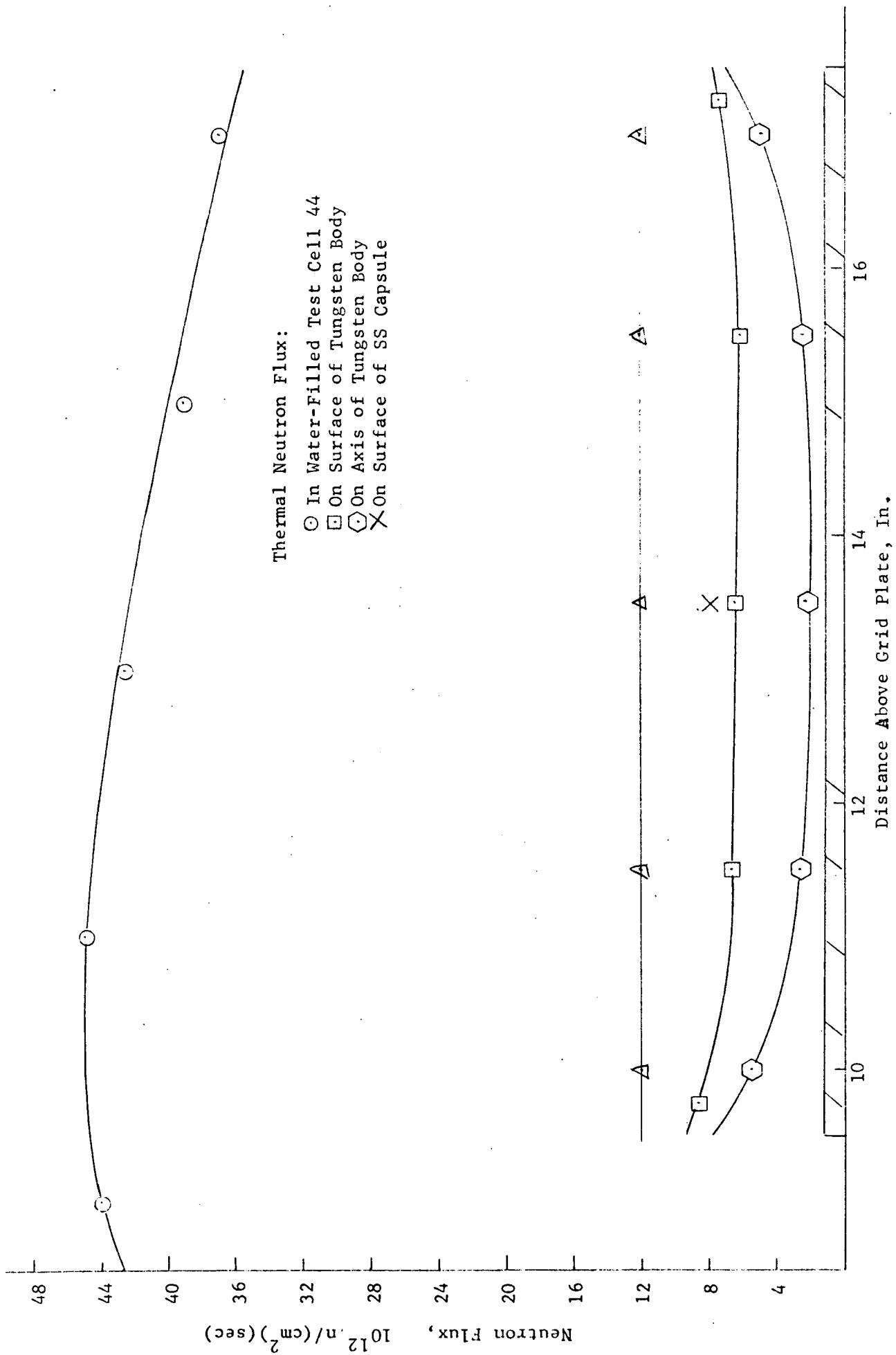


Fig. C6: NEUTRON FLUX PROFILES AT 2-MW REACTOR POWER

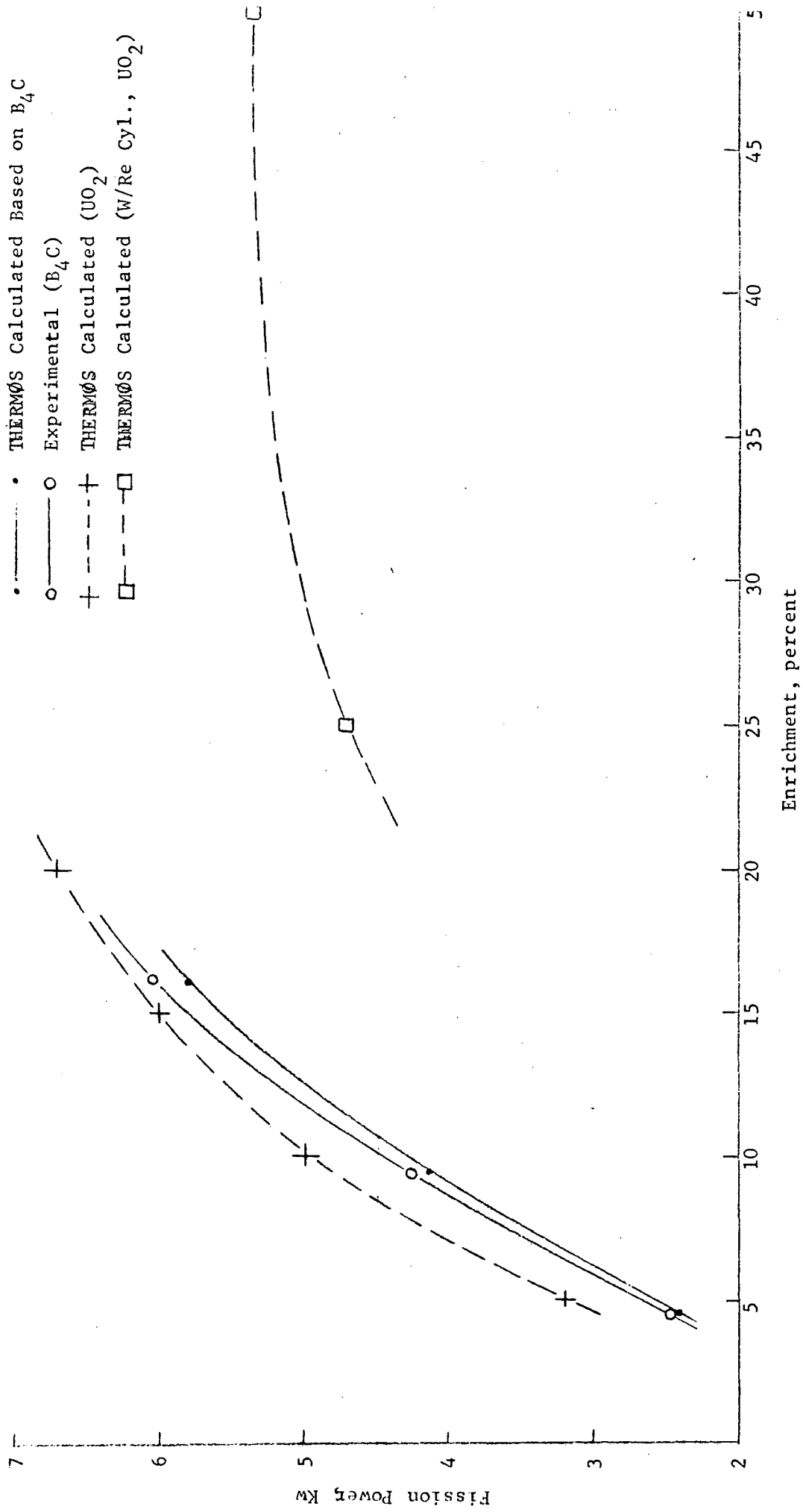
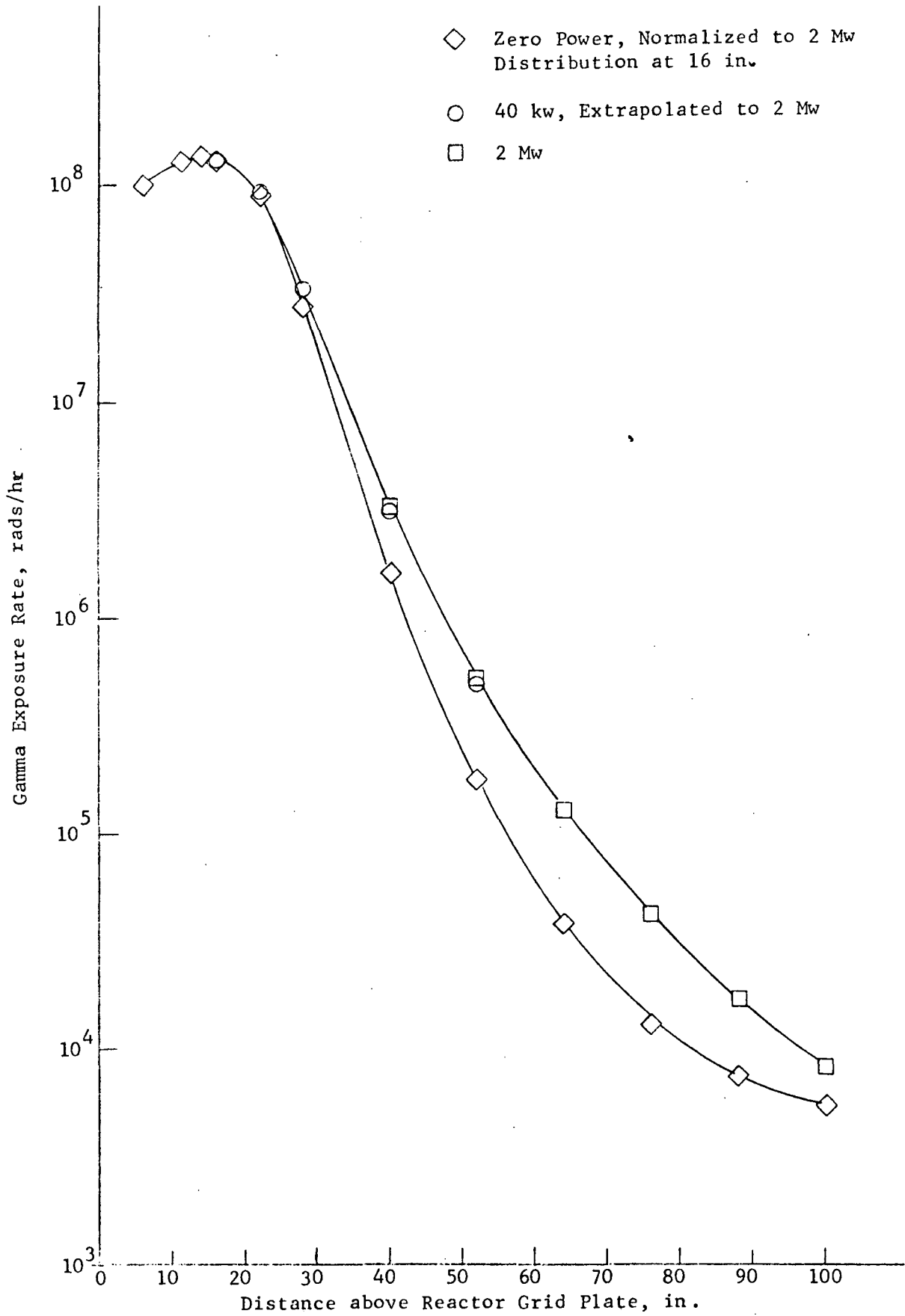


Fig. C7: FISSION POWER VERSUS FUEL ENRICHMENT

Fig. C8: MEASURED GAMMA DISTRIBUTION IN MOCK-UP CAPSULE



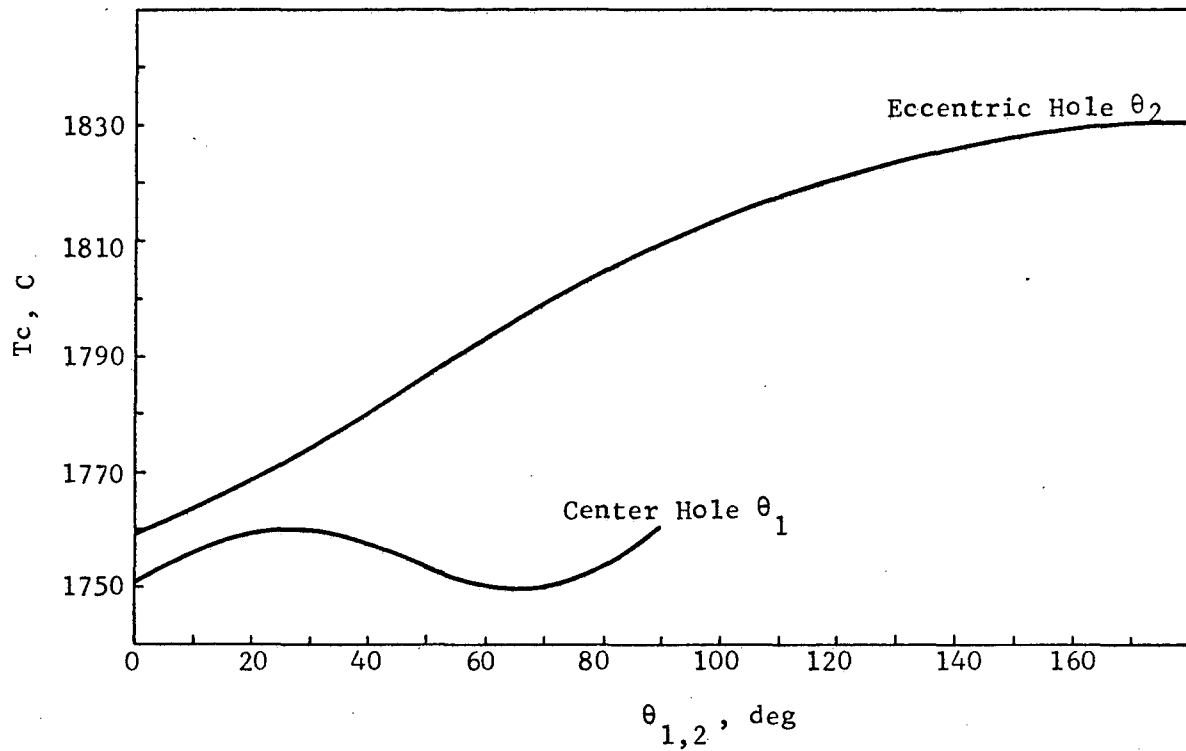


Fig. D1: PERIPHERAL TEMPERATURE PROFILE OF EMITTER AND FUEL CHAMBER

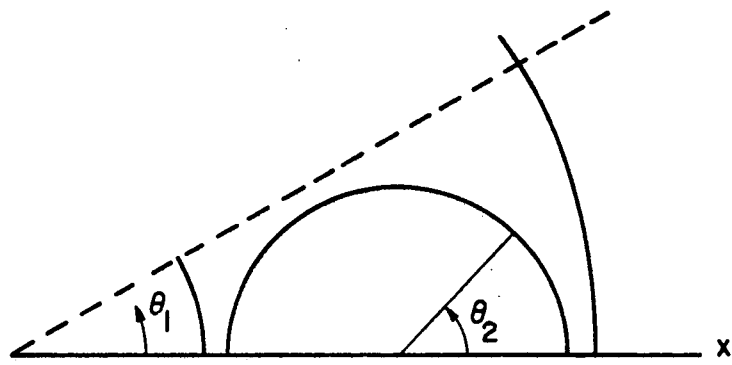


Fig. D2: 30-DEGREE CELL FOR THERMAL STRESS ANALYSIS

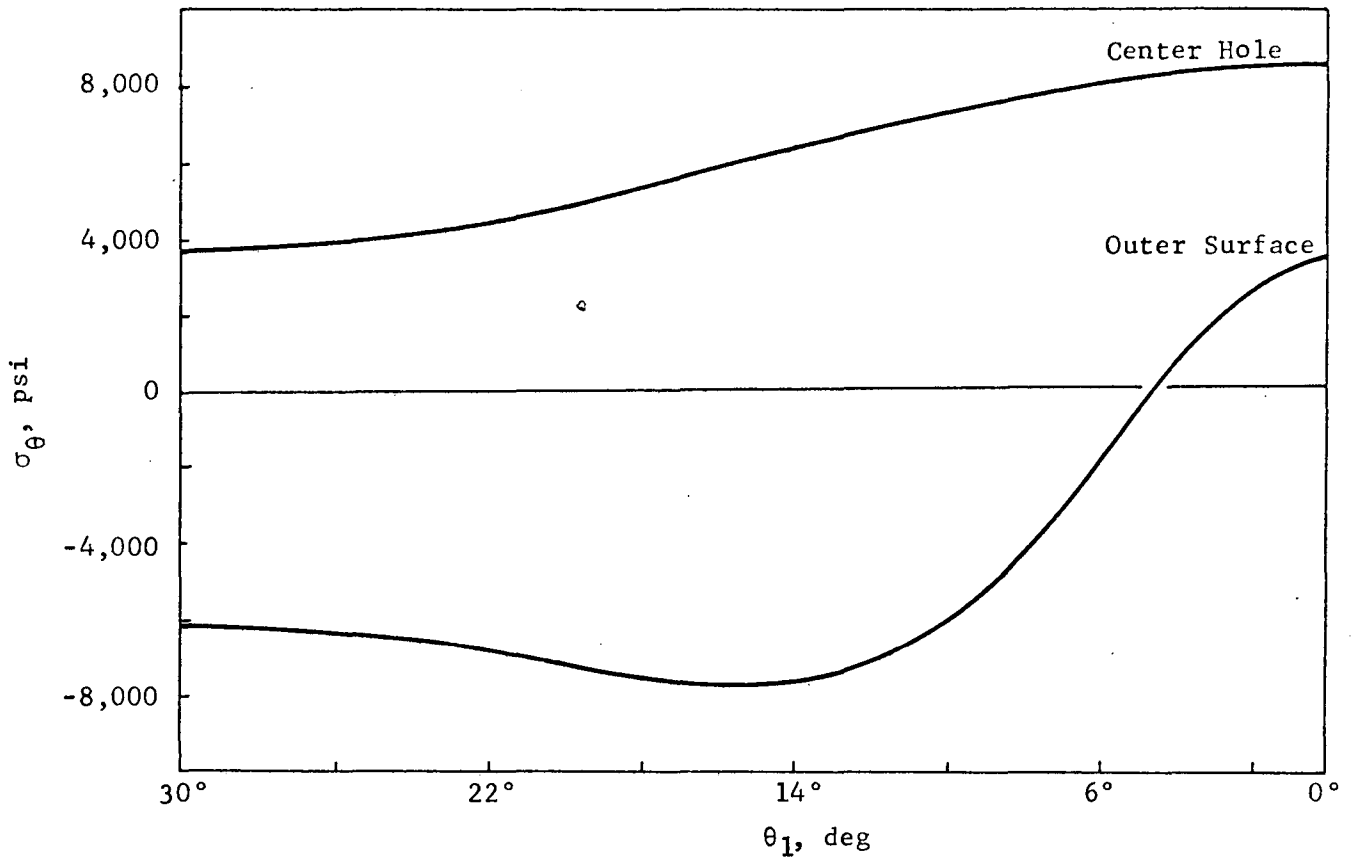


Fig. D3: TANGENTIAL STRESS AT BOUNDARIES OF EMITTER BODY

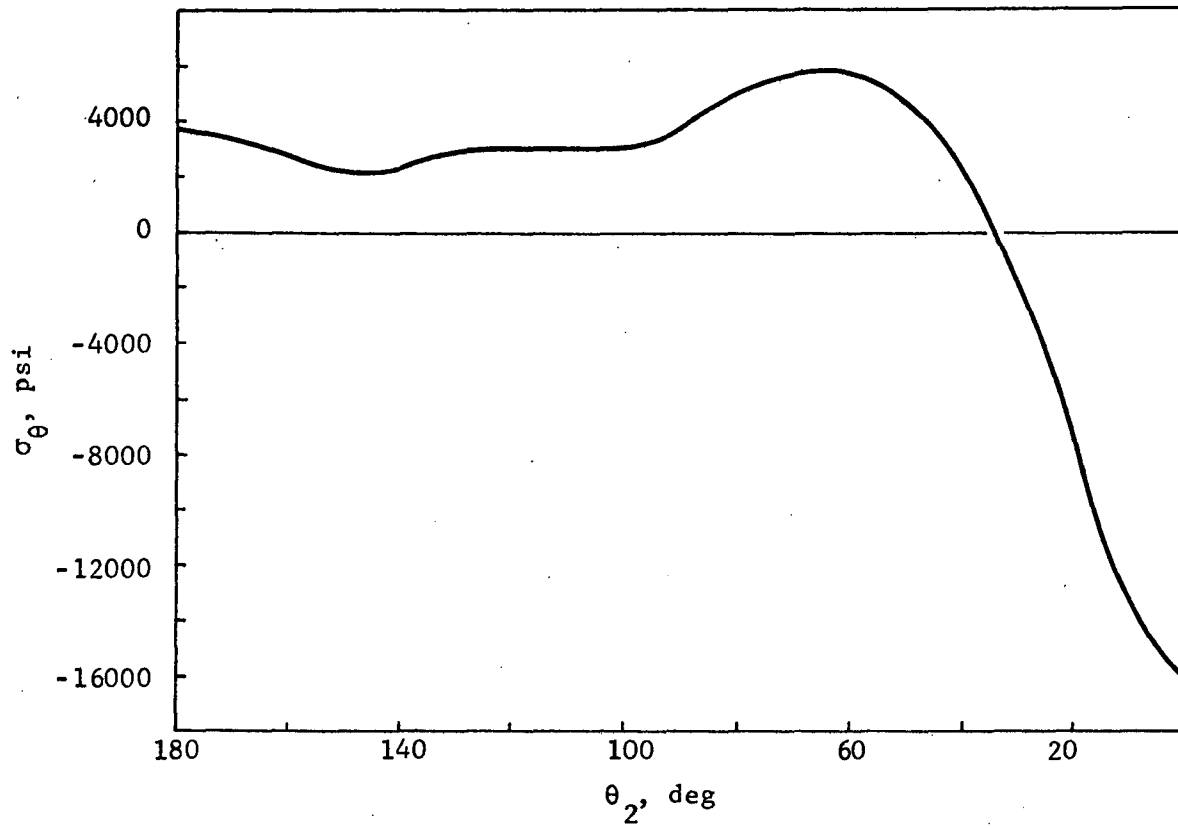


Fig. D4: TANGENTIAL STRESS AT FUEL CHAMBER BOUNDARY

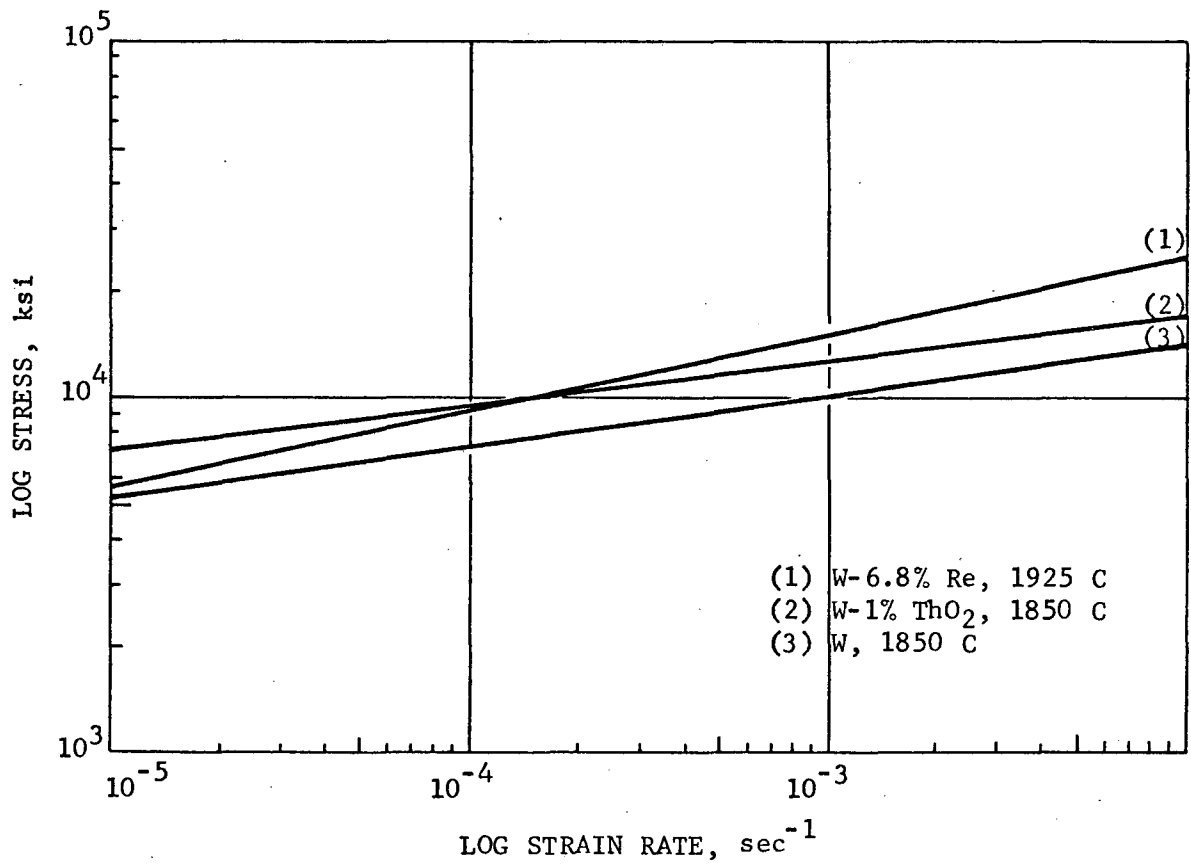


Fig. D5: HIGH-TEMPERATURE CREEP RATES OF TUNGSTEN ALLOYS

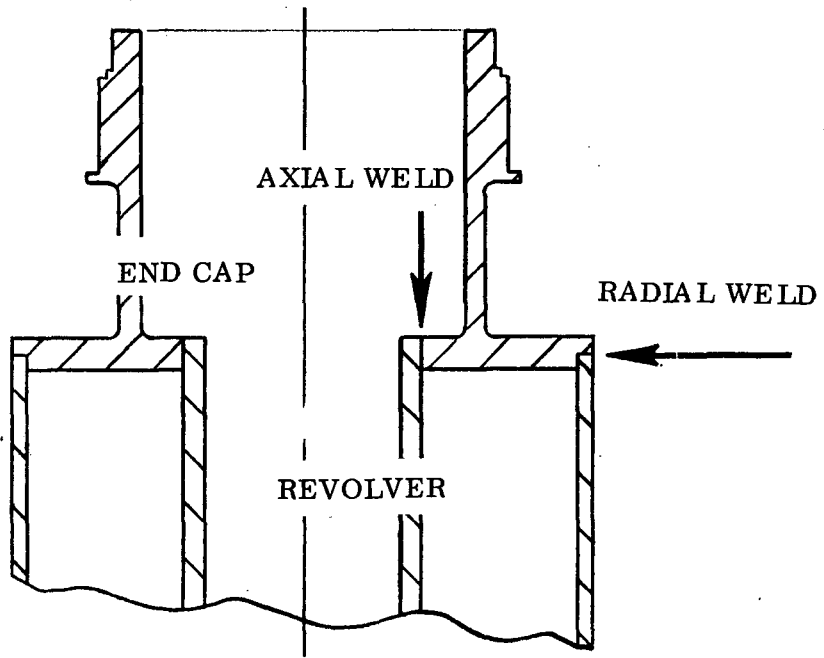


Fig. F1: CONFIGURATION OF END CAP-TO-REVOLVER WELDS

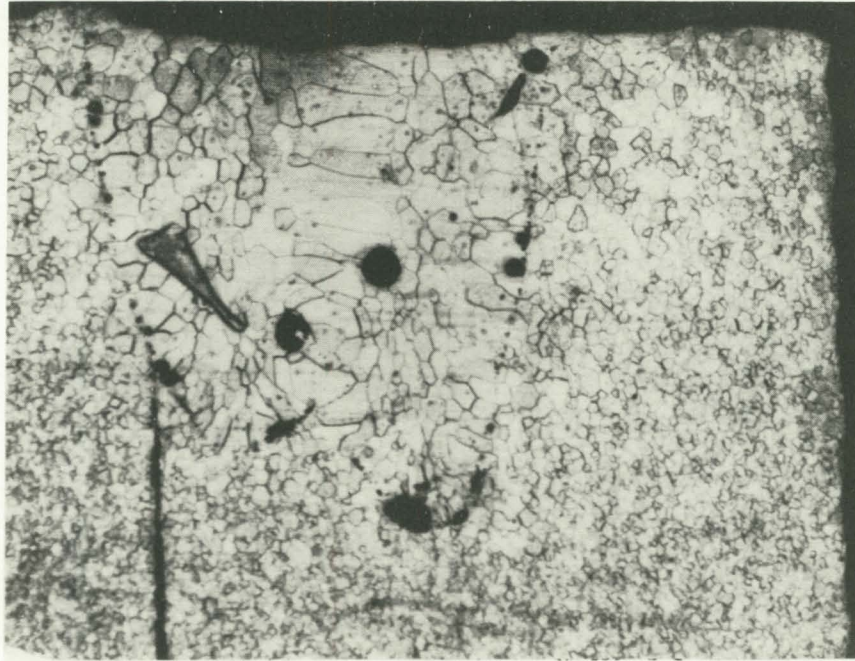


Fig. F2: AXIAL WELD, PM-TUNGSTEN TO PM-TUNGSTEN

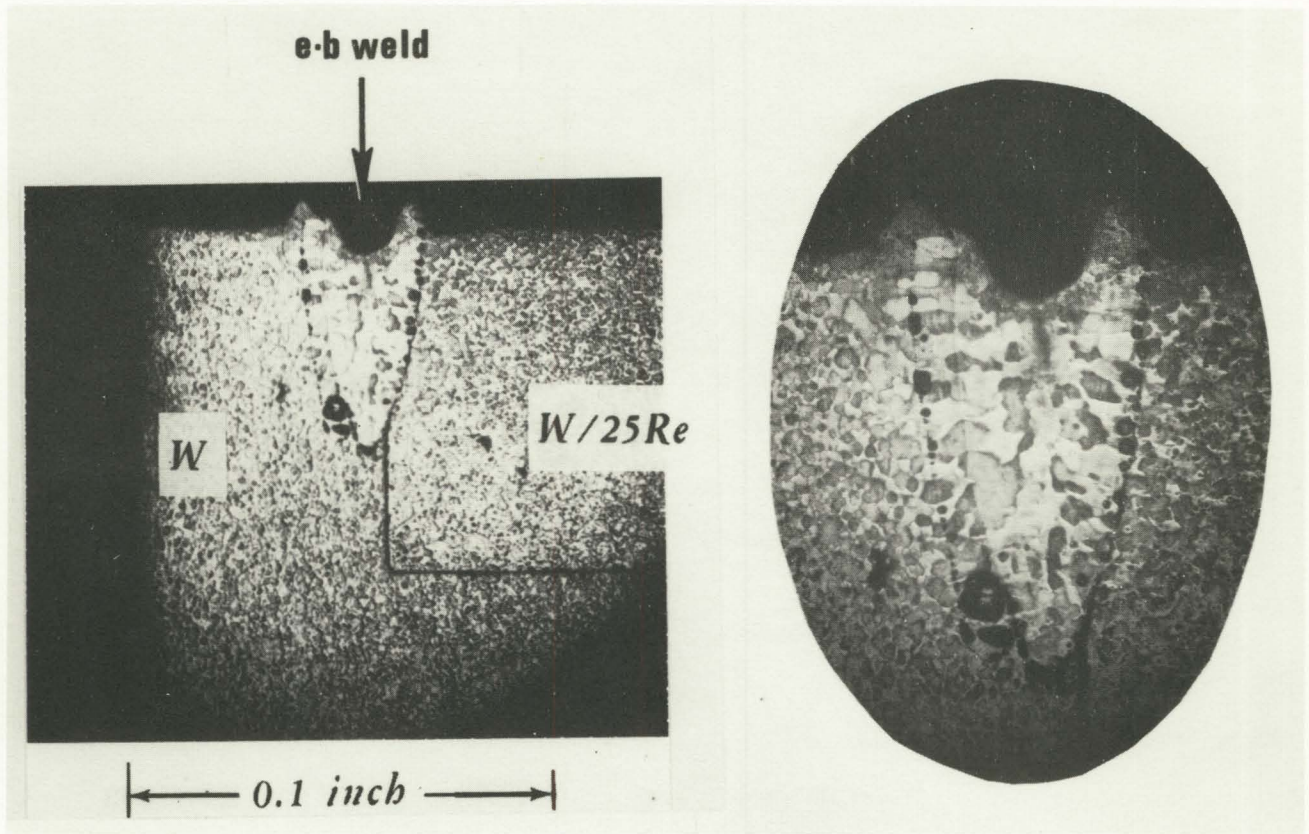
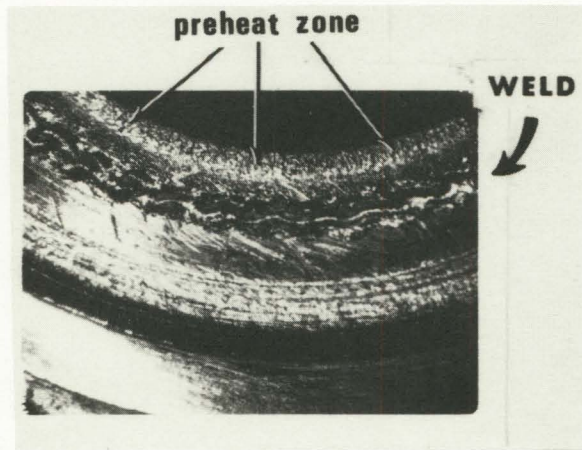
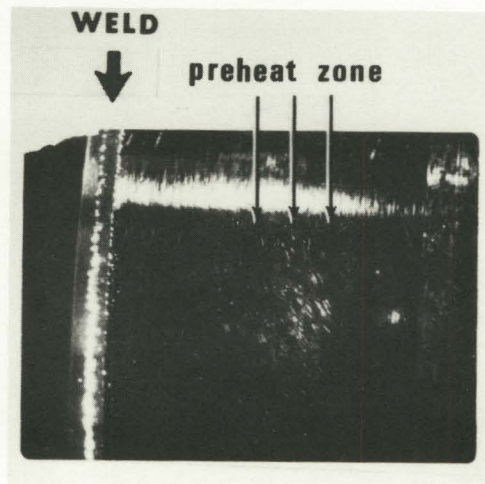


Fig. F3: AXIAL WELD, PM-TUNGSTEN TO PM-TUNGSTEN/25 RHENIUM



AXIAL



RADIAL

Fig. F4: SURFACE MACROPHOTOGRAPHS

PM-W/25RE END CAP TO AC-W REVOLVER WELDS WITH E-B PREHEAT

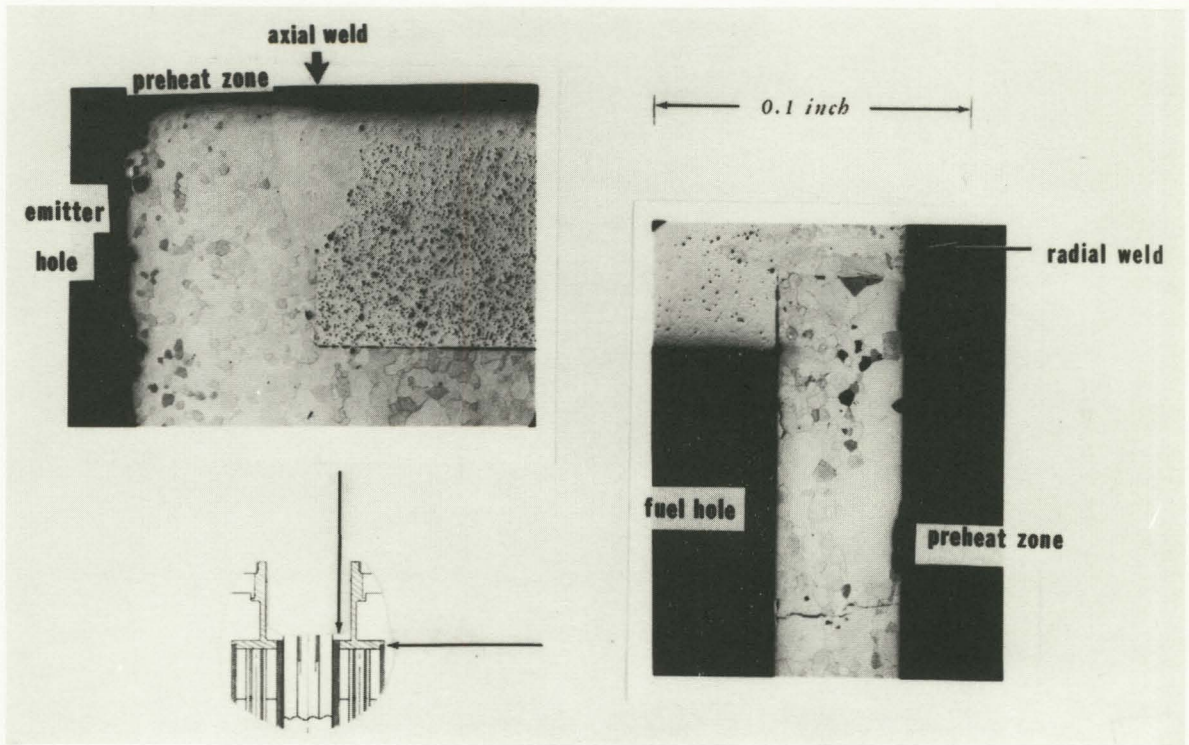


Fig. F5: CROSS-SECTIONS THROUGH WELDS SHOWING PREHEAT ZONES

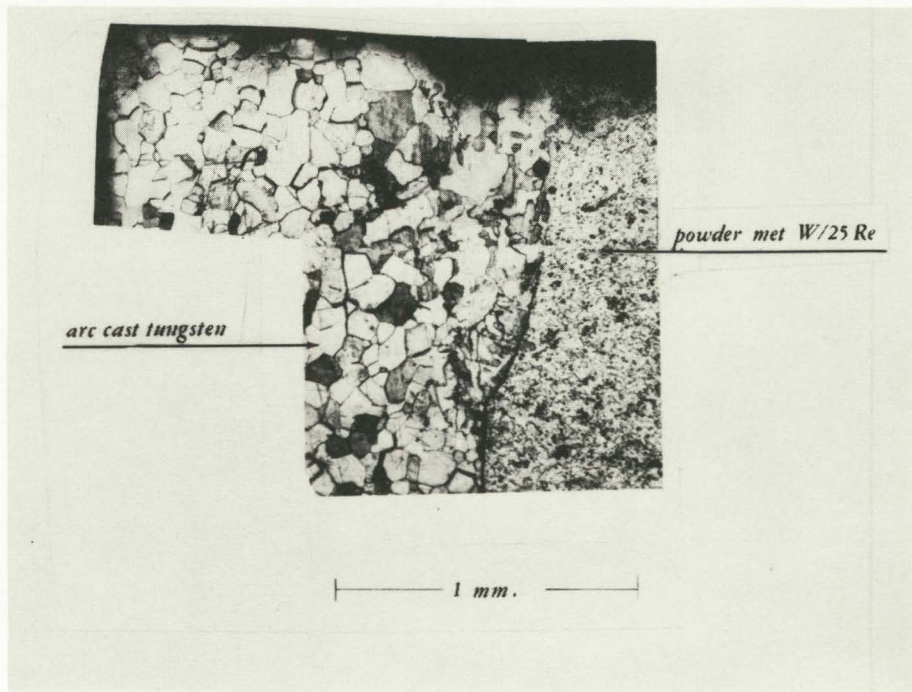


Fig. F6: ENLARGED CROSS SECTION THROUGH WEB OF FIG. F4 AXIAL WELD

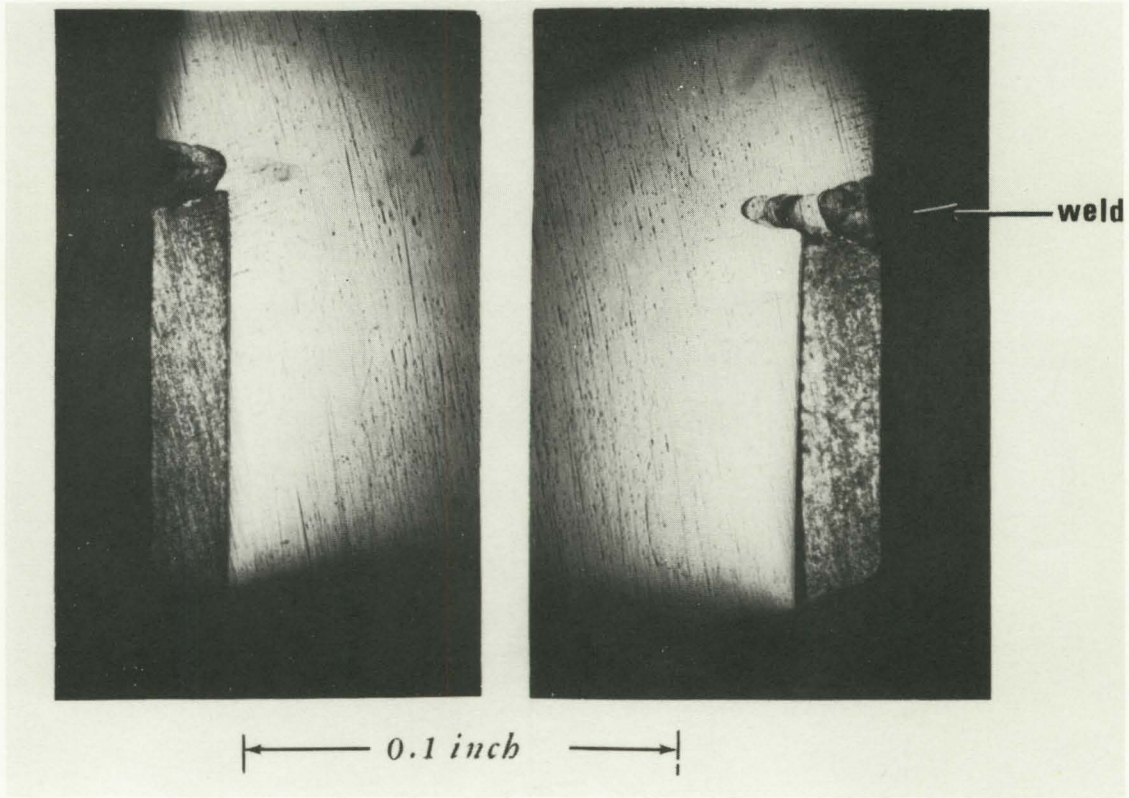


Fig. F7: NIOBIUM TUBE TO PM-TUNGSTEN/25 RHENIUM SLEEVE

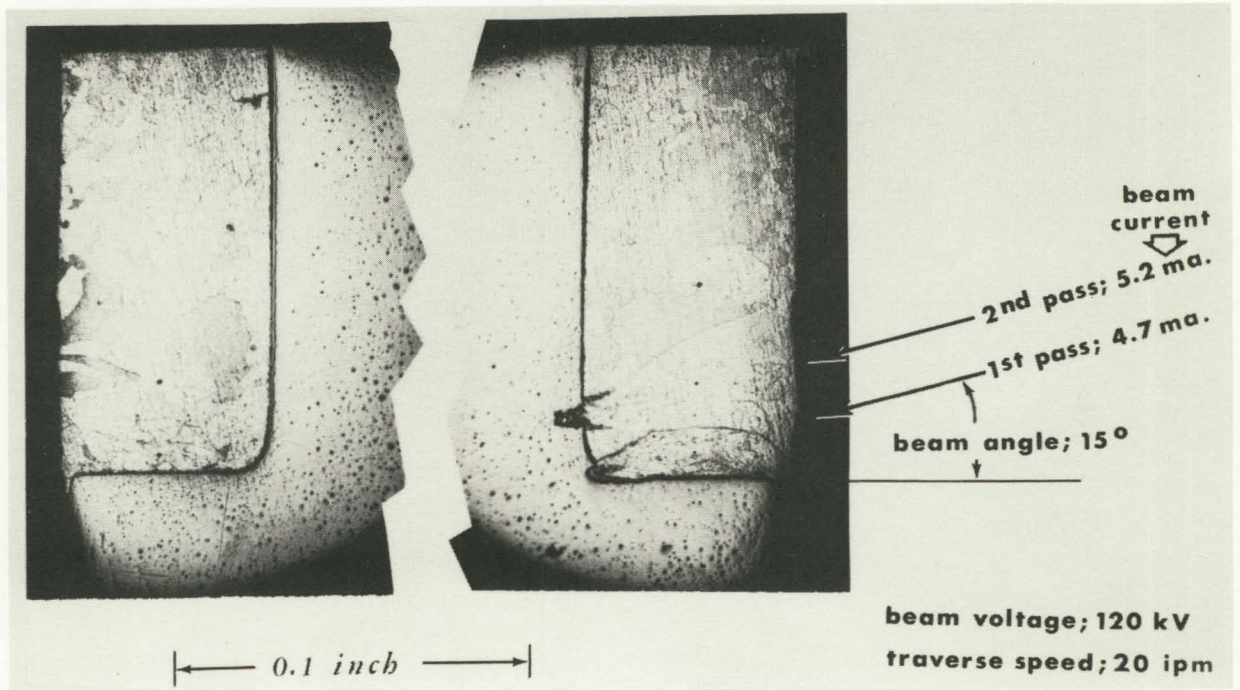


Fig. F8: E-B "SELF-BRAZE" JOINT; NIOBIUM TO PM-TUNGSTEN/25 RHENIUM

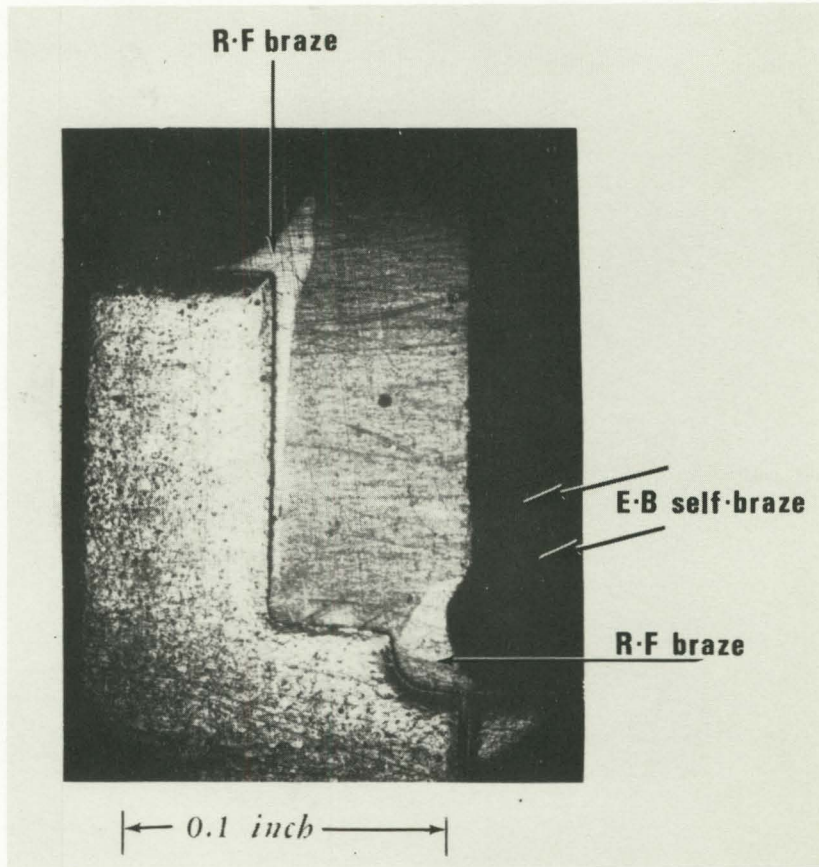


Fig. F9: NIOBIUM SEAL TO PM-W/25RE END CAP
SELF-BRAZE WITH RF BACKBRAZES

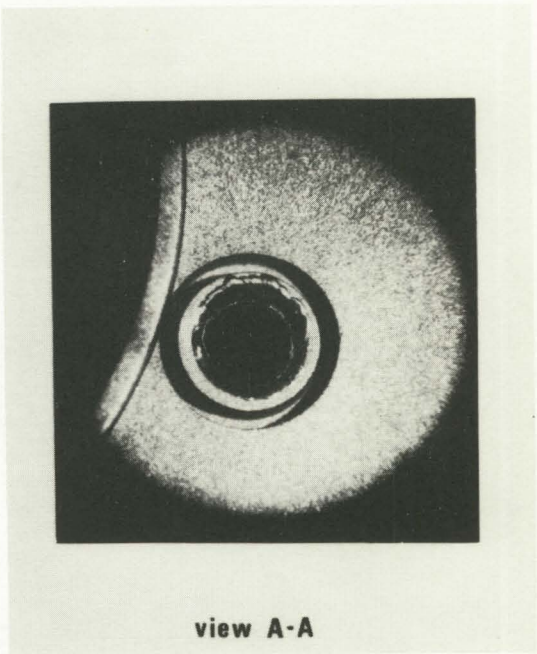
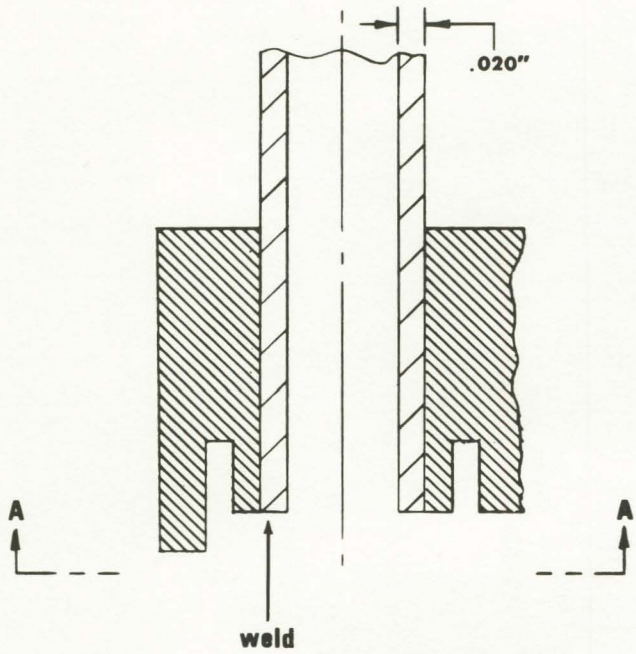


Fig. F10: NIOBIUM TUBE TO PM-TUNGSTEN/25 RHENIUM FLANGE BRAZE-WELD

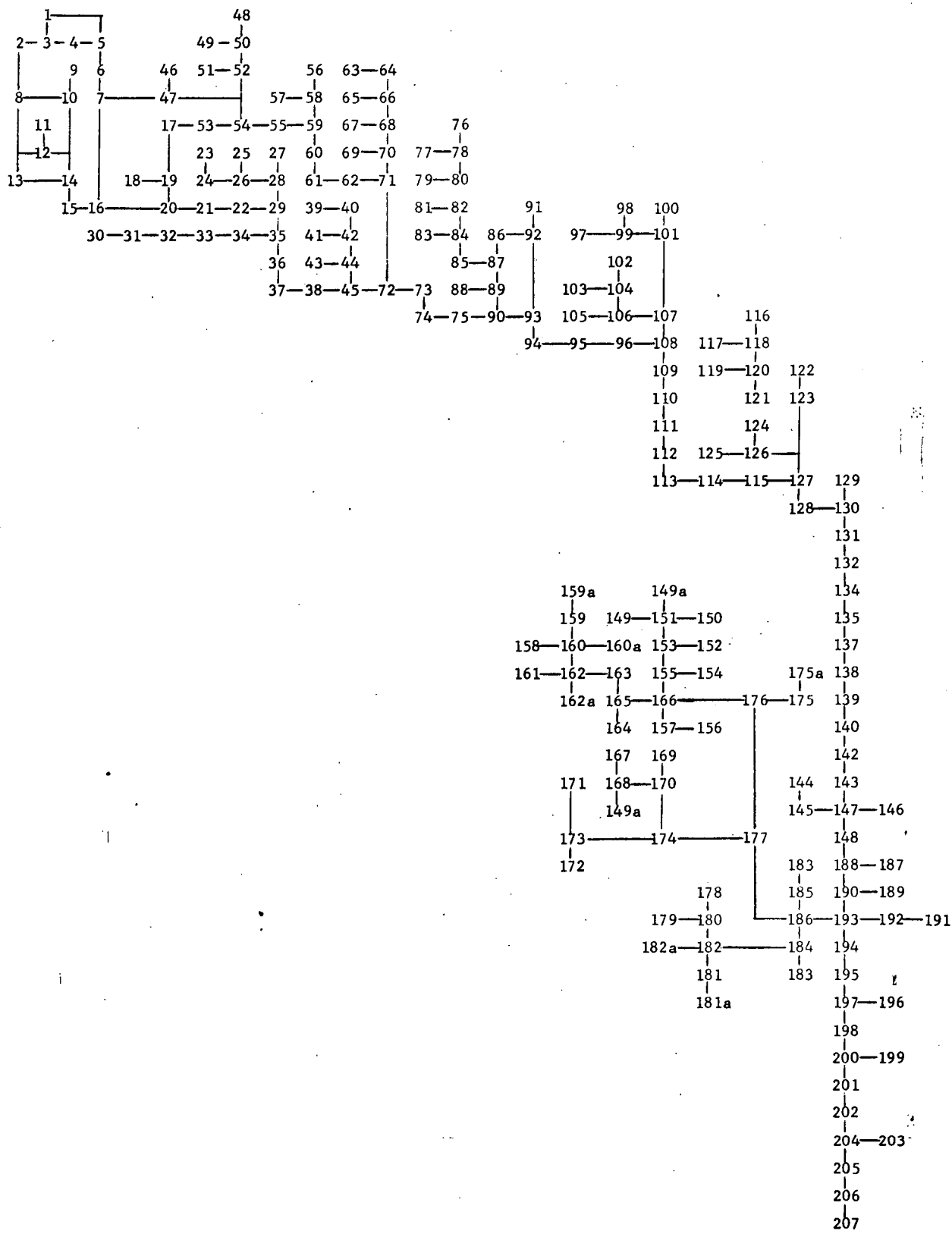


Fig. G1: CONVERTER FABRICATION AND ASSEMBLY SEQUENCE

FOLDOUT FRAME 1

FOLDOUT FRAME 2

FOLDOUT FRAME 3

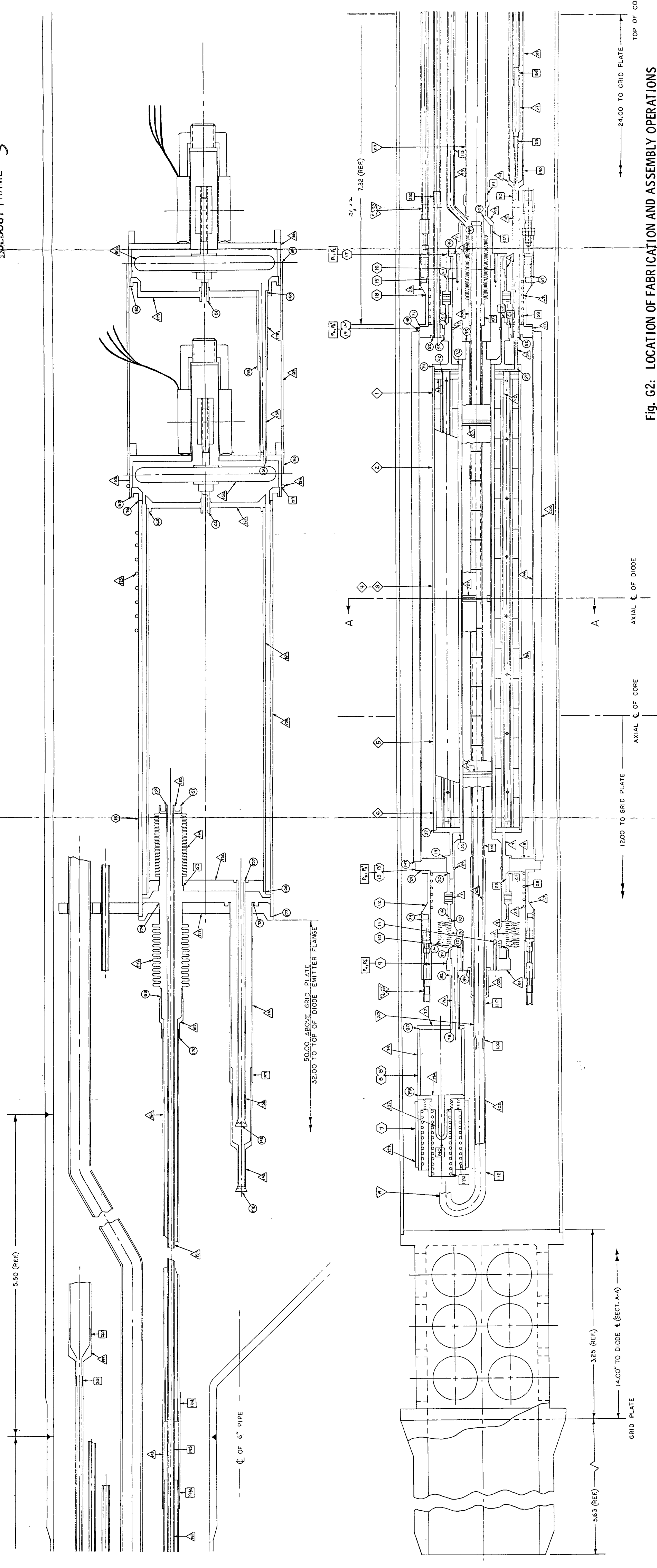


Fig. G2: LOCATION OF FABRICATION AND ASSEMBLY OPERATIONS